REPORT DOCUMENTATION PAGE		Form Approved OMB No. 0704-0188

1. AGENCY USE ONLY (Leave blank)	2. REPORT DATE 2.Nov.00	3. REPORT TYPE AND DATES COVERED THESIS

4. TITLE AND SUBTITLE
PERFORMANCE ANALYSIS OF A SPACE BASED GMTI RADAR SYSTEM
USING SEPARATED SPACECRAFT INTERFEROMETRY

5. FUNDING NUMBERS

6. AUTHOR(S)
2D LT HACKER TROY L

7. PERFORMING ORGANIZATION NAME(S) AND ADDRESS(ES)
MASSACHUSETTS INSTITUTE OF TECHNOLOGY

8. PERFORMING ORGANIZATION REPORT NUMBER

CY00438

9. SPONSORING/MONITORING AGENCY NAME(S) AND ADDRESS(ES)
THE DEPARTMENT OF THE AIR FORCE
AFIT/CIA, BLDG 125
2950 P STREET
WPAFB OH 45433

10. SPONSORING/MONITORING AGENCY REPORT NUMBER

11. SUPPLEMENTARY NOTES

12a. DISTRIBUTION AVAILABILITY STATEMENT
Unlimited distribution
In Accordance With AFI 35-205/AFIT Sup 1

12b. DISTRIBUTION CODE

13. ABSTRACT (Maximum 200 words)

14. SUBJECT TERMS

20001120 092

15. NUMBER OF PAGES
199

16. PRICE CODE

17. SECURITY CLASSIFICATION OF REPORT	18. SECURITY CLASSIFICATION OF THIS PAGE	19. SECURITY CLASSIFICATION OF ABSTRACT	20. LIMITATION OF ABSTRACT

Performance Analysis of a Space-Based GMTI Radar System Using Separated Spacecraft Interferometry

by

TROY L. HACKER

ABSTRACT

The development of a model to assess the radar performance capabilities of a sparse aperture space-based GMTI radar system is presented. Airborne radars have provided reliable detection of moving targets for many years. Recent technological advancements have allowed the deployment of radar systems in space to improve global coverage. Additional radar performance benefits from space-based platforms are made possible with clusters of collaborative microsatellites. Using quantitative capability metrics, specifically the probability of detection and the minimum detectable velocity, the performance of the radar system can be modeled to enable effective and unbiased comparison of candidate system architectures. A design study based on the space-based GMTI radar reference mission for the Air Force's TechSat 21 program was conducted to identify viable system design configurations that satisfy specific radar performance requirements. A comprehensive analysis of the cost, reliability, and performance considerations for the complete TechSat 21 system is proposed.

Thesis Supervisors:
Dr. Raymond J. Sedwick
Dept. of Aeronautics and Astronautics

Professor David W. Miller
Dept. of Aeronautics and Astronautics

20001120 092

Performance Analysis of a Space-Based GMTI Radar System Using Separated Spacecraft Interferometry

by

Troy L. Hacker

B.S. Physics
U.S. Air Force Academy, 1998

SUBMITTED TO THE DEPARTMENT OF AERONAUTICS AND ASTRONAUTICS
IN PARTIAL FULFILLMENT OF THE REQUIREMENTS FOR THE DEGREE OF

MASTER OF SCIENCE

at the

MASSACHUSETTS INSTITUTE OF TECHNOLOGY

May 2000

© 2000 Massachusetts Institute of Technology

Signature of Author . . . .
Department of Aeronautics and Astronautics
May 24, 2000
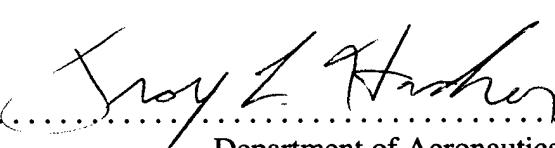
Certified by . . . .
Dr. Raymond J. Sedwick
Research Scientist

Certified by . . . .
Professor David W. Miller
Thesis Supervisor
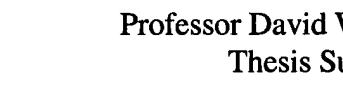
Accepted by . . . .
Professor Nesbitt W. Hagood
Chairman, Department Graduate Committee

ACKNOWLEDGMENTS

TABLE OF CONTENTS

LIST OF FIGURES

LIST OF TABLES

NOMENCLATURE

A_{cell}	cell area [m^2]
A_e	antenna effective area [m^2]
A_f	footprint area [m^2]
A_g	resolvable area of ground cell [m^2]
ASR	area search rate [m^2/s]
c	speed of light [m/s]
AZ	azimuth angle [degrees]
B	cluster baseline [m]
BW	bandwidth [Hz]
BW_n	noise bandwidth [Hz]
CPI	coherent processing interval [s]
CR	pulse compression ratio
CW	continuous wave
D	circular aperture diameter [m]
DC	transmission duty cycle
$DPCA$	displaced phase center antenna
EL	elevation angle [degrees]
f_c	carrier/transmission frequency [Hz]
f_D	Doppler shift [Hz]
$G_{(ap)}$	antenna (aperture) gain
G_{af}	array factor gain
G_{int}	interferometer gain
$(G)MTI$	(ground) moving target indication
h	orbital altitude [m]
k	Boltzmann constant [J/K/Hz]
L	square aperture length [m]
L_s	system losses [dB]
LW	spectral line width [Hz]
MDV	minimum detectable velocity [m/s]
n_c	number of coherent pulses
n_i	number of incoherent pulses
n_p	number of pulses
N	number of satellites in a cluster
$\overline{N}$	mean noise power level [W]
P_{avg}	average power [W]
P_d	probability of detection
P_{fa}	false alarm probability
P_t	transmission power [W]
PDF	probability density function
PRF	pulse repetition frequency [Hz]

PSF	point spread function
R	distance/range to target [m]
R_e	radius of the Earth [m]
R_g	ground range [m]
R_{max}	maximum detection range [m]
SCR	signal-to-clutter ratio
SIR	signal-to-interference ratio
SNR	signal-to-noise ratio
$STAP$	space-time adaptive processing
t_d	coherent dwell time [s]
T	interpulse period [s]
T_d	total dwell time [s]
T_s	system noise temperature (K)
v_p	orbital (platform) velocity [m/s]
v_T	target velocity [m/s]
Δf	frequency width of the Doppler bins [Hz]
Δf_D	spread of Doppler frequencies [Hz]
ΔF	total change in frequency of the transmitted pulse [Hz]
ΔR	range resolution [m]
Δv	velocity resolution [m/s]
ΔXR	cross-range resolution [m]
$\Delta \theta$	antenna beamwidth/angular resolution [rad]
$\Delta \theta_{cell}$	beamwidth of a sparse aperture interferometer [rad]
γ	clutter reflectivity
θ	off-boresight angle [rad]
λ	transmission wavelength [m]
σ_0	clutter cross section per unit area
σ	clutter radar cross section [m^2]
σ_T	target radar cross section [m^2]
τ	pulse width [s]
τ_c	compressed pulse width [s]
ϕ_c	Earth angle [degrees]
ψ	grazing angle [degrees]

Chapter 1

INTRODUCTION

1.1 Motivation

Examples of radar-like principles are everywhere around us. Bats and porpoises emit sound waves to detect small objects at great distances (sonar). A blind man taps his cane on the sidewalk to avoid obstacles in his path. The weather pictures we see on the nightly news as well as the positions of aircraft for air-traffic control are also provided by radar. The term radar stands for RAdio Detection And Ranging, and the underlying principle in all of these applications is the detection and location of objects based on the echoes they reflect. Radar is used to enhance our perception of the environment around us by extending the capability of our senses. It represents the greatest advance in remote sensing since the invention of the telescope because it can rapidly scan large angular regions in a short amount of time [Barton, 1988]. Furthermore, radar signals can penetrate the atmosphere in all forms of weather to provide much longer detection ranges and greater sensitivity than are possible in the visible spectrum.

Although there are well known cases of radar-like phenomena in nature, mechanical radar systems are a relatively new field of research. When radar was first developed in the World War II era, the typical system simply consisted of a ground-based antenna that transmitted a pulse, listened for its reflection, then started over. All objects illuminated by these ground-based radars showed up as simple blips in the user's display based on their respective ranges while azimuth information came from the direction in which the antenna

was pointed. However, there was no known system for identifying the various sources of these received echoes. With the advent of Doppler processing, the additional frequency information in the received signals helped the radar distinguish desirable target returns from sources of interference. Radars were soon placed on aircraft to give an improved reconnaissance capability characteristic of an airborne platform as well as an increased effectiveness at detecting targets beyond visual range. Airborne radar created a number of practical applications for civil and military use.

Airborne platforms benefit from strong signal returns with relatively low transmission power and can be deployed at a moment's notice, but they suffer from small coverage areas and operating ranges, vulnerability to enemy attack (military applications), and overall size limitations. In addition, the excessive deployment time, immense support structure, outdated technology, and high operating and maintenance costs are some of the major drawbacks of current airborne radar systems. All of these handicaps could be remedied from a space-based platform. Such a radar system could respond to new tasks almost instantly, requires relatively little support structure, incorporates cutting-edge technology, and is dominated by acquisition and deployment costs over operations and maintenance costs [Wickert, 1997]. In general, the advantages of space-based radar include a much larger search area as well as access to otherwise denied areas at the cost of large signal attenuation from free space loss and the presence of severe clutter return. While there are many differences between airborne and space-based radar, it is important to remember that they operate in much the same manner.

There are many issues that must be considered when deploying a radar system in space, including orbit selection, hazards of the space environment, and other difficulties associated with a wide variety of space missions. With a space-based platform, the coverage in space and time is limited only by the orbit selected and the number of satellites, the radar can perform multiple missions, atmospheric propagation problems can be minimized, and no overseas data relay stations are required [Cantafio, 1989]. Despite the numerous potential benefits of space-based radar, the technologies for these systems (antennas,

power systems, on-board processing, etc.) are in their primitive stages and the overall cost tends to be expensive. Each of these factors represents a key challenge in the development of an operational space-based radar system.

Beyond technology and cost concerns, increasing demands on performance have pushed the limits of modern radar systems to satisfy these target detection and angular resolution requirements at specified area search rates according to the system application. The probability of detecting targets is determined by the power-aperture product of the radar and the clutter rejection capability of the signal processor. The physical dimensions of the antenna set the angular resolution of the system. Although applications of airborne radar are much more limited than space-based alternatives, the shorter operating range inherently provides a higher level of performance for similar system designs. Space-based radars must employ some combination of larger apertures, higher transmission power, and increased computational capacity to meet the performance requirements dictated by various end users.

Since airborne radars operate from serviceable platforms, transmission power and aperture diameter are restricted solely by the physical limitations of the aircraft because additional energy is available through refueling. However, the same is not true for space-based radars that must be launched to and operated from a great distance in Earth orbit. These systems are not readily accessible and, therefore, the optimum combination of power (solar cells and batteries) and aperture must be considered in the system design phase. The aperture diameter can be increased (easing the power requirement), but not without an adverse affect on the area search rate of the system. For single aperture radar systems, the size of the footprint involves a trade-off between angular resolution and coverage area. A small aperture system provides a broad coverage area while limiting the smallest sized object that can be resolved within this area. On the other hand, a large aperture system provides high resolution but places a very small beam on the ground. Finally, robust computational algorithms can enhance the ability to suppress clutter contributions in the signal reflections received by the radar. All of these options for improving radar performance

from a space-based platform are ultimately subject to stringent size, weight, and cost constraints that allow the realistic implementation of only a partial subset of these improvements.

A novel concept that is only beginning to see serious consideration in space-based radar is the principle of interferometry. Instead of limiting an operational space-based radar system to a single aperture, the more capable alternative is to design a system with an array of sparse apertures that each transmit a pulsed waveform and combine their receiver inputs. The potential benefit of such a system is a significantly enhanced performance capability because the angular resolution is governed not by the diameter of the individual apertures but by the maximum separation distance between them. This means that multiple aperture radar systems can use reasonably sized apertures located on separated spacecraft to achieve superior angular resolution while maintaining a broad coverage area. Also, the signal combination provides an additional gain in the strength of the received signals after processing. This does not mean that sparse aperture radar is without its disadvantages, such as duplicated subsystems, a higher computational burden, and increased overall complexity. To study the technologies associated with distributed satellite systems, the Air Force Research Laboratory initiated a extensive research program called TechSat 21. The basic effects of separated spacecraft interferometry on a space-based radar system that detects ground moving targets are explored as the representative mission.

1.2 The TechSat 21 Concept

In a dramatic departure from current space systems, a new design approach is being explored where clusters of micro-satellites flying in formation and operating cooperatively are used to perform the function of much larger, complex, and expensive single satellites. Each smaller satellite communicates with the others in the cluster and shares the processing, communications, payload, and mission functions. Thus, the cluster forms a "virtual satellite", a revolutionary concept that will eventually lead to new paradigms in space systems [AFRL, 1998]. The TechSat 21 program was created to coordinate a wide
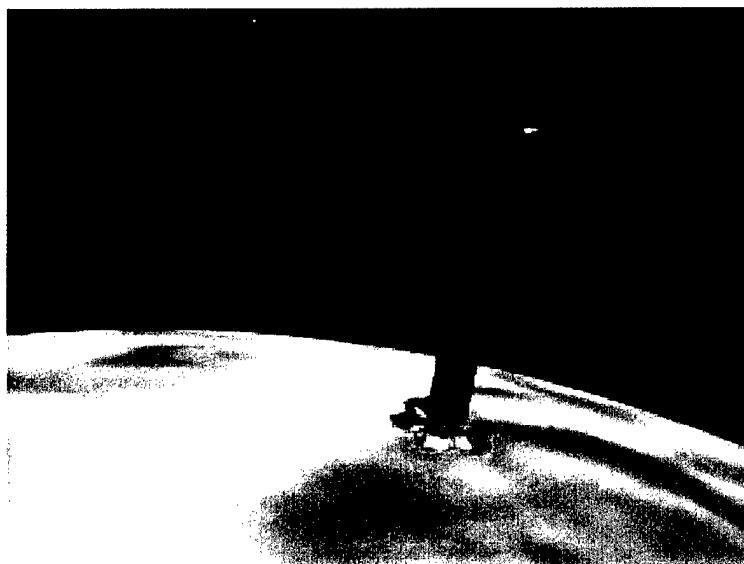
Figure 1.1 Illustration of the Operational TechSat 21 System [AFRL, 1998]

variety of research efforts in this area of distributed satellite systems. Although there are many different application missions for satellite clusters, including surveillance, passive radiometry, terrain mapping, navigation, and communications, the initial reference mission for TechSat 21 is space-based GMTI radar because it stresses many of the operational and hardware technologies required for a distributed satellite system. An artist's impression of the operational TechSat 21 satellite cluster is shown in Figure 1.1. This section briefly explains the TechSat 21 radar system as the representative application of the work presented in this thesis. For more information, please refer to the system factsheet on the internet [AFRL, 1998] as well as the numerous papers on this topic [Das et al, 1998, and Martin et al, 1999].

Proceeding with our discussion on the TechSat 21 radar mission, past space-based radar systems have required very large, high-power satellites to enable target detection in the presence of strong clutter return. At first glance, simply subdividing a satellite into several pieces does not seem to afford any savings since many subsystems are duplicated. However, the benefits of distribution fully justify this penalty, especially for space-based radar applications [Das et al, 1998]:

- Increased adaptability afforded by the ability to spatially reconfigure the cluster adds functionality

- Ability to upgrade a cluster by adding more satellites is made tenable

- The entire cluster capability could correspond to an equivalent single satellite that would be unlaunchable

- The mission survivability is increased because of proliferation of the number of satellites in the cluster

- Increased baseline, or spatial separation, increases the overall performance of the cluster

A satellite cluster offers additional cost savings through economies of scale resulting from the mass production of many identical units, graceful degradation in the event that individual satellites fail, and better use of a launcher's full capacity by being able to launch several satellites at a time. The resulting conceptual design for TechSat 21 consists of a constellation of clusters in low Earth orbit to provide global coverage with minimal revisit times. Each satellite weighs less than 100 kilograms, is deployed on-orbit, and incorporates gravity gradient stabilization.

The operational concept for a cluster of space-based radars still needs to be defined. Although problems such as high grating lobes arise from splitting a single large aperture into many smaller apertures, the improved angular resolution from a sparse array has the potential to overcome these obstacles by producing good spatial resolution on the surface and providing a high level of clutter suppression. In practice, the satellites would receive and process not only the returns from their own transmitters, but also the bistatic responses from the orthogonal transmit signals of every other satellite in the cluster. Since each satellite has a different geometry to the ground, the sparse array provides a wealth of independently sampled angle-of-arrival information in both the elevation and azimuth directions. This permits the simultaneous generation of multiple high resolution, high gain receive beams during post-processing to greatly enhance the performance capabilities of the radar system. The cluster footprint is scanned over a particular region to detect targets of interest. This operational approach is illustrated in Figure 1.2. Future research and
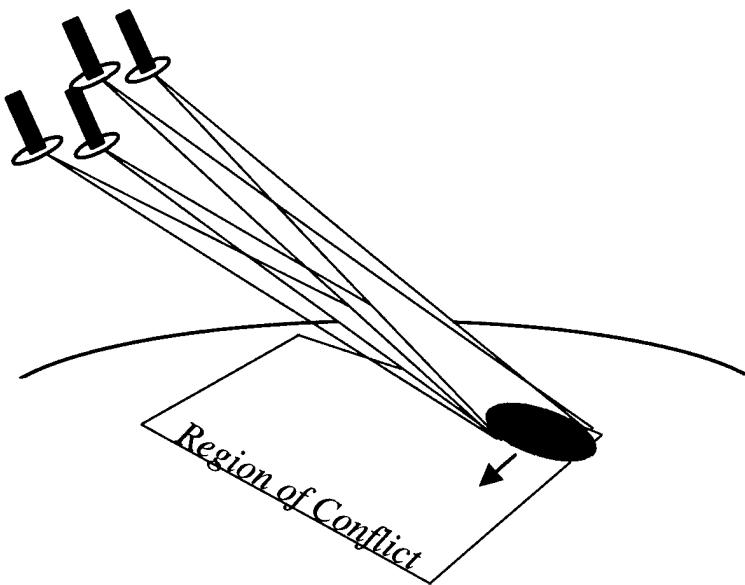
Figure 1.2 TechSat 21 Operations Concept

experimentation will demonstrate the feasibility of operating a space-based GMTI radar system with a cluster of sparse apertures.

The development stages of TechSat 21 have indicated a number of scientific and technological advancements are needed to enable this distributed satellite system concept. These technology challenges include the following [Martin et al, 1999]:

- Signal processing algorithms to enable detection of targets in severe clutter conditions

- Formation flying control strategies to maintain cluster configurations

- Accurate position sensing and actuation with micro-propulsion

- Development of new design tools to allow meaningful performance analysis of satellite clusters

- Validation and application of various microsatellite systems

- Assessment of propagation delay and refraction caused by the ionosphere

The actual satellite design incorporates innovative developments in power generation, multi-functional structures, micro-electro-mechanical systems (MEMS), payload components, and similar advancements in other subsystems. Following this initial research

phase, a significant on-orbit experiment will be conducted with three or four microsatellites to validate critical technologies and capabilities of distributed satellite systems.

1.3 Thesis Objectives

The primary objective of this thesis is to analyze the overall radar performance of candidate TechSat 21 system architectures using quantifiable metrics. This goal can be accomplished by constructing a model that incorporates the various system design parameters to evaluate the target detection and resolution capabilities of the space-based GMTI radar. It is imperative that this model captures the underlying principles of separated spacecraft interferometry applied to space-based radar. The model must also support an in-depth design study to identify viable system configurations for TechSat 21.

In summary, the objectives of this thesis are:

- Develop the fundamentals of space-based radar and separated spacecraft interferometry
- Construct a performance model that captures the physics of the TechSat 21 radar system
- Analyze the radar performance of candidate TechSat 21 system architectures

1.4 Approach and Outline

The development of a radar performance model for TechSat 21 is the overall theme of this thesis. The first step in this process is to explain the underlying principles of radar operation in the space environment that form the foundation of the model. In Chapter 2, the fundamentals of space-based radar are explained. Beginning with the basic detection and location concepts of radar, the general properties common to nearly all types of radar are specified by the transmitter settings, the antenna beam, and the pulsed signal. These parameters determine the range and Doppler measurement methods for the system. Target detection is a function of the signal strength reflected by targets and is limited by numerous sources of interference from noise and clutter.

Building on the basics from Chapter 2, Chapter 3 focuses on the wide range of issues raised by separated spacecraft interferometry in space-based radar. Interferometry can significantly improve the performance of a space-based radar system by providing both increased sensitivity and fine angular resolution. Operating in a cluster of sparse apertures, such a system must maintain sufficient spatial separation between the individual apertures. This allows the synthesis of a large aperture based on the maximum separation distance between the individual satellites. The adverse contribution of clutter in the received radar signals is removed with highly capable signal processing algorithms.

Following the extensive background in Chapters 2 and 3, the development of a comprehensive model to analyze the radar system performance of candidate TechSat 21 architectures is discussed in Chapter 4. The systems analysis methodology that serves as the framework for this model focuses on a defined set of capability metrics to evaluate the overall performance. The performance within a footprint can provide useful insight, but the viability of various system architectures can only be evaluated by modeling the performance at the complete system coverage area level.

Finally, the key results from a representative TechSat 21 design study are presented in Chapter 5. Based on the nature of the various system parameters that define the probability of detection from the power in the target signal, a design study is developed to yield system architectures that satisfy minimum performance requirements. The results specify minimum values for the product of the transmission power and the square of the number of satellites in the cluster for a range of aperture diameters. The chosen architecture involves additional cost, reliability, and performance considerations beyond the scope of the radar system analysis.

Chapter 2

FUNDAMENTALS OF SPACE-BASED RADAR

Before we can analyze the performance of a space-based radar system, we must first acquire an appreciation of the underlying physics of radar. In modern times, there are seemingly limitless applications for airborne and space-based radar, from reconnaissance to navigation to ground mapping and many others. The primary focus of this chapter is the detection of moving targets, or moving target indication (MTI) radar, but the vast majority of the principles presented in each section are also relevant in most other radar applications. Airborne and space-based radar systems are similar in many ways, so the majority of this chapter is based on the comprehensive background provided in the *Introduction to Airborne Radar* [Stimson, 1998]. When appropriate, meaningful differences between airborne and space-based radar are noted. Other useful resources on this topic are provided by Barton, 1988, Cantafio, 1989, Mahafza, 1998, and Skolnik, 1990. Section 2.1 begins the chapter by presenting the basic concepts that are fundamental to all radar applications. An explanation of the function of each device in a typical radar system is given in Section 2.2. The physical properties of the transmitted radar signal are illustrated in Section 2.3 followed by an introduction to the basic methods used to measure target parameters in Section 2.4. Finally, Sections 2.5 and 2.6 focus on the interference sources that airborne and space-based radars encounter and the methods used to reduce their overall impact. It is assumed that the reader has a reasonable familiarity with the elementary principles of electromagnetic waves, so a brief review in this area may be helpful if this is not the case. The goal of this chapter is to gain an understanding of the fundamental con-

cepts of radar because they form the foundation for the remainder of the work presented in this thesis.

2.1 Basic Radar Concepts

Even though we have many highly specialized and incredibly complex radar systems in existence today, there are a few simple characteristics that form the overall foundation for every one of them. First, the radar system must be able to detect the presence of a desired object in the signals that it receives. Once a target is detected, the next meaningful piece of information is its location with respect to the radar. The last step is to determine the relative speed (range rate) of the target by exploiting the Doppler effect in the received signals. Often, the implementation of these concepts varies from system to system, but a basic knowledge of their general function in radar is essential.

2.1.1 Target Detection

The vast capabilities of modern radar systems are rooted in one fundamental premise: detecting the presence of objects based on the signals they reflect. Therefore, it is natural to begin a discussion of radar by determining how an object or target is detected in received radar signals.

Nearly all objects reflect radio waves, much as they do light. The reason for using radio frequencies instead of light in radar is the ability of this form of electromagnetic radiation to illuminate objects day or night as well as travel with little or no attenuation through the atmosphere. Still, radio waves cannot penetrate solid objects, so targets must be within the line of sight of the radar if they are to be detected. To find a target, the transmitted energy from the radar (antenna beam) is scanned through the region where the targets are most likely to appear, and the reflected signal energy is processed to determine if any targets are located in the search area.

The most rudimentary form of a radar system includes a transmitter, a receiver, an antenna, and some sort of display for the user. The transmitter provides the signal to the antenna that is radiated throughout the medium surrounding the radar. Any signals that are reflected back towards the radar are gathered again by the antenna and fed to the receiver. The receiver determines if the reflected signals were caused by extraneous sources (external noise, ground clutter, etc.), or if there is in fact a target echo imbedded in the signals. If any desired targets are detected, this information is passed to the display to indicate these detections to the user.

One significant limiting factor that is common to all radar systems is the presence of interfering sources that contribute unwanted return in the received signals. The reflections from targets must compete with all noise sources in the transmission medium as well as signals from unwanted reflectors. The radar system must contend with these forms of interference to enable detection of target signals. In addition, the strength of the transmitted signals is diminished by a factor of $1/R^2$ as they propagate towards the target, where R represents the distance to a target. The signal power reflected by a target back towards the radar is also reduced by the same factor. Therefore, the power density of the received signals is inversely proportional to the target's range to the fourth power. Although the maximum range to which a radar can detect targets is influenced by many factors, the most important are the following:

- Antenna transmission power
- Antenna aperture size
- Transmission duty cycle
- Reflecting characteristics of the target
- Length of time the target is illuminated by the antenna beam
- Number of search scans in which the target appears
- Wavelength of the transmitted signals
- Strength of all interference sources

The mere presence of a target is normally of very little importance. Not only does the user need to know that a target of interest has been detected, but other information about the target such as its location and its relative speed is also extremely useful in airborne and space-based applications.

2.1.2 Determining Target Position

Once a target is detected, the next step is to pinpoint the precise location of a target. This positioning provides the user with the distance (range) to the target and its direction.

Range. The distance to a target is determined by measuring the round-trip transit time of the signals between the radar and the target. Since the radio waves travel at the speed of light (in most situations), the target range is simply one-half the product of the speed of light and the round-trip transit time (Δt), as shown in equation 2.1.

$$R = \frac{c\Delta t}{2} \tag{2.1}$$

It is often desirable to limit the width of the transmitted pulse to ensure that the returns from closely spaced reflectors do not overlap. This range resolution defines the spatial width of the bins used to measure range in the reflected signals (Section 2.4.1). In certain instances, measuring the range to a target may not be as simple as this, such as when a received signal arrives after the transmission of the following signal, but this issue will be addressed at a later time (Section 2.4.3).

Direction. For most radars, the direction to a target is measured in terms of the angle between the line of sight to the target and some reference coordinate system. Most of the time, this angle is divided into its horizontal (azimuth) and vertical (elevation) components and are measured based on the direction where the antenna is pointed. In space-based radar, the azimuth angle is measured from the velocity vector of the satellite while the elevation angle is measured from the nadir direction (Figure 2.1). Also, a parameter known as the grazing angle (ψ) is often substituted for the elevation angle because it
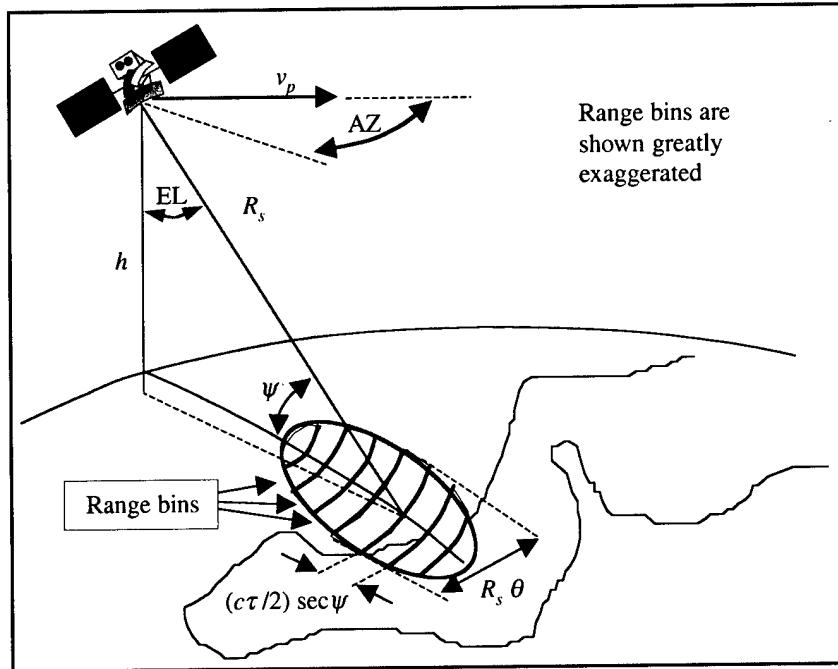
Figure 2.1 Geometry for a Space-Based Radar System [Shaw, 1998]

accounts for the curvature of the Earth in the patch of ground illuminated by the radar. The precision to which these angles can be measured is a function of the beamwidth of the antenna (Section 2.3.2). This concept is known as angular resolution and is a very important measure of the overall capability of the radar system.

By knowing the range and direction of a target, a radar system can use this information to track the target location as needed. Even though the location of a target is a particularly important piece of information to the radar user, the frequency content of the received signals can also be exploited to determine the speed of detected targets relative to the radar system.

2.1.3 The Doppler Effect

The Doppler effect refers to the shift in radio frequency between the signals transmitted by the radar and those reflected by a target. It is a very common occurrence that is used to

understand the relative motion of objects in everything from the change in pitch of a car's engine as it races by to the motion of galaxies in the universe. In radar systems, this phenomenon is caused by the relative motion of the target to the radar platform. As shown in equation 2.2, a target that is moving towards the radar (positive v_T) causes an increase in the frequency of the reflected signals [Mahafza, 1998].

$$f_r = f_c \frac{c + v_T}{c - v_T} \tag{2.2}$$

These signals are said to be "blue-shifted" since the color blue in the visual spectrum has the highest frequency. The opposite is true for targets moving away from the radar (negative v_T), causing a "red-shift" in the reflected signals.

Because of the Doppler effect, a radar can measure the rate of change of the target direction (range rate) based on the frequency (Doppler) shift in the received signals. Doppler shift is defined as the difference between the transmitted and received frequencies and depends on the relative motion of the target and the transmission wavelength.

$$f_D = \frac{2v_T}{\lambda} \tag{2.3}$$

Equation 2.3 is a simplified form of equation 2.2 due to the fact that the traveling speed of the radar waves is orders of magnitude greater than the velocity of any target. The difficulty with exploiting the Doppler effect in radar is that the motion of the target represents only a miniscule fraction of this propagation speed. Therefore, the Doppler shift caused by this motion is distinguishable only as a pulse-to-pulse shift in the radio frequency phase of the target echoes. This means that a radar system can measure the Doppler shift of a target only if it has a sufficient number of successive echoes from the target where the phase of each echo is the same. In addition to range rate, the availability of frequency measurements also allows the radar to separate target signals from competing clutter on the basis of their respective Doppler shifts. In the absence of this information, the targets would almost always be lost in the presence of these much stronger interfering sources.

2.2 Generic Radar System

Now that we have an understanding of the basic concepts common to nearly all airborne and space-based radar systems, our next step is to look at the devices that are used to make these radars work. Although the design of radar systems is strongly dependent on their intended applications, most contain the elements represented in the block diagram in Figure 2.2. The following paragraphs explain the role and the function of each device in the operation of a generic radar system.

Synchronizer. The role of the this unit is to send a stream of very short, evenly spaced timing pulses to the transmitter and the receiver in order to synchronize these devices. The pulses are used to switch the transmitter on and off and to provide timing information to the receiver.

Modulator. The modulator produces a high power dc pulse to the transmitter upon receipt of each pulse from the synchronizer. Often, the modulator and the synchronizer are combined into a single element known as an exciter that generates the signal for transmission and signal processing.

Transmitter. This device is basically an oscillator (usually a magnetron) that generates high-power radio frequency waves as the dc pulses are received from the modulator. The frequency of the waves can range anywhere from a few megahertz to hundreds of terahertz depending on the system application, but most of the time the frequencies lie in the few hundred megahertz to few hundred gigahertz range. The waves are radiated into a series of waveguides which propagates them to the duplexer.

Duplexer. This unit physically connects the transmitter and the receiver to the antenna. Because it is sensitive to the direction of flow of the radio waves, the duplexer essentially acts as a waveguide switch that allows the waves from the transmitter to pass through with negligible attenuation while blocking their flow to the receiver, or vice versa.
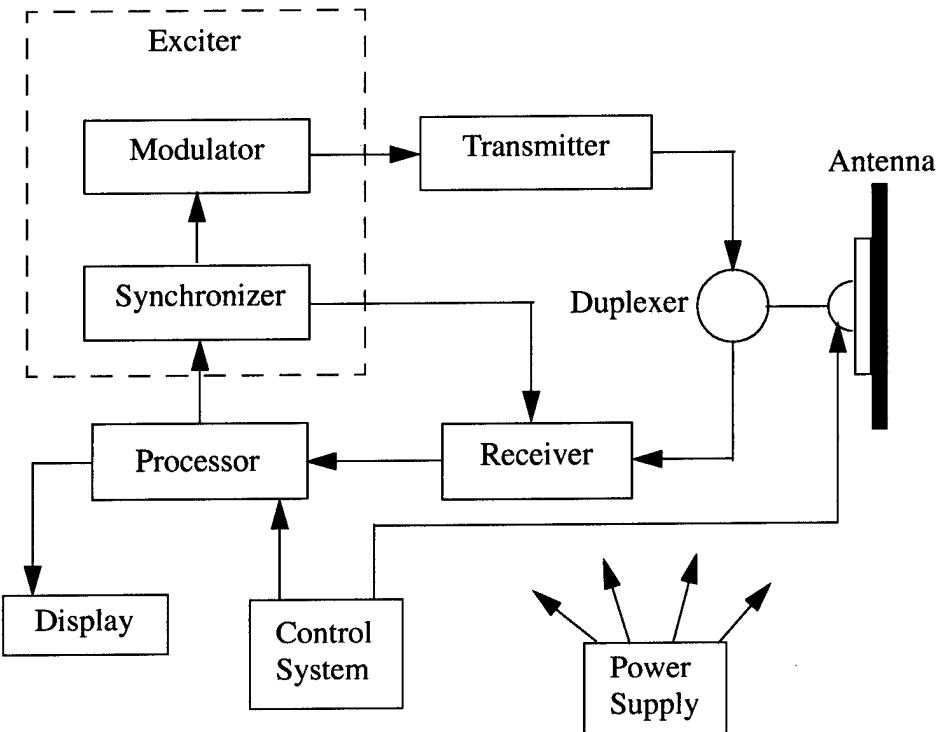
Figure 2.2 Common Elements of a Radar System

Antenna. The antenna generally consists of a radiator and a parabolically shaped reflector dish mounted on a common support. In its most simple form, the radiator is a horn-shaped nozzle at the end of the waveguide connected to the duplexer. It either directs the waves coming from the transmitter onto the dish and reflects them into the medium, or it intercepts waves gathered by the dish and conveys them to the receiver via the duplexer. Often, the antenna is mounted on a set of gimbals that allow it to be rotated about both elevation and azimuth axes. Another alternative is to employ a reflector that consists of an array of many individual radiators, each with its own waveguide, distributed over the surface. The waves transmitted from such an antenna can be electronically steered by applying a series of phase delays to the radiators. It is important to note that the design of the antenna for a radar system can be one of the most difficult tasks because the antenna dictates so many aspects of the overall system operation and performance. Many antenna

designs vary significantly from the example given here, but the purpose is to give a general understanding of the function of the antenna in a radar system.

Receiver. Typically, this device consists of a receiver protector device, a local oscillator, a mixer, an IF amplifier, and either an envelope or a synchronous detector. Due to the fact that some of the energy in the transmitted signal is invariably reflected back from the antenna, the role of the receiver protector device is to keep these signals from entering the receiver and causing significant damage. The device automatically blocks any signals that are strong enough to damage the receiver and passes everything else. The desired incoming waves are "beat" against the output of the local oscillator through the mixer to lower, or heterodyne down, their carrier frequency. This is known as the intermediate frequency (IF) and is used to allow a single operating frequency for the amplifier, thereby improving its efficiency. Next, the IF amplifier acts as a tuned circuit that not only amplifies the output from the mixer, but also filters out any interfering signals that lie outside the band of frequencies occupied by the received signals. Finally, the signals are passed through a detector that measures their maximum amplitude (envelope) or identifies the amplitude and Doppler frequency of each pulse if that information is available (synchronous).

Processor. The processor is the most important device in the radar system because this is where the usable information is extracted from the received signals. Based on the current operating mode of the radar, the processor first sorts the signals from the receiver into a series of range increments known as range bins. It then filters out unwanted clutter based on its Doppler frequency by forming a bank of narrowband filters for each range bin. These filters are used to integrate the energy from successive echoes of the same target so that the level of competing noise can be reduced. Once this stage of the process is complete, the signal amplitudes are measured (magnitude detection) and a target detection threshold voltage is set. All signal amplitudes that exceed this threshold are counted as targets and displayed to the user. The processor also monitors all operations of the radar system and provides fault-detection capability to the user in the event of a component malfunction. There are many additional operations that are performed by the processor to

enhance the strength of the target signal in the presence of interference and to accommodate different modes of operation. However, the simplified steps listed here are common to most types of radar.

Power Supply. This element converts the power from the spacecraft's primary power source to the various dc forms required by the radar system. The primary power is transformed to the required voltages, converted to dc, smoothed, and regulated to keep the resulting power level constant in the face of voltage and current fluctuations in the primary source.

Control System. Basically, the control system translates inputs from the user to the various components of the radar system. This may mean steering the antenna to a new location, selecting a different transmission or pulse repetition frequency, changing the waveform of the transmitted signals, switching between various operating modes (i.e. target search to automatic tracking), etc. A radar system is designed based on an intended application, but it must be able to adapt to a wide range of operating conditions to provide a sufficient level of performance.

2.3 Radar System Properties

Before the actual devices used in a radar system can be selected, the system engineer must first account for certain factors that significantly affect the overall design of the radar. For example, the intended use of the radar system and the environment in which it operates dictate the chosen transmission frequency and waveform. Furthermore, the characteristics of the antenna beam govern the radar's ability to detect targets and determine their positions with precision. Since most airborne and space-based radars transmit some form of a pulsed signal, the parameters of this type of signal strongly impact the makeup of the signals reflected by targets. These general properties of the radar system are crucial to both the operation and the performance of any radar system, meaning that each must be carefully addressed when trading between different aspects of the radar design.

2.3.1 Frequency and Waveform Selection

The primary consideration in the initial design of a radar system involves the selection of the transmitted wave characteristics. The first step is to select the radar's operating frequency. The system requirements play a significant role in this determination because the overall capabilities of the radar, such as detection range, angular resolution, and Doppler performance, are heavily influenced by the chosen transmission frequency. The waveform of the transmitted signal is also an important concern in radar because the design and operation of many of the individual devices in the system are based on the chosen waveform. Both the frequency and the waveform of the transmitted signal affect the size, weight, and cost of the radar system as well as its overall performance.

Frequency

Modern radars operate at a wide range of frequencies depending on the system application and the operational requirements. As a matter of convenience, the radio frequency spectrum is arbitrarily divided into several bands with specified frequency ranges. Furthermore, frequencies that fall in the microwave region (1-40 GHz) are subdivided into even narrower bands. These frequency bands are listed in Table 2.1. Most of today's radars fall in the VHF, UHF, microwave, and millimeter-wave regions.

The choice of radio frequency (or wavelength) has a significant impact on many other elements in the radar system. First of all, the physical dimensions of the hardware used to generate the transmitted waves at the specified frequency are proportional to wavelength. While lower frequencies (longer wavelengths) require large and bulky transmission hardware, higher frequencies (shorter wavelengths) allow a reduction in the overall size and weight of the system. The level of power that can be transmitted by the radar is also influenced by wavelength. In general, radars operating at longer wavelengths can transmit comparatively more average power that those at shorter wavelengths, although other system considerations such as weight, cost, and reliability tend to place stricter limits on power availability. In addition, the wavelength of the transmitted signal defines the

TABLE 2.1   Radar Band Designations [Skolnik, 1980]

Band	Frequency	Wavelength
HF	3-30 MHz	100-10 m
VHF	30-300 MHz	10-1 m
UHF	300-1000 MHz	1-0.3 m
L	1-2 GHz	30-15 cm
S	2-4 GHz	15-7.5 cm
C	4-8 GHz	7.5-3.75 cm
X	8-12 GHz	3.75-2.5 cm
Ku	12-18 GHz	2.5-1.67 cm
K	18-27 GHz	17-11 mm
Ka	27-40 GHz	11-7.5 mm
mm	40-300 GHz	7.5-1 mm

antenna beamwidth as well as the level of atmospheric attenuation and ambient noise. Finally, the amount of Doppler shift in the received signals is dictated by the chosen radio frequency. These factors weigh differently in basic radar design based on the system requirements and constraints. As a rule of thumb, most airborne and space-based radars operate at microwave frequencies due mostly to limitations on size and weight. It is worth mentioning that the X-band (10 GHz) region is very attractive for these systems because the atmospheric attenuation is relatively low, the narrow beamwidth provides superior angular resolution with reasonably small antennas, and the radar components are widely available from commercial industry.

Waveform

Once the frequency is selected, the next decision in the radar design involves the choice of the transmission waveform. If the radar transmits radio waves continuously while simultaneously listening for reflected echoes, this is known as continuous wave (CW) transmission [Mahafza, 1998]. The spectra of the received signals in these radars is concentrated around the transmission frequency shifted by the Doppler shifts of any moving targets in the returns. Consequently, CW radars can very accurately measure target range rates.

Range measurement, however, is generally not possible without some sort of modification to the transmitted waveform (FM ranging in Section 2.4.1). CW radars require separate antennas for the transmitter and the receiver since the transmitter is continuously sending out a signal. This means that CW transmission tends to be popular in ground-based and shipboard applications where there are fewer limitations on the physical dimensions of the radar system.

The other type of transmitted waveform in radar is a pulsed signal. These radars transmit their signals intermittently in short pulses and listen for echoes in the periods between pulses. Because space and weight limitations often allow for only a single antenna in airborne and space-based radar systems, pulsed operation is most often chosen for these radars to avoid transmitter interference with the receiver and to simplify range measurement. Therefore, the remaining sections in this chapter will assume that the transmitted waveform is pulsed. There is such a wide range of issues raised by pulsed transmission in radar that an entire subsection (Section 2.3.3) is devoted to the properties of these signals.

Ultimately, the system application and requirements must be carefully evaluated when selecting the best transmission frequency and waveform for a radar. The magnitude of this decision is evident in the overall impact these properties have on both the operation and performance of the radar as well as the physical dimensions of the system. Along with these features of the transmitted signal, the properties of the antenna beam must also be considered when analyzing radar system performance.

2.3.2 Antenna Beam Characteristics

Now that we understand the relationship between the transmission frequency and waveform of a radar and the physical dimensions and performance capabilities of the system, it is necessary that we gain a similar appreciation of the physical attributes of the antenna beam. The chief role of the antenna is to concentrate the energy radiated by the radar in a desired direction. This directivity of the antenna beam significantly impacts the overall capabilities of the radar system. Figure 2.3 illustrates the typical distribution of energy for

Figure 2.3 Radiated Energy Distribution in an Antenna Beam [Stimson, 1998]

an antenna "pencil" beam. While most of the radiated energy is concentrated in a conical region around the central axis, or boresight line, of the antenna, a substantial fraction is also radiated in nearly every direction. This radiation pattern is caused by diffraction, but a detailed explanation of this phenomenon is not required for a general understanding of the antenna beam properties. The important consequence here is the resulting lobe structure of the antenna beam, as shown in Figure 2.4. For a square aperture, this field strength (in volts) of the antenna beam is primarily a function of the angular distance from the boresight line according to equation 2.4

$$E = k \frac{\sin\left(\frac{\pi L}{\lambda} \sin\theta\right)}{\frac{\pi L}{\lambda} \sin\theta} \tag{2.4}$$

where L refers to the aperture length and λ is the transmission wavelength. The second term in this equation is known as a *sinc* (sin x/x) function and is a very fundamental relationship in radar. Often, the power of the radiated waves is the parameter of interest and can be found by squaring the field strength from equation 2.4, giving a *sinc*^{2} distribution. In general, signals that pass through the mainlobe represent desired returns while sidelobe signals are considered a form of unwanted interference.

Many meaningful capabilities of the radar can be ascertained from the radiation pattern of the antenna beam. For instance, the width of the mainlobe, known as the antenna beamwidth, defines the minimum separation distance of targets that can be resolved by the radar. This is known as the angular resolution and is proportional to the ratio of the transmission wavelength and the aperture length (equation 2.5) for a square aperture.

E(sinθ)

sinθ
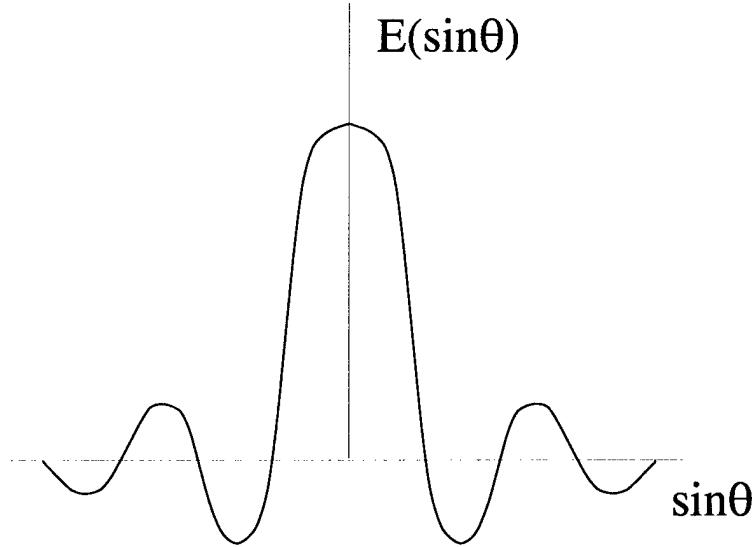
Figure 2.4 Lobe Structure of the Antenna Beam

$$\Delta\theta = 2\frac{\lambda}{L} \tag{2.5}$$

The radiation pattern also illustrates the ratio of the power per unit of solid angle radiated by the antenna. This is known as the gain of the antenna (receive gain), and it directly impacts the amount of power that is reflected back to the radar. The gain is calculated in equation 2.6 as a function of the effective receiving area of the antenna aperture (A_e).

$$G = \frac{4\pi}{\lambda^2}A_e \tag{2.6}$$

Finally, the sidelobe level is important to consider because not only does it represent power lost from the mainlobe, but sidelobes can also produce considerable return that interferes with the mainlobe signal. The sidelobes can be reduced by weighting the transmitted signal, but this comes at the cost of an increase in the antenna beamwidth. It is easy to see that the radiation pattern of the antenna is a strong representation of the performance capability of any radar system.

Another effect of the antenna radiation pattern that is found in all space-based radars is caused by the intersection of the mainlobe with the ground. This ground area illuminated by the radar is called the radar footprint (refer to Figure 2.1), and it represents the current area that the radar is scanning. The shape of the footprint is elliptical and elongates as the signal moves closer to the observable horizon due to distortions caused by the curvature of the Earth. The "toe" is the location in the footprint that is the greatest distance from the radar while the "heel" is the closest. Anything inside the footprint, including desired returns from targets and unwanted returns from miscellaneous objects (clutter), contributes to the overall strength of the reflected signals. This means that space-based radars must be able to suppress these clutter returns to enable detection of much weaker target signals. The consequences of dealing with clutter are major issues in space-based radar and will be addressed in greater detail in a later section (Section 2.6).

The main lesson here is to understand how the properties of the antenna beam affect the operation and the performance of the radar. Most of the information we get from the antenna is contained in the radiation pattern of the transmitted beam. In the end, the antenna design involves a trade between the desired gain and angular resolution of the radar and the actual physical dimensions of the antenna. To complete our discussion of the basic properties of a radar system, we now continue with an explanation of the characteristics of the pulsed waveform and the overall effects of this type of transmission.

2.3.3 Pulsed Signal Properties

As previously stated, most airborne and space-based radars utilize pulsed transmission waveforms to allow the use of a single antenna in the system. A discussion of the operation of a pulsed radar will be saved for a future section (Section 2.4), but first we need to understand the relationship between the physical parameters of the pulsed signal and the performance characteristics of the radar system.

The pulsed waveform, illustrated in Figure 2.5, has four basic characteristics: carrier (transmission) frequency, pulse width, pulse modulation, and pulse repetition frequency.
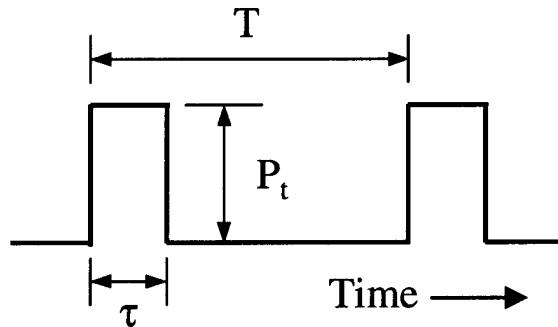
Figure 2.5 Parameters of a Pulsed Waveform

The carrier frequency is selected as described previously (Section 2.3.1), but it can be changed from pulse to pulse or even within pulses. The pulse width is the duration of the each pulse, which defines the range resolution of the radar (Section 2.4.1) and influences the overall strength of the received signals (Section 2.5.2). Pulse modulation refers to the frequency coding of successive increments of each pulse and is used to improve the detection range and range resolution in a technique known as pulse compression (Section 2.5.3). Finally, the pulse repetition frequency is the rate at which the radar's pulses are transmitted. The inverse of the PRF, known as the interpulse period, gives the time between transmitted pulses. Often, the PRF can be adjusted by the user, and this parameter has a considerable impact on the ability of the radar to measure the range and range rate of a target with accuracy (Section 2.4.3).

The pulsed waveform also contains information on the output power and the transmitted energy of the radar. The peak or transmission power is given by the amplitude of each pulse in the waveform, and the energy per pulse is simply the product of the peak power and the pulse width (equation 2.7). The average power refers to the product of the peak power and the transmission duty cycle, which is defined as the ratio of the pulse width to the interpulse period (equation 2.8).

$$E = P_t \cdot \tau \qquad\qquad (2.7)$$

$$P_{avg} = P_t \cdot DC = P_t \cdot \frac{\tau}{T} \qquad (2.8)$$

To maximize the detection range of a radar system, the average power can be boosted by increasing the transmission power, the pulse width, or the PRF.

Up to this point, this discussion of pulsed waveforms has focused on their time domain representation. However, many additional properties of the pulsed signal are best described by looking at its radio frequency spectrum. Figure 2.6 illustrates the spectrum of a standard square-pulse signal. The envelope represents the spectrum that would result from a single pulse. The spectrum is centered on the carrier frequency of the pulsed wave-
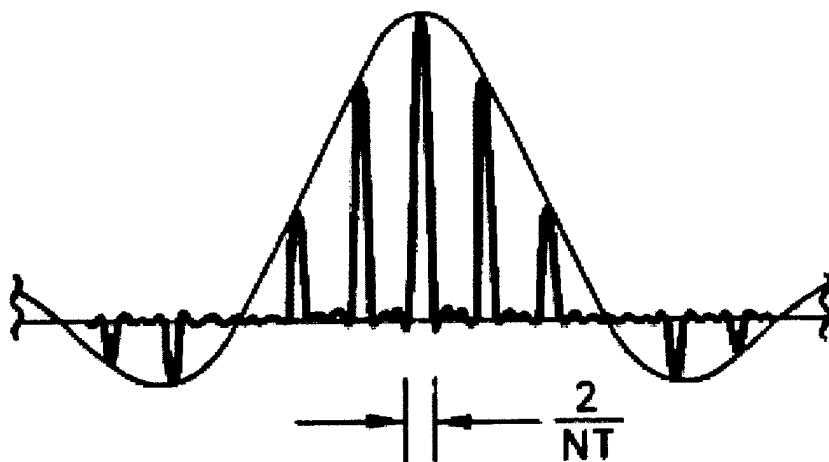
Figure 2.6 Pulsed Signal Spectrum [Stimson, 1998]

form and has a *sinc* shape with a series of sidebands, similar to the radiation pattern of the antenna. The null-to-null bandwidth of this envelope is calculated from equation 2.9 as a function of the pulse width.

$$BW = \frac{2}{\tau} \qquad (2.9)$$

The spectral lines in Figure 2.6, repeated at periods equal to the pulse repetition frequency, are caused by combining a series of coherent pulses. Coherence refers to the continuity of a signal's phase from pulse to pulse, and it allows the radar to integrate pulses. Pulse integration (coherent) leads to an improvement in the frequency resolution of the radar by narrowing the width of the spectral lines. This line width corresponds to the PRF and the total number of pulses integrated (n_c) as shown in equation 2.10.

$$LW = \frac{2}{n_c} PRF \tag{2.10}$$

Coherent integration will be discussed in greater detail at a later time (Section 2.5.4), but suffice it to say that any hope of detecting targets from space-based radars would be impossible without it.

2.4 Evaluation of Target Parameters

After reviewing the properties of the transmitted signal, the antenna beam, and the pulsed waveform and assessing their impact on the performance capability of a radar system, we proceed at this point with a discussion concerning the methods used to find the range and range rate of a target. Figure 2.7 illustrates the steps followed to measure this information in the radar processor. As described in Section 2.1.2, the distance to a target is primarily determined by the round-trip travel time of the transmitted signal reflected by a target. Various range measurement techniques have been developed to maximize the detection range of airborne and space-based radars. Once the range is known, the relative motion of a target to the radar is calculated by sensing the Doppler shift of the target echo (Section 2.1.3). This is accomplished by examining the spectrum of the reflected signals. After the range and Doppler measurement, the signal is further processed to determine if a target echo is present. Unfortunately, there is often a certain level of ambiguity associated with the range and range rate of a target that must be corrected to ensure accurate values for these parameters. The techniques used to measure the range and Doppler information

```
                          │
                          ▼
                 ┌─────────────────┐
                 │   IF Amplifier  │
                 └─────────────────┘
                          │
        ┌────────┬────┬───┼───┬────┬──────────┐
        ▼        ▼    ▼   ▼   ▼    ▼          ▼
  ┌──────────┐                          ┌──────────┐
  │  Range   │   ┊   ┊   ┊   ┊          │  Range   │
  │  Bin 1   │                          │  Bin n   │
  └──────────┘   ┊   ┊   ┊   ┊          └──────────┘
        │                                     │
        ▼        ┊   ┊   ┊   ┊                ▼
  ┌──────────┐                          ┌──────────┐
  │ Doppler  │                          │ Doppler  │
  │ Filters  │                          │ Filters  │
  └──────────┘                          └──────────┘
        │                                     │
        ▼                                     ▼
  ┌──────────┐                          ┌──────────┐
  │Magnitude │                          │Magnitude │
  │Detectors │                          │Detectors │
  └──────────┘                          └──────────┘
        │                                     │
        ▼                                     ▼
   ╭──────────────────────────────────────────────╮
   │            Threshold Detection               │
   ╰──────────────────────────────────────────────╯
```
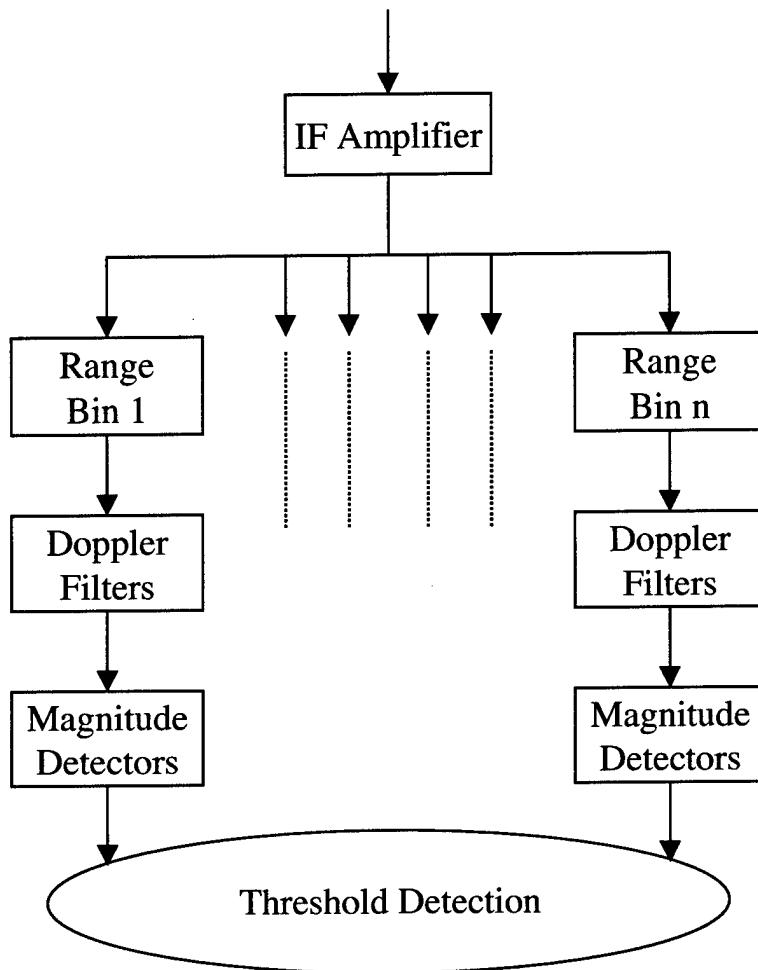
Figure 2.7   Block Diagram for Radar Signal Processing

in received signals are significant drivers in the operation and performance of nearly all airborne and space-based radar systems.

2.4.1 Range Measurement

Because it is simple and can be extremely accurate, the technique used by most airborne and space-based radars to measure the range to a target is pulse delay ranging. A transmitted pulse reflected by a target is passed through the receiver and on to a single range gate that periodically samples the amplitude (voltage) of the signal. Each sample is stored in a unique position in the radar processor known as a range bin. The size of these range bins,

which is proportional to the width of the transmitted pulse, defines the smallest range increment that can be resolved by the radar. In space-based radar, this range resolution, given in equation 2.11, also depends on the elongation of the footprint caused by the curvature of the Earth (Section 2.3.2).

$$\Delta R = \frac{c\tau}{2}\sec\psi \qquad (2.11)$$

This last point raises a key distinction between airborne and space-based radars. Airborne radars have a maximum range of interest that refers to the longest range from which target echoes are expected to be received. In certain cases, a target at a range greater than this maximum range may have a large enough cross section to cause a detection in the radar. The range to this target cannot be accurately determined in this situation, thereby causing an ambiguity in the range measurement. While space-based radars can also suffer from range ambiguities, the signals transmitted by these systems reach their maximum range when they come into contact with the ground. The nature of these ambiguous range measurements will be covered in Section 2.4.3, but the point here is that the different operating environments for these systems lead to unique explanations of the source of these ambiguities.

Another alternative for range measurement in radar is to vary the frequency of the transmitted pulses, thereby converting the time lag between transmission and reception to a frequency difference. This method is known as frequency modulation (FM) ranging and is most often used in radars that transmit CW or very high PRF waveforms. In simplest form, the frequency of the transmitter is linearly increased over a series of pulses. The radar measures the instantaneous difference between the frequencies of the received echoes and the transmitter, and calculates the round-trip transit time (t_r) of the signal by dividing this frequency difference (δf) with the rate of change (K) of the transmission frequency as shown in equation 2.12.

$$t_r = \frac{\delta f}{K} \qquad (2.12)$$

The Doppler shift of a moving target changes the frequency difference measured by the radar. To remedy this problem and still be able to detect a target's Doppler shift, the transmitter frequency is held constant for a brief moment during the modulation cycle. During this constant frequency segment, the measure frequency difference between the transmitted and received signal is caused solely by the Doppler shift of the target. In practice, FM ranging is limited by the frequency measurement accuracy of the radar and the number of individual target returns that can be resolved, which is why most airborne and space-based radars use some form of pulse delay ranging.

The range measurement capability of a radar system is a very important consideration in nearly all radar applications. This information, along with the direction in which the antenna is pointed when a target echo is received, allows the radar to determine the precise location of the target. Once the range is known, the frequency content of the received signals is used to calculate the relative speed of detected targets.

2.4.2 Sensing Doppler Frequencies

Doppler information is vital in nearly all airborne and space-based radar applications for two main reasons: the ability to separate returns received simultaneously from multiple objects while also determining range rates. This family of radars is commonly referred to as pulse-Doppler radars. The process used to measure these Doppler frequencies begins by forming a bank of narrow bandpass filters for each range increment (bin) that cover the spread of frequencies in the received signals. Starting at the low end of the frequency range, each filter is tuned to a progressively higher frequency. Ideally, these filters would produce an output only when a frequency in the received signal falls within its band. However, filter sidelobes may produce some output for signals whose carrier frequencies actually lie outside the band. The filters are made to overlap somewhat which helps prevent signal loss when a frequency in the signal falls on the border between the passbands of two adjacent filters.

The two main characteristics of the Doppler filter bank are the bandwidth of each filter and the passband of the entire bank. As stated before (Section 2.3.3), the frequency resolution of a radar is increased with the number of coherently integrated pulses. This means that the frequency width of each Doppler filter then is approximately equal to the inverse of the total coherent dwell time (equation 2.13).

$$\Delta f = \frac{1}{t_d} \tag{2.13}$$

The passband of the filter bank is a function of the pulse repetition frequency and the spread between the maximum positive and negative Doppler frequencies for all significant targets. If the PRF exceeds this spread, then the passband of the Doppler bank should be large enough to encompass this range of frequencies. However, the passband of the filter should not exceed the PRF when it is less than the anticipated spread in Doppler frequencies. In this situation, the received signals contain Doppler ambiguities that are explained in greater detail in the next subsection.

2.4.3 Range and Doppler Ambiguities

The range and Doppler measurement techniques presented in the last two subsections can individually provide highly accurate information to pinpoint the location and relative motion of a target. Unfortunately, it is impossible to have both at the same time due to the large extent of the footprints projected by airborne and space-based radars. Depending on the chosen pulse repetition frequency, ambiguities exist in either the range or Doppler measurements or both. Table 2.2 indicates the relationship between the transmitted PRF and the types of ambiguities that result in the received radar signals. Depending on the

TABLE 2.2 Resulting Ambiguities from PRF Selection

PRF	Range	Doppler
Low	No	Yes
Medium	Yes	Yes
High	Yes	No

system application, the PRF is selected based on the measurement that has the least toler-ance to ambiguity. There are various methods available that can be used to resolve ambig-uous return, but first we need to understand how these ambiguities are formed and the effect they have on range and Doppler measurement.

Range Ambiguities

As long as the reflection of an entire pulse is received by the radar before the transmission of the next pulse, the target range can be easily calculated from the round-trip transit time of the pulse. However, the range becomes ambiguous when the system cannot determine if a received echo is the reflection from a nearby target of the pulse most recently transmit-ted, or if the echo actually originated from a pulse transmitted earlier and subsequently reflected from a more distant target. In space-based radar, range ambiguities occur when multiple pulse reflections from different ranges are received by the radar at the same time as illustrated in Figure 2.8. This figure also shows that the returns from certain ranges are
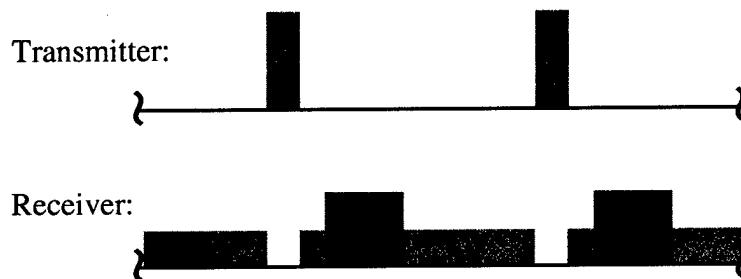
Figure 2.8 Range Ambiguities in Received Signals

blanked out if the complete reflection from a single pulse does not arrive at the antenna before the next pulse transmission. If the radar does not have the capacity to resolve these range ambiguities, the returns from multiple ranges cannot be separated and the measured range is meaningless.

In most space-based radar applications, precise range measurement is a necessity. To allow this to happen, the PRF must be low enough so that only one transmitted pulse is reflected by the ground at all times. The maximum range unambiguous PRF, given in equation 2.14, mainly depends on the length (X) of the footprint.

$$PRF_{max} = \frac{c}{2X}\sec(\psi)$$

(2.14)

From this equation, we see that there are no range ambiguities in the footprint as long as the spatial separation between successive pulses (c/PRF) is at least twice the projection of the footprint length in the radar's line of sight (X/sec(ψ)). There are situations where such a low PRF is infeasible given the operational constraints of the system. When this is the case, the radar must find ways to separate the pulses that arrive simultaneously from different ranges.

Doppler Ambiguities

The frequency spread of the ground return (Section 2.6.1) combined with the Doppler shift from the maximum anticipated target velocity is used to set the frequency passband of the Doppler filter bank. In Section 2.3.3, we mentioned that the spectrum of a received signal is repeated at intervals of the PRF when a number of successive pulses are integrated. As long as the PRF is greater than the passband of the filter bank, these sidebands do not cause any problems because they fall outside this passband regardless of the actual target Doppler shift. However, two situations can cause the Doppler measurement to become ambiguous: when the PRF is less than the filter bank passband or when the target Doppler shift places the center spectrum outside the passband. In the first case, the repeated spectra begin to overlap which has profound consequences when ground clutter is present in the received signals (Section 2.6.2). When the target Doppler shift is too large, the radar cannot recognize that the measured target Doppler shift actually results from one of the sidebands and not from the actual Doppler profile of the target echo (Figure 2.9). If Doppler ambiguities need to be avoided, then the minimum PRF must equal the passband of the Doppler filter bank as shown in equation 2.15, where the two
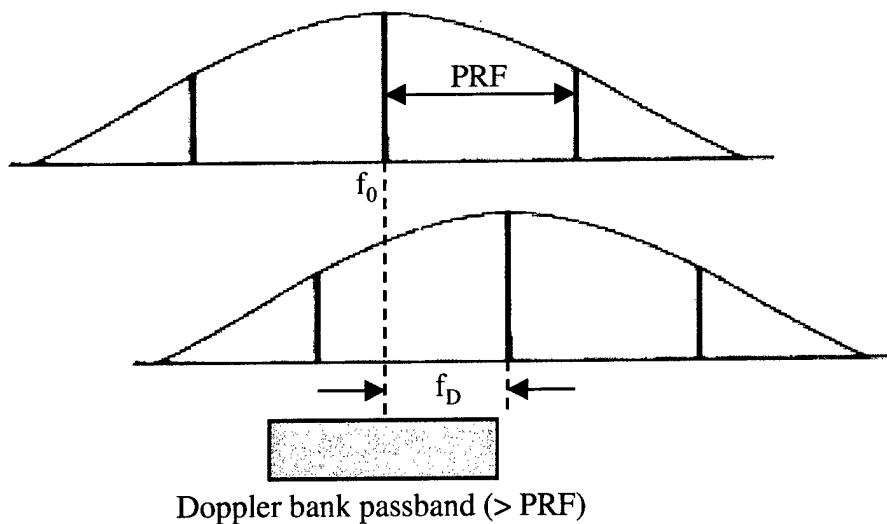
Figure 2.9 Doppler Ambiguities in the Received Signal Spectrum

terms represent the Doppler spectra of the ground return and the fastest moving target respectively [Cantafio, 1989, and Mahafza, 1998].

$$PRF_{min} \cong \frac{2v_p}{L} + \frac{2v_{Tmax}}{\lambda}$$ (2.15)

Again, the presence of Doppler ambiguities in received radar signals renders the Doppler filter bank useless because the true spectrum cannot be distinguished from the sidebands. Without accurate Doppler information, the overall performance of the system is severely degraded because the target and ground returns are no longer separable based on the difference in their frequency profiles. Also, the radar cannot separate the echoes from multiple targets located at the same range. Since most space-based radar applications favor unambiguous range measurement, methods are needed to eliminate the resulting Doppler ambiguities to obtain accurate frequency information from received signals.

Various techniques have been developed to resolve both range and Doppler ambiguities in received radar signals. For instance, range ambiguities can be removed by modulating the amplitude, width, or frequency of each transmitted pulse and applying this modulation to the received echoes to identify the original pulse to which each echo belongs. Unfortu-

nately, "tagging" the transmitted pulses in this manner is rather limiting because the accurate processing of the received echoes can be very difficult. Another example, known as range differentiation, approximates a target's range rate by measuring how its range changes over time. This value is used to estimate the true Doppler shift of the target that yields a correction factor for the measured Doppler shift. This method is also somewhat uncommon since it relies on an approximation of the target range rate that can be highly inaccurate, especially when the range resolution is poor or a high number of Doppler ambiguities are present. The most widely used technique to resolve range and Doppler ambiguities is PRF switching. By changing the PRF of the transmitted pulses, the apparent range and Doppler measurements for a target are shifted based on the total number of ambiguities in the footprint. The application of PRF switching, with an emphasis on resolving Doppler ambiguities, will be further explained in Chapter 3. In the end, the accurate measurement of a target's range and Doppler shift is essential in radar. Although we must deal with a certain level of ambiguity in these measurements based on the chosen PRF, we do have ways around this problem to help us maximize the target detection capability of airborne and space-based radar systems.

2.5 Noise-Limited Target Detection

Unfortunately, the signals received by a radar are not solely caused by the reflection of the transmitted waveform from targets in the antenna beam. The echoes from targets must compete with signal energy from a variety of interfering sources. These sources are classified into two categories: noise and clutter. Detecting targets in the presence of background noise is the focus of this section while the effects of clutter will be addressed in the next section. The level of noise in the received signals is a driving factor in the overall detection range of the radar. Therefore, it is necessary that we first understand the different types of noise that are present in a radar's receiver as well as the general properties of this noise. Then we discuss methods that can be used to improve this detection range such as pulse compression and pulse integration. The goal is to gain an appreciation of the con-

sequences associated with noise in received radar signals and the significant impact it has on the radar system performance.

2.5.1 Detection Range

One of the most important properties of a radar system is the maximum range at which it can detect targets. In airborne applications, this range is often limited by obstructions in the line of sight. However, a space-based platform avoids this shortcoming by placing the radar above all possible obstructions. Beyond this line of sight concern, the maximum range of a radar is the point where the return from a target becomes indistinguishable from competing clutter and noise signals. Most types of clutter can be eliminated on the basis of its Doppler spectrum (Section 2.6.1). Electrical background noise, however, is electrical energy of random amplitude and frequency and cannot be characterized in the same manner. Therefore, noise energy is a substantial contributor to the total power in received signals and is often the limiting factor in the radar detection range. There are two primaries noise sources in radar: noise that is generated internally in the receiver and noise that radiates from external sources.

Internal Noise. This type of noise is mainly generated in the input stages of the receiver and is subsequently amplified by the full gain of the receiver. Internal noise is commonly expressed as the ratio of the receiver noise output to its gain. To become more familiar with internal noise, it is useful to introduce the concept of the ideal receiver that provides the same gain but generates no internal noise. We can now represent the internal noise level as the voltage in a resistor that is connected across the receiver's input terminals. This voltage results from the random thermal motion of free electrons in the resistor. Typically, internal noise is reduced by adding a low-noise preamplifier ahead of the receiver's mixer stage that increases the signal strength relative to the noise level while contributing very little noise itself.

External Noise. All objects surrounding a radar continuously radiate radio waves caused by thermal energy. These sources of radiation are extremely weak but nevertheless may

still be detected by the receiver and added to the total noise in its output. The principal external noise sources are the ground, the atmosphere, and the sun. The radiation from these sources is mainly a function of their absolute temperatures, but it is also influenced by other miscellaneous factors such as the absorption properties of the ground and the atmosphere or the presence of the sun in the antenna beam. Additional external noise sources include the antenna and the waveguides connecting it to the receiver, and again their contribution is proportional to their absolute temperatures.

In general, noise causes thermal agitation of free electrons inside the receiver, thereby causing a detectable voltage that is spread almost uniformly across its entire frequency band. The mean noise power can be approximated by defining the equivalent noise temperature of the entire system. This system temperature is simply a combination of the absolute temperatures of all the noise sources times their respective loss coefficients. The mean noise power is then calculated from equation 2.16.

$$\overline{N} = kT_sBW_n \qquad (2.16)$$

In reality, the actual noise power level measured at any one moment in time is a statistical quantity due to the random nature of the noise. Referring to Figure 2.10, the measured noise power follows a Rayleigh distribution about the mean level from equation 2.16. The vertical black line in this figure represents the target detection threshold. Anytime the noise level alone exceeds this threshold, the radar indicates the presence of a target that
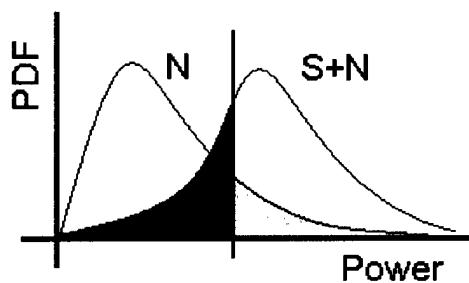
Figure 2.10   Statistical Representation of the Signal and Noise Power Returns

does not actually exist. This is known as a false alarm, and the probability of this occurring equals the area of the lightly-shaded region in Figure 2.10.

When a target signal is present, the measured signal-plus-noise power is now normally (Gaussian) distributed where the mean level has been increased by the signal power in the target echo (see equation 2.17). If the total signal and noise power is not large enough to exceed the detection threshold, the radar is not able to detect the target. Again in Figure 2.10, the probability of this missed detection equals the area of the darkly-shaded region. The chosen detection threshold for a radar involves a trade between the false alarm probability and the probability of a missed detection. If a low number of false alarms is desired, then the end user must accept a higher chance of not detecting a target signal, and vice versa.

The quantity of interest here is the probability of detection, which equals the area of the signal-plus-noise distribution that is above the detection threshold. This parameter is used to gauge the overall performance of a radar system because the ability to detect targets with varying degrees of certainty is of considerable importance to the end user. In most instances, a minimum probability of detection is specified in the system requirements for a radar. This quantity is used to determine the minimum signal-to-noise ratio (SNR) that is needed to satisfy the required probability of detection (see Chapter 4). From the minimum SNR, we can calculate the maximum detection range for a radar using the radar range equation.

2.5.2 Radar Range Equation

The range at which a radar can detect target echoes is a function of many parameters. As stated before (Section 2.1.1), the power transmitted by the radar is diminished by a factor of the distance to the target squared. The power that is intercepted and reflected by the target undergoes the same distance-squared loss, resulting in a total reduction in the power density of the received signals equal to $1/R^4$. The amount of power that a radar receives from a target is a function of the following quantities:

- Transmission power (P_t)

- Radar cross section of the target (σ_T)

- Effective area/gain of the antenna (A_e, G)

- Mean noise level (kT_sBW_n)

- System losses (L_s)

- Minimum signal-to-noise ratio for target detection (SNR_{min})

All of these quantities are captured in a single equation used to define the maximum detection range of the radar. Equation 2.17 is known as the radar range equation and is one of the fundamental relationships in radar [Cantafio, 1989].

$$R = \sqrt[4]{\frac{P_t G A_e \sigma_T}{(4\pi)^2 kT_s BW_n L_s (SNR_{min})}} \tag{2.17}$$

From this equation, it is easy to see that the maximum detection range of a radar can be improved in multiple ways. However, many of these potential improvements are limited by certain system constraints including size, weight, and cost. This means that the design of any radar system must trade between the capabilities of the transmitter and the antenna to maximize the detection range while meeting these constraints. The following paragraphs contain more complete explanations of certain key terms in the radar range equation.

Minimum Signal-to-Noise Ratio. The minimum detectable signal power from a target in the presence of noise depends mainly on the signal processing capability of the radar. Looking at the return from a single pulse, the overall SNR can be improved by increasing the average power, the gain of the antenna, or the length of the pulse (prolonged time on target). The remaining quantities that determine the amount of energy received from a target are either fixed dimensions of the radar, including the size of the antenna, or are properties of the target itself, such as the radar cross section. Most of the time in space-based radar, the power in a single pulse reflected by a target is not distinguishable from the background noise level, so some technique must be devised to improve the strength of the tar-

get signal. A more detailed discussion of some of these techniques, such as compressing individual pulses (Section 2.5.3) and integrating a stream of pulses (Section 2.5.4), is given in future subsections.

Mean Noise Level (Time on Target). The amount of time that a radar antenna dwells on a target determines the frequency resolution of the received signals (Section 2.4.2). A longer time on target reduces increases this resolution, thereby lowering the mean noise level in the system. For a single pulse, it would be desirable to increase the pulse width of the transmitted pulses which would correspond to a smaller noise bandwidth. The problem here is that a point is soon reached where the returns from successive pulses reflected by closely spaced targets overlap when they arrive at the radar, meaning that the individual target returns cannot be resolved in range. The remedy is to transmit a series of pulses of narrow width and combine them when they return (Section 2.5.4). Again, this leads to a reduction in the mean noise level of the received signals, but not at the expense of range resolution.

Radar Cross Section. This property is not only a function of the physical dimensions, or geometric cross section, of a target but also its reflectivity and directivity. Reflectivity refers to the fraction of the intercepted power that is reradiated or scattered by the target. Directivity is defined as the ratio of the power scattered back in the radar's direction to the power that would have been scattered isotropically. If a target is thought of as consisting of a great many of individual reflectors covering its surface, then its directivity signifies the extent to which the scatter from these reflectors combines constructively. Equation 2.18 consolidates all of these properties into a single expression for the radar cross section (RCS) of a target.

$$\sigma_T = 4\pi \frac{P_{backscatter}}{P_{incident}} \tag{2.18}$$

The top term in the fraction is the power per unit of solid angle (steradian) backscattered by a target and the bottom term is the power density of the transmitted signal. Typical

RCS values for air and ground targets viewed from space-based radars are given in Table 2.3. It must be remembered that while a target's geometric cross section remains unchanged, its RCS is not a constant but depends on the relative configuration and orientation of both the radar and the target as well as the wavelength and the polarization of the transmitted signal.

TABLE 2.3 Target RCS Values at Microwave Frequencies [Skolnik, 1980]

Object	RCS (m^2)
Conventional missile	0.5
Small, single-engine aircraft	1
Fighter	2-6
Bomber/jet airliner	20-40
Jumbo jet	100
Pickup truck	200
Automobile	100

Although the radar range equation is a very powerful tool in evaluating the maximum detection range of a radar, it does have some limitations. Certain properties of the radar and potential targets are not accounted for in this equation. First of all, the level of attenuation in the radar signal caused by the atmosphere, although very small at radio frequencies, is neglected. Another example concerns the physical dimensions of the antenna. An increase in the antenna size means that more surface area is available for receiving target echoes. However, a larger antenna gives a smaller beamwidth meaning that the antenna is forced to spend less time on one region in a specified volume to cover the same amount of space in the same time. Eventually this could lead to a decrease in the time on target and give no improvement in the detection range. Finally, the RCS of a target fluctuates as its orientation with respect to the radar changes, which may cause a detected target to disappear and then reappear according to these fluctuations. Nevertheless, the radar range equation captures the majority of the radar and target properties that together define the maximum detection range of the radar. Too often, this range does not meet the require-

ments set by the user, so something must be done to increase it. The next subsections describe some techniques that are used to improve both detection range and range resolution in radar.

2.5.3 Pulse Compression

Ideally, long detection range and fine range resolution could be provided with extremely narrow pulses of exceptionally high peak power. Most of the time, however, this is not possible because there are practical limitations on the level of peak power one can use. This means that airborne and space-based radars must transmit fairly wide pulses to provide adequate detection range at reasonable power demands, thus limiting the capable range resolution of these systems. One solution to avoid this dilemma is known as pulse compression. In this method, transmitted pulses are internally modulated in a prescribed pattern. The received echoes can then be compressed by decoding their modulation. This allows the radar to transmit sufficiently wide pulses for long detection ranges while still providing fine range resolution. The two most common coding methods for pulse compression are linear frequency and binary phase modulation. Other codes have been developed, but the remainder of this subsection will focus on these two methods.

Linear Frequency Modulation (Chirp)

The basic premise behind this form of coded modulation is that the frequency of the transmitted pulses is either increased or decreased at a constant rate throughout its length. Once target echoes are received, they are passed through a filter that introduces a linear time lag to the signals as a function of frequency. The leading increment of each pulse (lowest frequency) takes the longest time to pass through the filter while the trailing segment experiences almost no time lag. The resulting compressed pulse is a fraction of the width of the transmitted pulse and has a proportional increase in peak power (Figure 2.11).

When using a chirp, the uncompressed pulses are divided into a series of individual segments depending on the total frequency change (ΔF) over the duration of these pulses. The difference in frequency (Δf) between each of these segments is based on the fre-
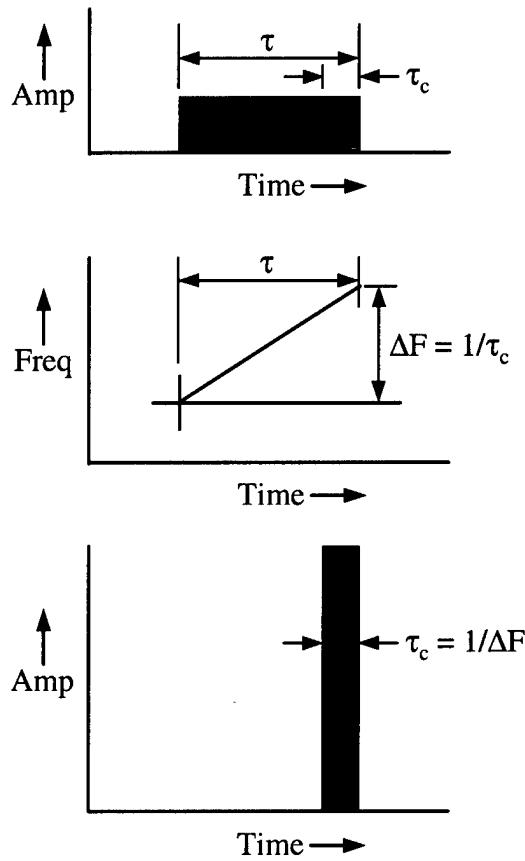
Figure 2.11   Compressed Pulse in Linear Frequency Modulation

quency sensitivity of the time lag filter. If the returns from two closely spaced targets are to be separated on the basis of their frequency difference, the width of the uncompressed signals that pass through the filter must be long enough to provide the required frequency resolution. A useful quantity known as the pulse compression ratio is defined in equation 2.19.

$$CR = \frac{\tau}{\tau_c} = \frac{\Delta F}{\Delta f} = \tau \Delta F \qquad \qquad (2.19)$$

The last term in this equation is also referred to as the time-bandwidth product. The fact that these quantities are equal point to some interesting relationships. For instance, if the uncompressed pulse width is kept constant, the pulse compression ratio can be increased by extending the total frequency range in the modulation of the transmitted pulse. The

overall significance of this quantity is evident in the improvement it represents in both range resolution and detection range provided by pulse compression.

Binary Phase Modulation

This type of coding introduces a 180° shift to the radio frequency phase of certain segments in the transmitted pulse according to a prescribed binary pattern. The received echoes are passed through a delay line that provides a total time delay equal to the duration of the uncompressed pulses. An example 3-segment binary phase modulation sequence and its resulting delay line output is given in Figure 2.12. The delay line is divided into the
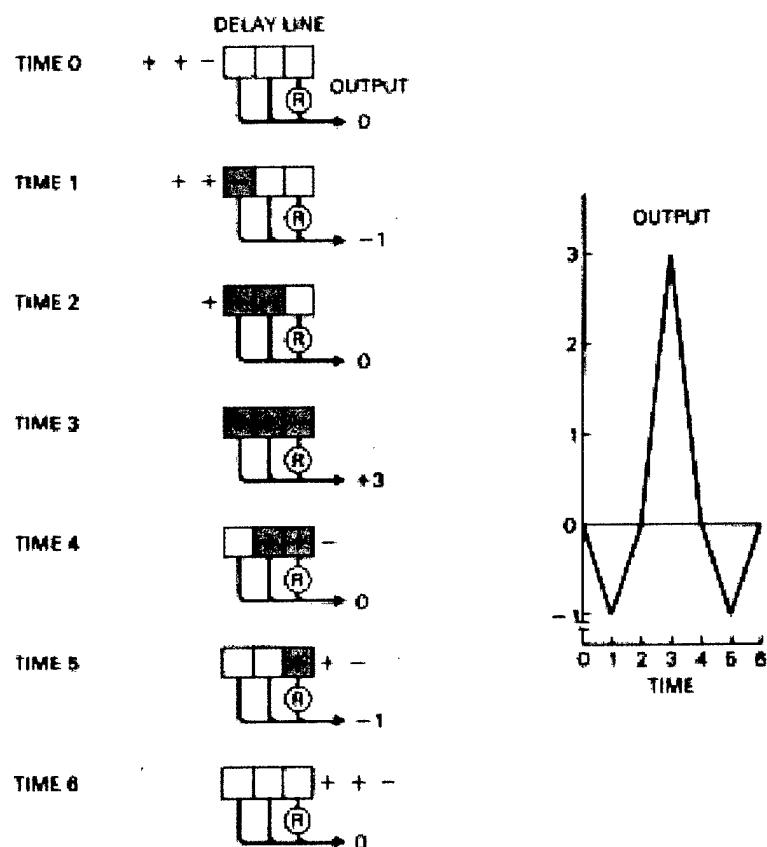
Figure 2.12   Illustration of Binary Phase Modulation [Stimson, 1998]

same number of segments as are contained in the transmitted pulse. An output tap that feeds into a single output terminal is provided for each segment. In certain taps, 180° phase reversals are inserted whose positions correspond to the phase shifted segments of the transmitted pulse. As the received echo travels through the delay line, the total output is based on the current location of the pulse in the delay line. Most of the time, the delay line outputs combine in a destructive manner because some of these outputs are out of phase with one another. However, a point is eventually reached where all of the segments add together in phase when the pulse completely fills the delay line (time 3 in Figure 2.12). In the resulting compressed pulse, the total number of segments is the factor by which the amplitude is increased and the pulse width is reduced. This again gives a longer detection range and finer range resolution for the radar.

The increase in detection range that results from both pulse compression methods is caused by the boost in the peak power of the compressed pulse. The width of this pulse also leads to enhanced range resolution as illustrated in Figure 2.13. This figure shows that the returns from two closely spaced targets that are merged indistinguishably at the input to the time lag filter are able to emerge separately. The reason for this is that the
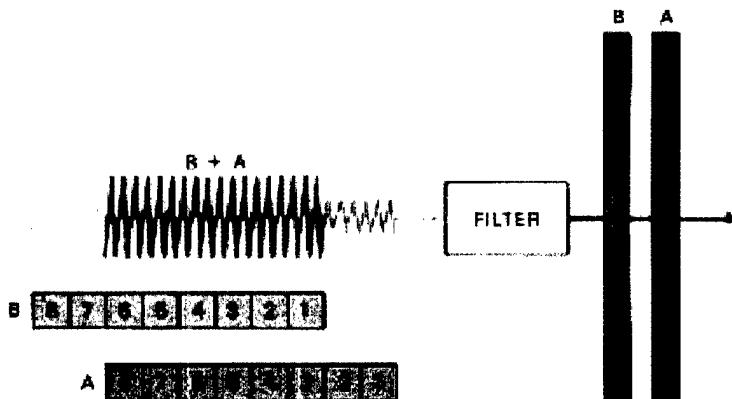
Figure 2.13 Improved Range Resolution from Pulse Compression [Stimson, 1998]

modulation coding in each pulse allows each segment of the echo from the near target to emerge from the filter at the same time as the first segment of this echo. The same is true for the echo from the far target. The end product is two compressed pulses separated by the length of time that the transmitted pulse took to travel from the near target to the far target and back. The resulting range resolution now depends on the width of the compressed pulse. In the end, the desired amount of pulse compression and how to achieve it is a key trade-off in radar system design.

There are some limitations that are inherent in pulse compression. For instance, a series of range sidelobes is formed when the modulated pulses are compressed that is similar to the lobe structure of a pulsed signal's Doppler spectrum (refer to the output pulse in Figure 2.12). In linear phase modulation, the sidelobes can be reduced to acceptable levels by tapering the amplitude of the uncompressed pulse at its leading and trailing ends. Binary phase modulation, on the other hand, minimizes sidelobes by using of a unique set of binary codes in the modulated signal. These are known as Barker codes, and they produce sidelobes whose amplitudes are no greater than the amplitude of the uncompressed pulse. It turns out that certain combinations of these codes can completely eliminate range sidelobes. In addition to sidelobes, pulse compression also has certain disadvantages associated with measuring target Doppler shifts. In spite of these limitations, the overall merits of pulse compression are very desirable in most airborne and space-based radar systems.

By now it is easy to see that pulse compression is an extremely useful technique to help improve the range resolution and detection capabilities of a radar system. The chosen form of pulse modulation is a function of the assumed Doppler characteristics of anticipated targets and the personal preferences of the radar designer. The maximum detection range of a radar can be further improved by integrating a number of successive pulses reflected by a target.

2.5.4 Pulse Integration

In most cases, a certain amount of pulse integration is required to provide an adequate signal-to-noise ratio for target detection. Pulse integration is accomplished by combining a number of successive reflected pulses to improve the overall strength of the resulting target signal. If the integration is performed before the magnitude detection in the processor, it is referred to as predetection or coherent integration and uses both the amplitude and phase of each pulse to take advantage of the random nature of the background noise. Otherwise, postdetection or noncoherent integration is performed where only the amplitudes of the pulses are needed to help reduce the statistical variance in the noise.

Coherent Integration

This form of pulse integration can provide a substantial improvement in the detection range of a radar, but its application places certain strict limitations on the relative properties of each pulse. Specifically, the actual radio frequency phase of the transmitted pulses has to be constant (Section 2.4.2). In addition, the receiver must provide several parallel channels tuned to slightly different frequencies to account for all possible target Doppler shifts [Shaw, 1998]. These steps allow the radar to maintain a constant phase between successive pulses prior to integration. Once the target Doppler shifts exceed this anticipated frequency range, the pulse coherence is lost so they can no longer be integrated in this manner. The total length of time where coherent integration is possible is known as the coherent processing interval (CPI) or coherent dwell time (t_d), and the total number of pulses available for integration is simply the product of this period and the PRF (equation 2.20).

$$n_c = PRF \cdot t_d \qquad (2.20)$$

Coherent integration is essentially performed by tuning a filter to the Doppler frequency of a target echo and integrating the energy that passes through this filter over a series of successive pulses. It uses both the amplitude and the phase information of the input signal to boost the signal power while keeping the noise power constant.

To understand how coherent integration is performed, we must recall that any signal can be expressed in terms of its amplitude and phase with phasors. Since the amplitude and phase of the target signal are essentially constant from pulse to pulse, each integrated pulse combines constructively. Noise, on the other hand, has random amplitude and phase variations between pulses. This causes the noise signals from each pulse to cancel to a large extent when they are integrated due to the randomness of phase. The signal that results from coherent pulse integration has the same mean noise power as that contained in each individual pulse. However, the target signal power is multiplied by the number of integrated pulses which causes a corresponding increase in the maximum detection range of the radar. Most of the time, the coherent processing interval is shorter than the total time on target. When this happens, the detection range can be further improved with post-detection (noncoherent) integration.

Noncoherent Integration

While not capable of improving the actual SNR of received radar signals, this form of integration can still provide a considerable improvement in target detection capability by reducing the minimum required SNR. Noncoherent integration is performed after the phase information of the individual pulses has been removed and, therefore, does not have to meet the same stringent phase requirements as coherent integration. This means that the amount of integration in this case is bounded only by practical limitations on total dwell time over a particular area (T_d). The total number of noncoherently integrated pulses is calculated from equation 2.21.

$$n_p = \frac{T_d}{t_d}$$
(2.21)

Basically, noncoherent integration is nothing more than averaging. It is performed by adding together successive outputs of the processed signal after their amplitudes have been measured. The result is a reduction in the overall variation of the noise from pulse to pulse. Also, the fluctuations in the integrated signal tend to cancel out, which greatly

reduces the destructive interference from noise that can lead to missed target detections. Overall, the benefit of noncoherent integration is a decrease in the minimum voltage required to signify the presence of a target (detection threshold) while maintaining the same false alarm probability. This minimizes the number of target signals that miss detection and again increases the maximum detection range.

Another form of postdetection integration sometimes used in radar is known as binary integration. This method requires that a specified number of coherently integrated pulses cross the detection threshold to signify the presence of a target. If only a single threshold crossing is needed to indicate a target detection, isolated noise spikes can produce false alarms. The chance of this occurrence can be reduced if more than one threshold crossing is required as a condition for detection. This again allows a reduction in the target detection threshold without an increase in the false alarm probability, meaning that more distant targets can be detected.

2.6 Clutter-Limited Target Detection

In addition to noise, target echoes must also compete with unwanted reflections from miscellaneous objects on the ground. This type of interference is known as ground clutter, and it is a major contributor to the overall strength of the signals received by the radar. Certain airborne radars completely avoid returns from ground clutter when their transmitted signals do not reflect off any objects on the ground. The same is not true for space-based radars because their antennas are always pointed towards the ground. In this situation, the strength of the clutter return masks the presence of target signals. We must, therefore, find a method for either suppressing or eliminating its contribution to ensure detection of targets. The principal means used to separate targets from clutter is Doppler resolution. For airborne and space-based radar, targets and clutter are both moving with respect to the radar. Consequently, the radar processor must be able to separate these returns based on the individual frequency characteristics (Doppler spectra) of both targets and clutter. In this section, we begin by explaining the properties of the different types of

ground clutter that are encountered in these operating environments. We move on to a discussion of the adverse effects on the clutter spectrum caused by range and Doppler ambiguities and conclude by briefly mentioning a few methods that are used to separate targets from clutter. In the end, the contribution from clutter in received signals plays a substantial role in the design, operation, and performance of a space-based radar system.

2.6.1 Sources of Ground Return

While the return from any object that is not a viable target in the system application can be classified as clutter, the main form of clutter that contributes the greatest return in space-based radar originates from the ground. There are three categories that are used to classify ground clutter: mainlobe, sidelobe, and altitude returns. Each has its own return strength and Doppler spectrum, and this information can be used to separate target returns from clutter. In space-based radar, a critical concern in the system design is the relationship of the clutter spectrum to the Doppler frequencies of anticipated targets. The power that is returned by clutter is calculated in much the same way as it is for a target signal with a few modifications, as shown in equation 2.22 [Shaw, 1998].

$$C = \frac{P_t G A_e \bar{\sigma}}{(4\pi)^2 L_s R^4} \tag{2.22}$$

where

$$\bar{\sigma} = \sigma_0 A_g \tag{2.23}$$

The main reason why the signal strength of clutter reflections is significantly higher than target returns can be attributed to the relative difference in radar cross section. The radar cross section of clutter in equation 2.23, or clutter cross section ($\bar{\sigma}$), equals the product of the backscattering coefficient (σ_0) of the terrain within the radar footprint and the ground area that can be resolved by the radar (A_g). Equation 2.24 defines the backscattering coefficient as a function of the reflectivity of the ground clutter within the radar footprint and the footprint grazing angle.

$$\sigma_0 = \gamma \sin(\psi) \tag{2.24}$$

The clutter reflectivity (γ) depends on both the reflective properties and the relative orientations of the illuminated objects on the ground. Table 2.4 lists some typical values of gamma for various types of terrain encountered in space-based radar.

TABLE 2.4 Clutter Reflectivities for Land Terrain [Nathanson, 1969]

Terrain Type	γ (dB)
Deserts and roads	-25
Cultivated land	-22
Open woods	-16
Wooded hills	-14
Cities	-11

In most situations, the clutter RCS is one to two orders of magnitude higher than any target echo in the signals received by the radar, which explains why ground clutter returns must be suppressed to enable target detection. The next paragraphs explain the origins of the three types of ground clutter that are encountered in airborne and space-based radar.

Mainlobe Clutter. The mainlobe return refers to the reflection from the area on the ground within the radar footprint. Since the ground in the mainlobe of the antenna is amplified by the same gain as any targets in the footprint, the signal-to-clutter ratio (SCR) for mainlobe clutter (MLC) depends only on the RCS values of the target and the clutter (equation 2.25) [Cantafio, 1989].

$$SCR = \frac{\sigma_T}{\bar{\sigma}} \tag{2.25}$$

The Doppler spectrum of mainlobe clutter (large spike in Figure 2.14) is calculated from equation 2.26 based on the velocity of the radar, the transmission wavelength, and the angle between the direction of motion and the location of the footprint (α).
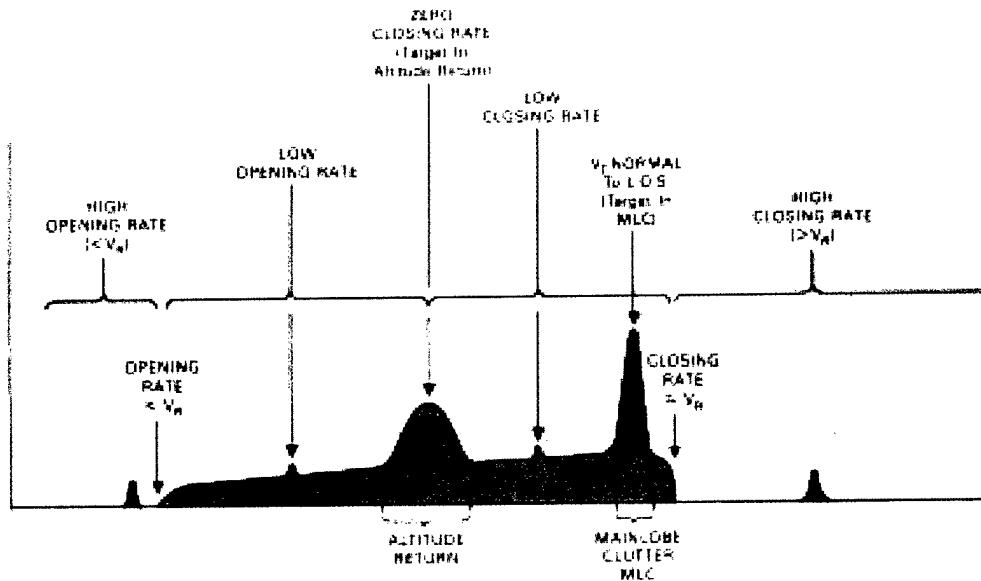
Figure 2.14 Clutter Spectrum for a Forward-Looking Radar [Stimson, 1998]

$$f_D = \frac{2v_p}{\lambda}\cos(\alpha) \tag{2.26}$$

From this equation, we see that the mainlobe return is at its highest Doppler shift when looking to the front (positive) and to the rear (negative). As the footprint is moved throughout the coverage area of the radar, the range of frequencies covered by mainlobe clutter fluctuates based on the footprint location and the beamwidth of the antenna. This Doppler spread defines the minimum target velocity that permits detection by the radar in equation 2.27 [Cantafio, 1989].

$$MDV = \frac{\lambda}{L}v_p\sin(EL) \tag{2.27}$$

Any target with a velocity less than this minimum (MDV) cannot be detected because there is not sufficient Doppler shift in its echo to separate it from the mainlobe clutter return. The issues raised by the Doppler frequency properties of mainlobe clutter will be addressed in much more detail in Chapter 4. For now, we only need to appreciate that the

strength and spectral variability of this type of clutter make it very difficult to contend with when trying to detect targets.

Sidelobe Clutter. Sidelobe clutter is composed of any and all signals that are received through the sidelobes of the antenna. This type of return is not amplified by the full gain of the antenna, but the sidelobe return can still be significant because the total area illuminated by sidelobes is quite large, and it is often located at shorter ranges. The SCR for sidelobe clutter is calculated by multiplying the mainlobe SCR from equation 2.25 with the mainlobe-to-sidelobe ratio of the antenna radiation pattern. Because sidelobes radiate in every direction from the antenna, the sidelobe spectrum is spread (Figure 2.14) over a wide range of frequencies based on the maximum Doppler shift of the ground within view of the radar ($\pm 2v_p/\lambda$). This means that for most reasonable target Doppler shifts, the target echo is going to have to compete with some level of sidelobe clutter.

Altitude Return. Altitude return is a special type of sidelobe clutter that originates from the patch of ground directly below the radar. This region on the ground has a fairly large extent where every point is so close to being at the same range that the sidelobe return appears as a single spike on the frequency spectrum (Figure 2.14). This spike is located around zero frequency because this patch of ground has very little relative motion with respect to the radar. The strength of altitude return is generally similar to that of mainlobe clutter, but since its Doppler frequency is easily predictable, this form of clutter is easily identified in the spectrum of the received signals.

Looking once again at Figure 2.14, we see that only the signals from the fastest moving targets are not adversely affected by ground clutter returns. If the Doppler shift of a target places its echo within the spectrum of either the mainlobe clutter or the altitude return, the target signal is most likely masked in the presence of these much larger interfering sources. Otherwise, most target returns normally have to compete with some amount of sidelobe clutter. In general, the overwhelming contribution of ground clutter in reflected signals is one of the major disadvantages in airborne and space-based radar. Many signal

processing methods have been developed that reduce the overall strength of the clutter return without diminishing the target signal. But first, we need to discuss the concerns raised when range and Doppler ambiguities exist in the received radar signals.

2.6.2 Effect of Ambiguities on Ground Clutter

Even though the return from ground clutter is much stronger than most target signals, a radar can still detect these targets by taking advantage of their individual Doppler profiles. Based on the direction in which the antenna is looking, the clutter frequency spectrum can easily be determined because the clutter is stationary. Since the goal is to detect moving targets, the resulting Doppler shifts in the target signals cause these returns to fall outside the clutter spectrum in the vicinity of the target. However, they must still compete with clutter originating from other areas of the footprint. In the case of fast-moving (airborne) targets, the Doppler shift places them outside the entire clutter spectrum. These signals now compete solely with noise and, therefore, have a much higher probability of detection. Separating target returns from clutter, essential to the operation of most space-based radars, is a difficult process that requires a some form of clutter suppression in the processing of received signals. Target detection is further complicated when range and Doppler ambiguities are present in these signals since they significantly alter the ground return. Our previous discussion on range and Doppler ambiguities focused on their overall impact on target signals (Section 2.4.3). However, the consequences of these ambiguities on ground clutter can severely limit the target detection capability of a radar.

Range ambiguities exist when the PRF of the transmitted pulses is too high and the reflections from multiple pulses are received by the radar at the same time. From a space-based platform, this situation occurs when multiple transmitted pulses continuously illuminate the footprint. Figure 2.15a shows two range ambiguities in the footprint, meaning that the echoes from R1 and R2 have the same apparent range when received by the radar. Any target signals in these reflections are combined with the return from ground clutter. While the target and mainlobe clutter returns from the same range can be resolved using the tech-

a) Range Ambiguous   b) Doppler Ambiguous
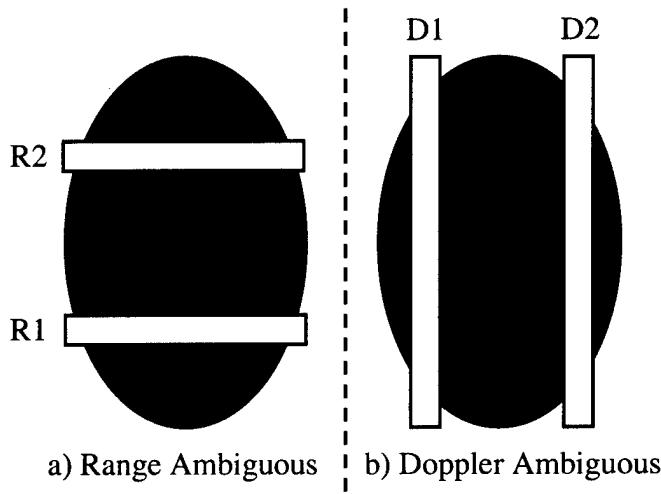
Figure 2.15   Ambiguities in a Radar Footprint [Sedwick et al, 2000]

niques described in Section 2.4.3, some of the sidelobe clutter remains superimposed because this type of ground return is received from all directions. If a target Doppler shift does not exceed the frequency spread of the clutter spectrum, its echo is forced to compete with a larger amount of interference from clutter which increases the likelihood that the target will miss detection. In most situations, the adverse effect of range ambiguities on ground return can be eliminated by using normal resolving methods such as PRF switching. Doppler ambiguous ground return, on the other hand, is not so easily resolved and can greatly limit a radar's ability to separate target signals from clutter.

As we learned in Section 2.4.3, the Doppler spectrum from a reflected pulse is easily measured as long as the transmission PRF exceeds the anticipated range of frequencies in the received signals. Once this is not the case, the true Doppler spectrum is overlapped by the spectra repeated at multiples of the PRF. The combined spectrum no longer represents the actual Doppler profile of the reflected pulse but contains additional artifacts from these sidebands. Referring to Figure 2.15b for a side-looking radar, the received signals contain Doppler ambiguities when the PRF is not high enough to cover the frequency extent of the footprint. The spectra centered at D1 and D2 overlap, meaning that a target signal may have to compete with ground clutter whose true Doppler profile is quite different from the

target's. This can substantially reduce the clutter-free regions in the received signal spectrum, thus making it even more difficult to detect targets in the presence of clutter.

Unfortunately, the methods for resolving Doppler ambiguities are not very helpful when dealing with ground return because they simply move around blocks of clutter in the filter bank passband. Therefore, the frequency difference needed to isolate target returns from clutter is still washed out by the Doppler ambiguities. As these ambiguities become even more severe, the mainlobe clutter return will eventually span the entire Doppler bank passband and make target detection nearly impossible. To avoid this outcome and attain the highest probability of target detection, the chosen PRF must attempt to minimize the number of range ambiguities while maintaining a sufficient frequency separation between the main and sideband Doppler spectra of the received signals. This can be a crippling constraint for many space-based radar systems because good performance in one area comes at the cost of poor performance in the other. A potential remedy is to combine the signals received by multiple radar antennas, a concept that will be further explained in the next subsection. Otherwise, the radar must find ways to suppress the level of competing clutter in received signals at the low PRFs required in most space-based radar applications.

2.6.3 Separating Targets from Clutter

If the Doppler shifts from most targets of interest are high enough to place their echoes outside the range of frequencies occupied by clutter in the same vicinity, then target detection is simply noise-limited and clutter returns are rejected by the radar. When this is not the case, particularly with ground-moving targets, the target signals are embedded in clutter return. For space-based radar, the competing clutter originates from the mainlobe due to its very large Doppler extent [Rabideau et al, 1999]. The problem of separating target signals from clutter can be somewhat reduced by employing an antenna that produces a very narrow beamwidth in specific directions or by switching the PRF to change the frequency location of the mainlobe clutter return. However, these solutions produce modest results at best and can place unreasonable constraints on the operation of the radar system.

This means that the radar signal processor must provide an acceptable level of clutter suppression to allow detection of targets, especially from space-based platforms. There are numerous techniques that have been developed to suppress the amount of competing clutter in received signals. Some are used in a wide range of radar applications while others are relatively new. Sections 3.4 and 3.5 in the next chapter concentrate on a selection of these clutter suppression methods that have the potential to provide the highest level of performance for space-based radars.

Chapter 3

SEPARATED SPACECRAFT INTERFEROMETRY

The radar fundamentals presented in the last chapter are applicable to all types of airborne and space-based radar. We now change our focus to a new topic that is only recently finding use in radar applications. The vast majority of past and present radar systems use the signals received by a single antenna to detect targets. This requires the radar engineer to make a choice between area search rate and resolution in the system design. If the radar must be able to determine a target's location with a high degree of precision, a large antenna is needed to provide the necessary resolution. The consequence of this option is a reduced area search rate due to the small antenna beamwidth, meaning that the radar must either increase the total dwell time over a specified area to do a complete search or provide multiple systems on separate platforms to reduce the total area that a single radar must cover. When a high area search rate is required, the resolution must be sacrificed in favor of a larger transmission beamwidth with a smaller antenna. In addition, the design for a single antenna radar must attempt to maximize the performance capabilities of the system while working within a number of constraints on size, weight, and cost. This is especially true in space-based radar where concerns over launching the system into orbit and operating it in such a hazardous environment can place severe restrictions on the radar design. A potential remedy is to locate multiple apertures on individual spacecraft flying in formation, thereby creating a large sparse array in which the signals received from the ground are combined in a process known as interferometry. In this configuration, the radar system can utilize small antennas to provide the necessary beamwidth while also achieving

high resolution in the combined signals. The overall cost of the system can also be decreased by using smaller satellites at lower orbital altitudes. This chapter begins with a brief overview of interferometry in Section 3.1. Section 3.2 addresses the concerns that arise from the need to maintain a tight formation for each cluster of satellites followed by Section 3.3 that explains how interferometry and cluster geometry are applied to sparse aperture synthesis in space-based radar.

The remainder of this chapter concentrates on the issues surrounding the detection of targets in the presence of clutter. Ever since radars were first placed on aircraft, strong clutter return has been a persistent problem anytime the transmitted signal comes into contact with the ground. For space-based GMTI radars that always look down to detect targets, the consequences of clutter are amplified due to the continual ground return and the much larger distances involved. The large spatial extent of the illuminated footprint in this case causes a greater frequency spread of the clutter Doppler spectrum, which makes it difficult to detect even fast-moving targets. It may seem at this point that placing a radar system in space is infeasible and undesirable in many situations. On the contrary, the overwhelming advantages of space-based radar, including a wider field of view and a higher area search rate, significantly outweigh the potential difficulties that arise from operating in such an environment (Chapter 1). To limit the adverse effects that result from the presence of clutter in received signals, numerous solutions are available to the radar system engineer that fall into two general categories. First of all, the physical design of the radar can aid in suppressing clutter by providing high resolution in certain directions with a long antenna, switching the pulse repetition frequency to shift around the clutter sidebands, or combining the returns from multiple antennas. The other option is to employ a signal processing strategy that takes advantage of the predictable nature of clutter to reduce its overall contribution to the received radar signals. Section 3.4 presents two clutter suppression techniques that been successfully implemented in existing single aperture airborne and space-based GMTI radar systems. Since the theme in this chapter focuses on clusters of satellites, Section 3.5 discusses some signal processing strategies that adapt the principles of sparse aperture interferometry to clutter suppression in received radar signals. Although

the implementation of separated spacecraft interferometry in space-based GMTI radar promises to be a difficult and demanding process, the hope is that the reader eventually appreciates the overwhelming improvements in performance that can be achieved with this potential system design.

3.1 Overview of Interferometry

For space-based GMTI radar, the ability to separate closely spaced targets, or angular resolution, is an important capability metric of the operational system. Traditionally, high angular resolution requirements have been satisfied by expanding the physical dimensions of the antenna aperture. The difficulty with this trend is that these increasingly large apertures are becoming prohibitively expensive to remain feasible and cost-effective. Only recently have the principles of interferometry been applied to space-based radar to help alleviate this problem. The main advantage of interferometry is the decoupling of the angular resolution of the system from the aperture diameter. By combining the signals received by multiple apertures, a new aperture is synthesized where the angular resolution is now specified by the maximum separation distance, or baseline, between the apertures. This means that the sensitivity requirements of the system are the only factors that affect the aperture diameter [Jilla, 1998]. The potential for significant improvement in the performance of space-based GMTI radar systems provided by interferometry is now beginning to be studied on a large scale.

Interferometry has its origins in astronomical observations [Enright, 1999]. The instrument works in practice by combining the signals collected by a series of widely separated apertures at the same location to provide a single data point. Since radars operate at radio frequencies, the signals from the various apertures can be recorded and correlated at a later time. The output of each correlation is a single complex value that gives the magnitude and phase information of the source's spatial Fourier component at a particular baseline [Kong, 1998]. These spatial frequencies in Fourier space, or u-v points, correspond to a

unique vector baseline between a pair of apertures. Equation 3.1 is used to calculate the u-v points based on the x and y coordinates of the i and j apertures.

$$u_{ij} = \frac{\pm |x_i - x_j|}{\lambda}$$
$$v_{ij} = \frac{\pm |y_i - y_j|}{\lambda}$$

(3.1)

Each measured u-v point contributes to the visibility map of the source object. The brightness image of the source is obtained by taking the inverse Fourier transform of the visibility map. The overall quality of the interferometric image is determined by the number of measurements taken at different u-v points, but only partial coverage of the spatial frequencies in the Fourier plane is required to obtain valuable images [Jilla, 1998].

The angular resolution of an interferometer is defined by the maximum separation between the apertures projected normal to the line-of-sight to the observed source (equation 3.2).

$$\Delta\theta = \frac{\lambda}{B\cos\theta}$$

(3.2)

Herein lies the benefit of using interferometry, since far fewer resources are required to provide the same angular resolution as a much larger antenna. This alternative is especially attractive for space-based radar systems, where the cost of putting resources into orbit is very expensive.

3.2 Satellite Cluster Geometry

For an interferometric remote sensing system orbiting the Earth, the received signal wavelength has a significant impact on the geometry of the cluster. Systems operating at optical wavelengths would be forced to maintain a rigid cluster configuration to ensure equal path lengths between the satellites for real-time interference. Fortunately, separated spacecraft radar systems have a low enough transmission frequency that the received sig-

nals can be digitized and recorded, thus allowing the signal correlation to be accomplished during post-processing. As a result, time delays can be introduced when interfering any two signals, meaning that the distance of any satellite from the illuminated ground area no longer matters. Therefore, the selection of cluster geometries for TechSat 21 is not determined by performance requirements but by other system constraints. The following subsections explain the reference frame used to evaluate the satellite motions and the candidate orbit trajectories for a sparse aperture space-based GMTI radar system. The discussion is based largely on the previous work by Kong, 1998, and Sedwick et al, 1998, and is intended to provide the reader with an overall familiarity of the motion of satellites in clusters.

3.2.1 Equations of Motion

Since the size of the cluster is relatively small compared to the size of its orbit, the local movements of the satellites can be approximated by assuming a perfectly spherical Earth and linearizing the motions about the cluster orbit. The resulting linearized set of equations govern the relative motion of two spacecraft where one is traveling in a circular Keplerian orbit while the second is perturbed from this orbit. These are known as Hill's equations and are given by

$$
\begin{aligned}
x'' - 2y'n - 3n^2x &= a_x \\
y'' + 2x'n &= a_y \\
z'' + n^2z &= a_z
\end{aligned}
\tag{3.3}
$$

where n is the frequency of the reference orbit in radians per second, and the acceleration terms on the right account for all non-central force effects (drag, thrust, etc.) [Hill, 1878]. The x-variable in equation 3.3 refers to the displacement along the zenith-nadir line, the y-variable gives the displacement along the orbital velocity vector, and the z-variable corresponds to the cross-axis displacement perpendicular to the velocity vector [Kong, 1998].
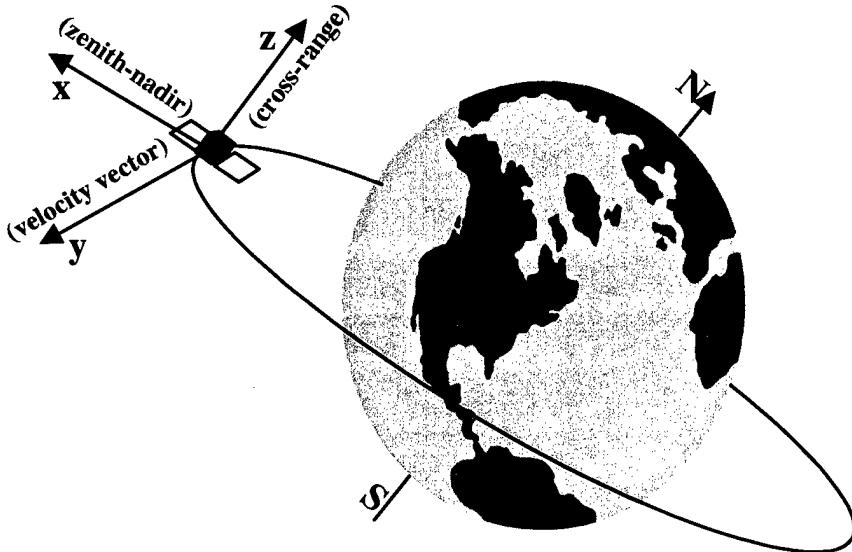
Figure 3.1 Hill's Coordinate Frame for an Earth-Orbiting Cluster [Kong, 1998]

The coordinate system in this accelerating reference frame, represented in Figure 3.1, is called Hill's frame.

In reality, there are many different ways to create local satellite clusters. One option is to force the satellites to fly in a rigid formation where their relative positions and orientations are kept constant. The other alternative is to maintain the separations between the satellites by allowing them to follow free orbit trajectories in Hill's frame. While the former preserves constant x-y-z values for each satellite, the latter constrains these coordinates to certain orbit trajectories [Shaw, 1998]. Since the propellant requirements for rigid clusters are prohibitively high [Sedwick et al, 1998], the only reasonable cluster geometry for TechSat 21 requires free orbit solutions to Hill's equations.

3.2.2 Free Orbit Trajectories

Looking again at equation 3.3, we can set the acceleration terms equal to zero and solve the resulting set of differential equations to get the free orbit motion. The solution is a family of elliptical orbits that are governed by equation 3.4

$$x = A\cos(nt + \alpha) + x_0$$

$$y = -2A\sin(nt + \alpha) - \frac{3}{2}nx_0 t + y_0 \qquad (3.4)$$

$$z = B\cos(nt + \beta)$$

where A and B are the semimajor and semiminor axes of the ellipses, and α and β are phasing angles. From equation 3.4, we can see that the motion along the z-axis is uncoupled from the other directions and exhibits simple harmonic motion resulting from the inclination of the orbit relative to reference. The coupling between the x and y equations imposes the following requirements:

- Each satellite follows a two-by-one elliptical trajectory in the vertical plane of motion

- Offsets in the positive x-direction cause drift along the negative y-axis and vice versa

This second result is caused by the satellite being in a higher orbit of longer period where the corresponding velocity is lower [Sedwick et al, 1998].
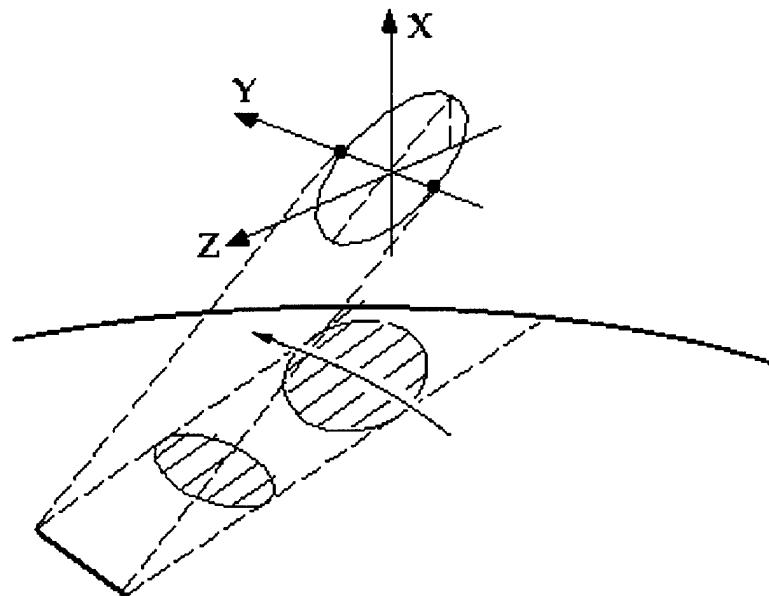
Figure 3.2 Free Orbit Solution to Hill's Equations

In the absence of perturbing forces, satellites placed in orbits governed by equation 3.4 would continue to follow these trajectories forever. Provided configurations could be found that satisfy whatever requirements have been set, this solution would be optimal since no propellant is required to maintain the cluster formation. Free orbit cluster geometries for TechSat 21 must remain closed, requiring that the x_0 term in equation 3.4 always equals zero to prevent the secular motion caused by offsetting a satellite in the vertical direction. If we also demand that the satellite trajectories project a circle at nadir while recognizing that motion in the cross-track direction (z-axis) can be independently specified, then we can place the satellites in an inclined plane relative to the ground. In this case, the phasing angles are equal and the width of the elliptical orbit is twice the height [Sedwick et al, 1998]. This orbit trajectory is shown in Figure 3.2. We can easily see that although the spatial extent of the cluster is maintained in the vicinity of nadir, the projected geometry degenerates to a line in certain directions.

To remedy this problem, some of the satellites in the cluster can be located in a different orbital plane such that a cluster projection of adequate spatial extent is provided in all directions within the field of regard. One possibility is to mirror the orbit in Figure 3.2 but rotated 180° about the vertical axis. Figure 3.3 illustrates this option. From this diagram,
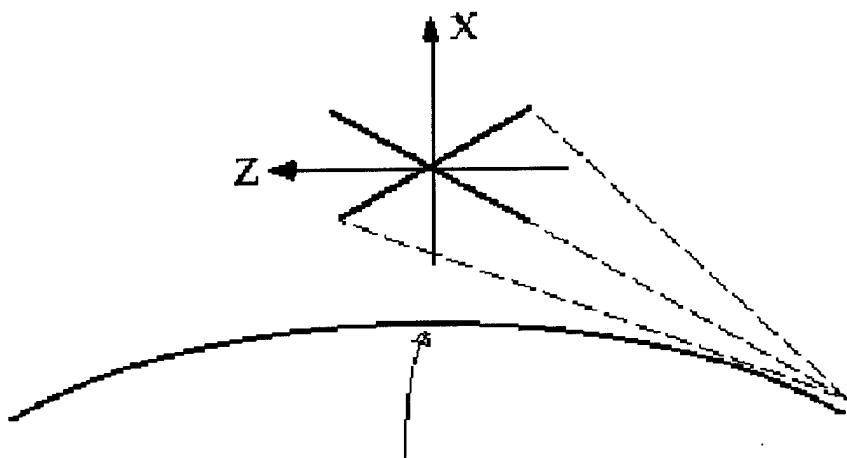
Figure 3.3 Non-Degenerate Cluster Geometry

we notice that as the projection of some of the satellites degenerates, the others open up, thereby maintaining the necessary spatial extent across the cluster. As long as this requirement on the projected spatial extent is always fulfilled, then the radar performance of the cluster does not depend on the individual locations of the satellites because a sufficient number of baselines for remote sensing are always provided when the cluster projection does not degenerate.

3.3 Sparse Aperture Synthesis

In Section 3.1, we learned that the combination of signals received by multiple apertures through interferometry synthesizes a aperture with a diameter proportional to the maximum separation distance between the apertures. This new aperture has much finer angular resolution but maintains the same footprint area, so no penalty is paid concerning the area search rate. The properties of the synthesized aperture from a sparse array are presented in this section. The focus will remain on space-based GMTI radar systems, but most of the results are applicable to all types of interferometry. Although interferometry in radar places a considerable computational burden on the processing of the received signals, the potential for greatly improved capability and performance far outweigh the drawbacks of this technique.

3.3.1 Radar Interferometry

A good space-based GMTI radar system must have high spatial and frequency resolution to enable the detection and isolation of a wide variety of moving targets. While frequency resolution can be improved by increasing the dwell time over the search area, high spatial resolution is only achieved through the use of large antenna apertures. These antennas can be physically large or synthetically produced through signal processing. One option of the latter type is synthetic aperture radar (SAR) which combines multiple views from a thin aperture as it travels along-track to provide fine resolution in the range direction [Stimson, 1998]. The problem with this choice is that a very wide aperture is needed to obtain ade-

quate cross-range resolution. In the end, the size requirement for single large antennas or even SAR antennas is excessive from both production and launching standpoints.

The only remaining alternative is to design a space-based GMTI radar system with a number of small apertures and apply the principles of separated spacecraft interferometry to achieve the level of spatial resolution demanded by modern users. With this improved resolution in both the range and cross-range directions, the footprint projected on the ground by the radar can be divided into a cell grid as demonstrated in Figure 3.4 (the cell sizes are intentionally exaggerated for clarity). Aside from resolution concerns, sparse
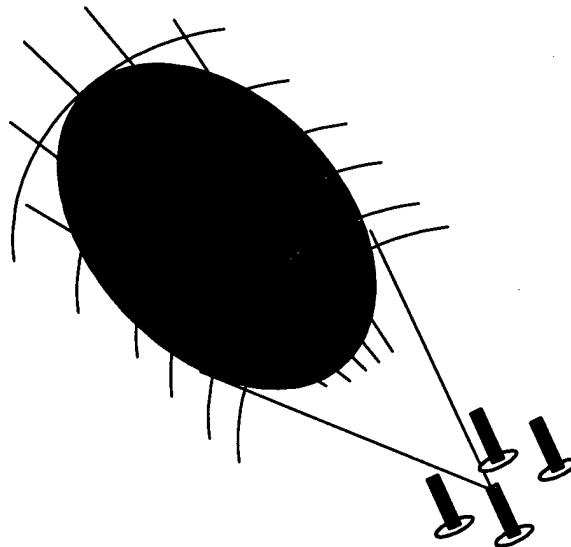
Figure 3.4   Cell Grid in a Cluster Footprint

aperture systems also benefit from an enhanced clutter rejection capability. In a single aperture system, the clutter return is spread in frequency throughout an entire range bin making it very difficult to detect targets at any speed. The increased resolution in cross-range with multiple apertures narrows the clutter spectrum within a given cell, thus lowering the minimum detectable velocity in the system. For each cell in the footprint, we can calculate the range, Doppler shift and spread, and clutter cross section to aid in the processing of the received signals. The cell size is physically set by the mainlobe width of the

receive antenna gain. This can be seen by studying a parameter known as the point spread function.

3.3.2 Point Spread Function

The response of an interferometer to a point source, the spatial equivalent to an impulse response in the time domain, is commonly termed the point spread function (PSF). Ideally, the PSF should approach that of a filled aperture where an intensity map with a single peak is produced when imaging a point source. However, the central peak is spread due to diffraction and a number of low intensity rings, or sidelobes, are observed in the intensity map [Kong, 1998]. The PSF is equivalent to the antenna gain of the radar. For a uniformly illuminated circular aperture, the antenna gain is based on the aperture diameter, transmission wavelength, and off-boresight angle (θ) as shown in equation 3.5

$$G_{ap} = \left[\left(\frac{\pi(1 + \cos\theta)D}{\lambda}\right)\left(\frac{J_1\left(\frac{\pi D \sin\theta}{\lambda}\right)}{\frac{\pi D \sin\theta}{\lambda}}\right)\right]^2 \qquad (3.5)$$

where $J_1(*)$ refers to the Bessel function of the first kind. Figure 3.5 illustrates the PSF for a filled aperture and represents the optimal point source response that can be achieved with a multiple aperture system.

In the case of an interferometer, with a series of identical apertures, the gain of the antenna is obtained by convolving the gain of a single aperture with impulse functions corresponding to the aperture locations in the physical domain. When working in the image domain, which is the inverse Fourier transform of the system, the gain contribution due to the separation of the apertures is known as the array factor gain, given in equation 3.6 as a function of the image angular coordinates (ψ_i, ψ_j) and the physical projection (x_n, y_n) of the n-th aperture position in the array [Kong, 1998].
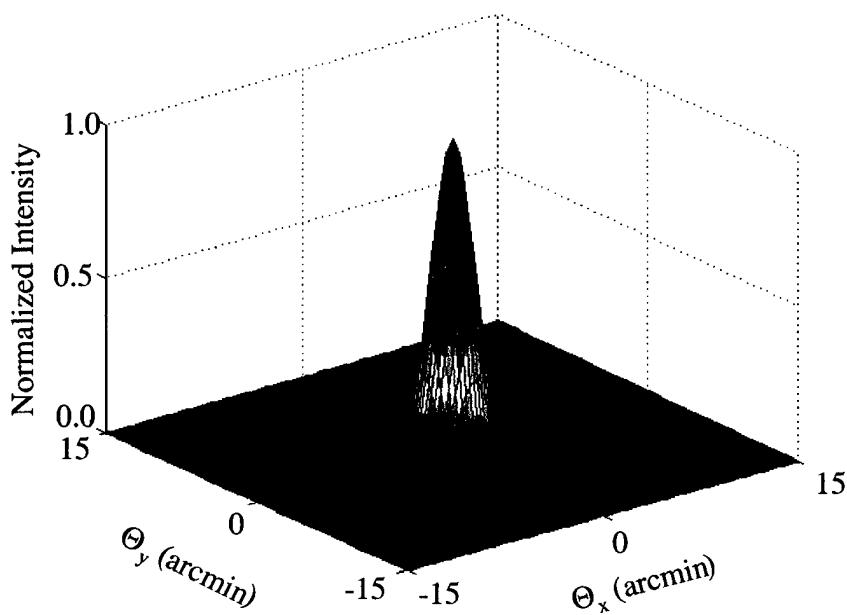
Figure 3.5   Nominal Point Spread Function [Kong, 1998]

$$G_{af} = \left| \sum_{n=1}^{N} \exp\left(-\frac{2\pi i}{\lambda}(\psi_i x_n + \psi_j y_n)\right) \right| \tag{3.6}$$

The resulting gain of the interferometer is the product of the single aperture gain and the square of the array factor gain according to equation 3.7.

$$G_{int} = \left[\left(\frac{\pi(1+\cos\theta)D}{\lambda} \right) \left(\frac{J_1\left(\frac{\pi D \sin\theta}{\lambda}\right)}{\frac{\pi D \sin\theta}{\lambda}} \right) \left| \sum_{n=1}^{N} \exp\left(-\frac{2\pi i}{\lambda}(\psi_i x_n + \psi_j y_n)\right) \right| \right]^2 \tag{3.7}$$

Rather than squaring the inverse Fourier transform of the antennas in the physical domain to obtain the gain of the interferometer, equation 3.7 can also be derived by first taking the auto-correlation of the antennas in the physical domain, which describes the spatial frequencies sampled by the interferometer, and inverse transforming the resulting auto-correlation function. We can take either of these two approaches because convolution in the
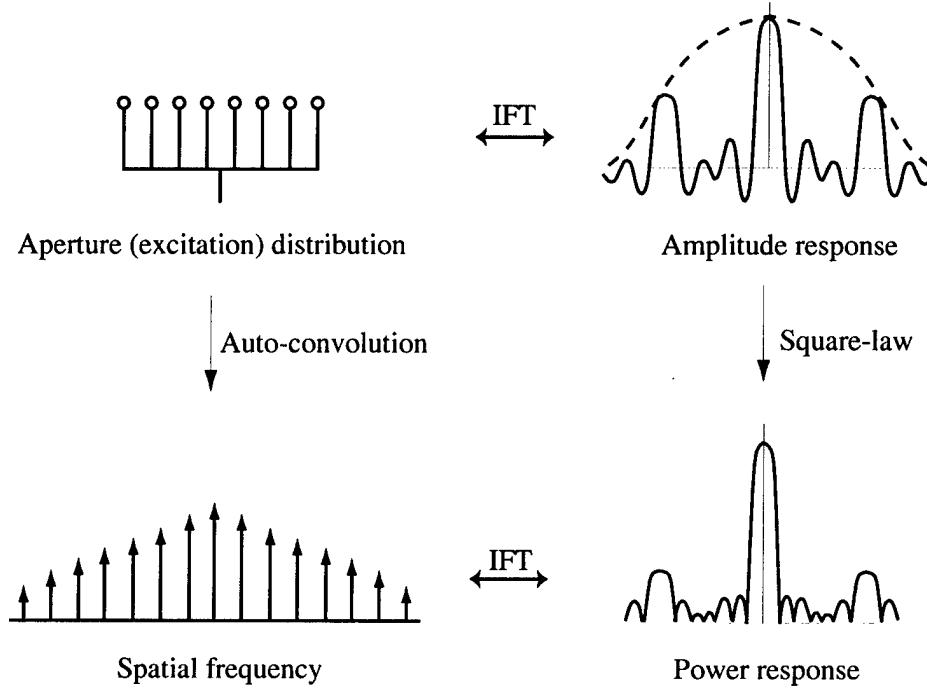
Figure 3.6 Aperture Synthesis with a One-Dimensional Array [Shaw, 1998]

physical domain is equivalent to multiplication in the Fourier domain. The physical interpretation of calculating the interferometer gain via these two methods is demonstrated in Figure 3.6 for a one-dimensional array. In processing the received signals, the PSF is made to scan the entire footprint to ensure the maximum probability of detection is provided for each cell.

3.3.3 Footprint Scan

In single aperture radar systems, the footprint produced by the intersection of the antenna mainlobe with the ground is scanned across the region of interest to detect moving targets. The scan of an individual footprint is intuitively similar to this concept where the region of interest is now represented by the footprint. However, in an interferometric system, the footprint scan does not involve moving the antenna throughout the footprint but is accomplished by post-processing the received signals.
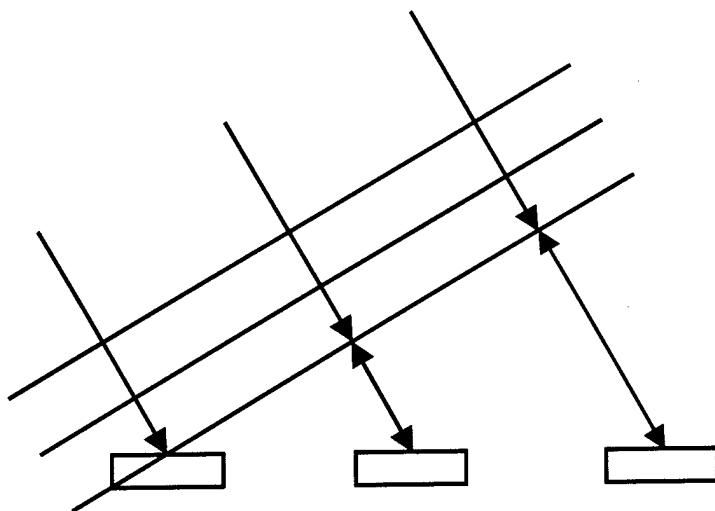
Figure 3.7   Array Steering With Time Delays

A description of this process begins with a series of recorded time domain signals corresponding to the receiver input for each aperture in the cluster from a single transmitted pulse train. By inserting coordinated time delays into each of the signals and adding them together, the wavefronts from a particular direction add constructively, as shown in Figure 3.7. By changing the time delays between the apertures, the mainlobe beam of the synthesized aperture can be made to scan across the footprint, hence the term PSF scan. Ideally, the PSF would solely consist of this mainlobe beam (filled aperture) and reconstruction of the target data could be easily achieved because a small amount clutter return in each cell results from the PSF scan and very little of it would compete with the anticipated target Doppler shifts in these cells. However, a number of grating lobes are present in the PSF corresponding to the finite number of apertures in the array. These grating lobes bring in extraneous data from other areas of the footprint outside the cell that is being scanned. This requires additional processing of the received radar signals to remove this unwanted information. The ability to accomplish this footprint scan post-processing means that the coverage area of the radar system is determined by the diameter of the individual satellite apertures, not the synthesized aperture, thus yielding a much higher area search rate corresponding to the larger footprint area.

3.4 Introduction to Radar Signal Processing

At this point, we shift our focus to the implications of separated spacecraft interferometry on the processing of received radar signals to separate target signals from clutter. In certain radar applications, such as ground mapping, altimetry, and Doppler navigation, ground return is a viable signal. Other radars are able to operate relatively free of ground return because their antenna beams are directed away from the ground. However, nearly all space-based radar systems must contend with ground clutter in order to detect targets. The echoes from fast-moving targets are sometimes isolated from local clutter returns due to the large differences in their respective Doppler profiles. Slow-moving ground targets, on the other hand, do not produce enough Doppler shift in their reflections to separate their signals from mainlobe clutter. In reality, it is difficult to detect targets at any speed from a space-based platform because the large spectral width of the mainlobe clutter dominates the frequency space of the Doppler filter bank [Murray et al, 1997]. Consequently, the level of competing clutter must be suppressed with some form of signal processing to enable detection of these targets. Since the radar platform is remote in space-based applications, on-board processing is desirable [Rabideau et al, 1999]. In the process of designing the signal processor, the system engineer must also consider additional factors such as computational load and efficiency, data storage requirements, system reliability, and overall cost versus performance. This section introduces us to a few prevalent signal processing procedures that have successfully demonstrated high levels of clutter suppression for airborne and space-based GMTI radar systems operating in clutter rich environments. The intent here is not to give a mathematically rigorous development of each individual step that is followed to cancel the clutter return. Instead, the discussion centers on the basic concepts of each method as well as their overall benefits and shortcomings. Ultimately, the best option for radar signal processing from a space-based platform depends on the overall application of the system as well as the requirements and constraints levied by the end user.

3.4.1 Displaced Phase Center Antenna

Due to the platform velocity of the radar, the Doppler spectrum of the ground clutter is spread over a wide range of frequencies caused by the forward displacement of the radar antenna phase center from one interpulse period to the next. If this motion can somehow be eliminated over a series of successive pulses, then the resulting mainlobe clutter spectrum is reduced to a narrow line centered at zero frequency. By adjusting the PRF of the transmitted signal and dividing the antenna into a number of receive segments, the phase center of the antenna when side-looking can be fixed at a precise point in space to cancel the platform motion. This is the premise behind DPCA, one of the simplest clutter suppression methods in radar.

To gain a better understanding of how the antenna motion is removed, consider the three-pulse DPCA example given in Figure 3.8. Between pulse transmission, the antenna moves a distance equal to the product of the platform velocity and the interpulse period (v_pT). The use of segments of the antenna on receive causes the phase center (plus signs in Figure 3.8) to be displaced in the opposite direction by $2v_pT$ between pulses. This effectively fixes the location of the phase center for the three pulses shown. The distance
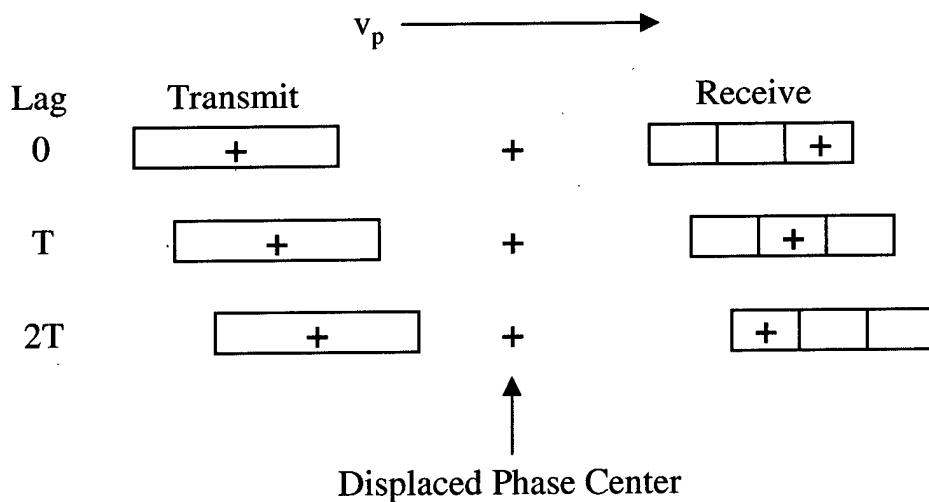
Figure 3.8   Three-Pulse DPCA Cycle

covered by the antenna between transmit and receive corresponds to the round-trip transit time of each pulse to the ground and back. Once the pulse reflections are received, the signals in the forward and middle segments are delayed by $2T$ and T respectively, and the signals from adjacent antenna segments are then subtracted to cancel the contribution from clutter [Cantafio, 1989]. The returns from moving targets remain due to the Doppler shifts that results from their motion relative to the radar. For a more in-depth discussion of DPCA beyond this simplified example, refer to Chapter 18 in Skolnik, 1990 or Chapter 11 in Cantafio, 1989.

Although DPCA is an effective technique for suppressing clutter returns, it does have some disadvantages. Specifically, the limitations of DPCA include the following [Stimson, 1998]:

- The PRF is tied to the platform velocity of the space-based radar
- Very tight constraints are placed on the motion of both the spacecraft and the antenna
- The phase and amplitude characteristics of the antenna segments and of the receive channels for all segments must be precisely matched
- Only a fraction of the aperture is used to receive at any one time

Various methods have been developed to alleviate some of these constraints. For instance, phase and amplitude variations can be corrected by comparing the signals in adjacent range bins [Murray et al, 1997]. In addition, certain correction factors can be applied to the received signals when the antenna is not side-looking [Cantafio, 1989]. In situations where the radar needs to be able to scan its entire field of regard or requires more freedom in selecting the PRF, a more generalized signal processing strategy is necessary that does not suffer from the same limitations as DPCA. The most popular alternative for space-based GMTI radar is space-time adaptive processing.

3.4.2 Space-Time Adaptive Processing

Since the reflections from targets and the ground received by space-based radars are functions of space and time, the method used to cancel the clutter return while preserving the

target signal must operate in the same dimensions. Concurrent spatial and temporal processing of the signals received by multiple apertures allows the formation of a narrow two-dimensional notch that nulls the competing clutter at little or no expense to the target signal [Klemm, 1998-1]. This form of signal processing is commonly known as STAP. Actually, DPCA is a special case of STAP because multiple looks from the same point in space at different times is a specific application of space-time processing. A more generalized application of STAP that does not suffer from the same drawbacks inherent in the DPCA method is presented in this subsection. Those who require a more rigorous treatment should consult the comprehensive works by Ward, 1994, and Klemm, 1998-2. Furthermore, a wealth of literature focuses on the implementation of STAP signal processing in myriad airborne and space-based radar applications, including more recent publications by Kogon et al, 1999, and Rabideau et al, 1999. The STAP method can significantly improve the target detection capability of a space-based radar system provided a few necessary conditions are met.

For the STAP processing of received signals, the idea is to emphasize the signals arriving from the angle and Doppler frequency that corresponds to a hypothetical target location and velocity while rejecting all other significant energy. To accomplish this task in theory, a series of temporal taps (based on the PRF) for each subarray of the radar antenna are needed to formulate the covariance matrix of the interfering sources and calculate its inverse. Transforming this matrix from the space-time domain gives the angular locations and Doppler spectra of the received clutter. Unfortunately, the computational requirements associated with the real-time implementation of this method are overly excessive for realistic numbers of spatial and temporal channels. As a result, sub-optimal STAP approaches are necessary that still provide good probabilities of detection at a smaller computational cost [Nohara, 1995]. In most cases, the clutter covariance matrix is estimated from the received signals based on a statistical model of the clutter in the footprint. As long as this model accurately represents the true clutter returns in these signals, then the STAP method virtually guarantees optimal system performance [Kogon et al, 1999].

The choice of either DPCA or STAP for processing received signals in space-based radar involves the consideration of a number of issues. Although STAP is not restricted to specific PRFs and side-looking antenna arrays, the improved capabilities of this technique come at the cost of an increased antenna complexity and computational burden. In addition, DPCA requires a somewhat rigid geometry for the antenna subarray while the presence of target echoes in the reflections used to estimate the clutter covariance matrix in STAP causes attenuation of the target signals [Nohara, 1995]. Finally, the angle measurement precision for both signal processing methods is degraded because they are not able to extract the angular location of target returns in the antenna beam [Stimson, 1998, and Kogon et al, 1999]. Despite the successful demonstration of DPCA and STAP in many airborne and space-based applications, the weaknesses in each of these techniques calls for a more capable signal processing architecture in future space-based radar systems.

3.5 Signal Processing for Multiple Aperture Systems

When working with a sparse aperture space-based radar system such as TechSat 21, the challenge for the system engineer is to select the best signal processing strategy that utilizes the benefits of separated spacecraft interferometry to achieve an even higher level of clutter suppression than is attainable in single aperture systems. The key is to suppress the clutter that appears in the same range-Doppler cell as a target using the inherent spatial resolution of the satellite cluster [Miller, 1999]. This section starts off with a discussion of the STAP method tailored to sparse aperture systems, then presents a recently developed technique for eliminating clutter in space-based radar applications known as deconvolution.

3.5.1 Adaptation of Current Methods

Although STAP has been extensively used in existing airborne and space-based radar systems with single apertures, only recently has it been adapted to multiple aperture systems to address the problem of clutter suppression in ground-looking radars [Miller, 1999]. DPCA is not a viable option for TechSat 21 because the system must be able to scan any

ground location within its field of regard. STAP processing takes advantage of the high spatial resolution resulting from the narrow pencil beam formed by the synthesized aperture of the cluster. By combining this spatial resolution of a multiple aperture system with the fine range and Doppler resolution inherent in MTI radars, ground clutter located in the same range-Doppler cell as a target can be suppressed. The level of clutter suppression achievable by STAP determines the likelihood that targets are detected in the footprint.

One STAP method begins by combining the received radar signals that are each sampled with a different set of time delays. This forms a synthesized antenna gain pattern (the PSF from Section 3.3.2) with a rich set of lobes and nulls resulting from the limited number of apertures in the cluster. The processing assumes some hypothetical target location and velocity, which requires a large set of target state hypotheses to ensure detection of any target in the radar footprint. STAP is designed to extract the target returns by placing a null of the antenna gain pattern over the ground regions that have a range rate corresponding to what was assumed for the hypothetical target (Figure 3.9). The width of this null is
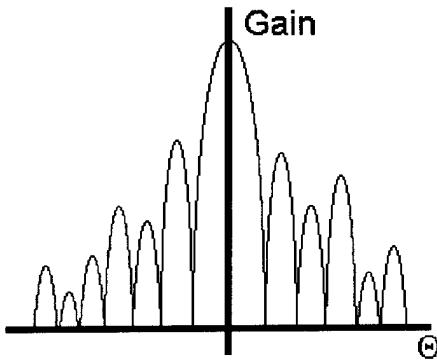
Figure 3.9   Simplified Representation of STAP

proportional to the number of apertures in the cluster and the cluster baseline [Nohara, 1995]. Since the null locations are matched to a target state hypothesis, any actual targets that match this state are amplified by the full gain of the antenna, thus allowing the signal to rise above the competing clutter. In the end, this form of STAP processing for multiple

aperture space-based GMTI radar functions by optimizing the placement of nulls in the footprint to boost the SNR for the assumed target.

As demonstrated in Section 3.3.1, the idea of applying the concepts of interferometry to improve the performance of radar systems is not new. However, there are several drawbacks to current signal processing methods such as STAP:

- Clutter is treated in much the same way as noise, whereby an assumed statistical distribution is used to characterize how large the return would be from any given cell

- The limited number of apertures in the cluster restricts the number of interference sources that can be eliminated

- Some requirement is placed on the cluster geometry to maintain an adequate distribution of the apertures

- The processing methods utilize only a small portion of the available information from the system

Because the clutter return is a statistical quantity, the only option is to ensure that the model used to estimate the clutter contribution in the received signals is as accurate as possible. It is also important that we carefully determine the positions of the clutter nulls to suppress the strongest interference sources since an insufficient number of degrees of freedom exist to cancel all of the competing clutter. Our past approach to remedy the remaining disadvantages of STAP began by trying to optimize two-dimensional cluster geometries for TechSat 21, thereby enhancing the isolation capability of the system [Kong, 1998, and Sedwick et al, 1999]. It was quickly determined that although stationary geometries could be found which promised excellent performance, propagation of these geometries in time as a result of orbital motion quickly cause the performance to degenerate to an unacceptable level. We then began to attempt an optimization of the satellite configurations over all time, thereby generating a level of performance that may be suboptimal at any given time but is acceptable over all times [Hacker et al, 1999]. Application of statistical methods were investigated, partially in hope of demonstrating that the reliance on the cluster geometry could be avoided by somehow utilizing the diversity of the PSF over time. Perhaps by using the additional information available as the geometry

changed, the variations in performance could be averaged out, and increased overall. It was along these lines of thought that we discovered an abundance of available information in the received signals that was not being used when only a single snapshot in time was considered. This eventually led to the development of a new signal processing technique for multiple aperture space-based radar.

3.5.2 New Approach: Deconvolution

We now see that prevalent signal processing techniques such as STAP can be adapted to multiple aperture systems and still provide sufficient target detection capability. However, the STAP method must still work with a statistical representation of the competing clutter in the received signals to determine the null locations. The inherent weakness here is that there are times when the actual clutter statistics do no match the model in the system, limiting the achievable suppression level and increasing the interference with the target signal. In addition, careful maintenance of aperture positions in the cluster is necessary to achieve an adequate level of clutter suppression. Although STAP is extremely useful in single aperture systems, signal processing for multiple apertures requires a better approach.

A potential remedy is to redesign the radar signal processor in such a manner that takes advantage of the spatial diversity of the apertures to cancel the entire clutter return in received radar signals. The best option at this time is a technique derived from image processing called deconvolution. This method depends not on the clutter statistics but solely on the Doppler profile of the clutter. While the former is random in nature, the latter is exact because it is based on the known angular locations of the cells in the footprint. Therefore, this signal processing algorithm is able to distinguish between targets and clutter in the signals received by the radar due to the difference in their respective frequency characteristics. By separating the clutter and target returns in this manner, noise becomes the only source of interference in the system, thus maximizing the probability of detection. After briefly discussing the origins of deconvolution, the next two subsections explain

how perfect cancellation of clutter return is achieved for multiple aperture space-based radar systems. Overall, the deconvolution method promises significant advancement in the progress towards the development of an operational separated spacecraft GMTI radar system.

The deconvolution method has its roots in image processing [Sedwick et al, 2000]. In this process, the scan of the footprint (Section 3.3.3) is conducted without isolating the frequency content of the received signals. Mathematically, this scanning can be represented by convolving the PSF with the intensity map of the ground scene. For a sufficiently large aperture, the PSF can be approximated with a delta function, giving the convolution relationship in equation 3.8.

$$I(AZ, EL) \cong \int \delta(\overline{AZ}, \overline{EL}) S(AZ - \overline{AZ}, EL - \overline{EL}) d\overline{AZ} d\overline{EL} \qquad (3.8)$$

In this ideal case, the ground scene is perfectly mapped into the image that is recorded. The convolution in spatial angle from equation 3.8 becomes a product relationship when transformed to the spatial frequency domain (Section 3.1) as shown in equation 3.9.

$$\tilde{I}(u, v) = \overline{G}(u, v)\tilde{S}(u, v) \qquad (3.9)$$

For a true delta function corresponding to an aperture of infinite extent, all spatial frequencies in the ground scene are identically mapped to the resulting image. Since the aperture is finite, certain spatial frequencies are weighted higher than others proportional to the *sinc* shape of the gain pattern (Section 2.3.2). The image is constructed by recording these spatial frequencies directly rather than conducting the PSF scan across the scene. Dividing this image by the PSF to obtain the true ground scene describes the deconvolution process for a single large aperture.

If we now consider a sparse array of much smaller apertures, which can be approximated as a series of delta functions for each aperture in the spatial frequency domain, only certain spatial frequencies are sampled according to the baselines in the array (Section 3.1). The resulting PSF contains grating lobes that bring unwanted information from other reso-

lution cells in the ground scene into the mainlobe cell during the convolution. In theory, we would like to deconvolve the PSF from the image to obtain the true ground scene by dividing out the gain pattern matrix. However, since this matrix contains zero gain values corresponding to the unsampled spatial frequencies, the matrix cannot be simply divided out. Keep in mind that this operation is not a matrix divide, but is done element by element. In this case, a number of deconvolution algorithms such as CLEAN and maximum entropy [Thompson et al, 1994] have been developed to reconstruct the ground scene from the image data.

The deconvolution concept has been successfully implemented in a wide variety of multiple aperture imaging applications. For example, the CLEAN algorithm was studied by Enright in the context of acoustic interferometric imaging [Enright, 1999]. In addition, Winings applied the deconvolution method to extract the scene change between two infrared images of the same location taken at different times [Winings, 1997]. With radar signal processing, we have an additional dimension provided by the frequency content in the received signals to aid in the deconvolution process.

3.5.3 Generalized Example

To gain a better understanding of the implementation of deconvolution in space-based radar, we present the following example from Hacker et al, 1999, to illustrate the clutter cancellation capabilities of this signal processing method. It is useful to express the deconvolution process in terms of linear algebra. As the PSF scan is performed across the range bin (Section 3.3.3), the mainlobe is placed over each cross-range cell and power contributions from clutter and any targets are filtered through the bank of Doppler bins. Let's assume that our simplified radar system is currently side-looking and consists of three cells in the range bin, five Doppler bins, and an asymmetric point spread function as illustrated in Figure 3.10. The targets are represented by their individual normalized radar cross sections in the cells where they are located and the clutter is assumed to have a constant RCS ($\bar{\sigma} = 15$) over the entire range bin.

Point Spread Function   Cross-Range Cells
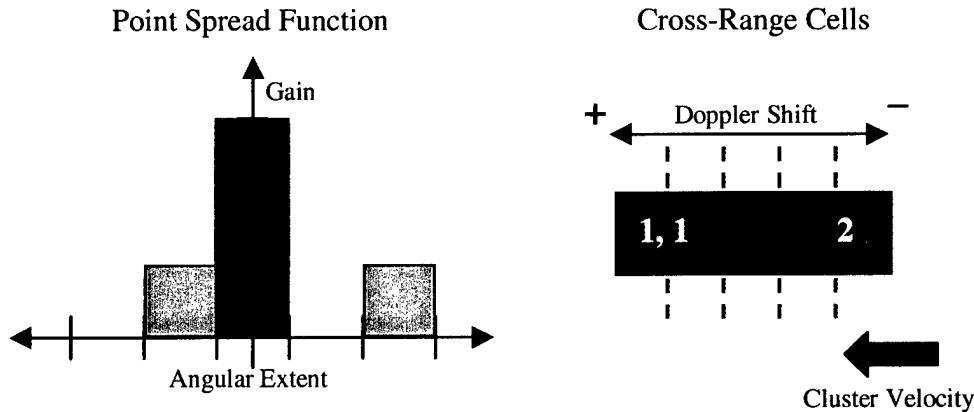
Figure 3.10 Simplified Radar System to Demonstrate Deconvolution

As each cell is scanned, the RCS values of the clutter and any targets in the cell are multiplied by the mainlobe gain of the PSF. We must also remember that grating lobes in the PSF cause additional contributions from clutter and targets located in other cells. The resulting power contributions are filtered into a set of frequency bins based on the respective Doppler shifts of the sources. Equation 3.10 demonstrates this process for our example problem.

$$
\underbrace{\begin{bmatrix} 27 & 20 & 3 & 6 & 12 \\ 9 & 15 & 28 & 9 & 1 \\ 0 & 9 & 9 & 21 & 27 \end{bmatrix}}_{y} = \underbrace{\begin{bmatrix} 3 & 0 & 1 \\ 1 & 3 & 0 \\ 0 & 1 & 3 \end{bmatrix}}_{A} \underbrace{\begin{bmatrix} 9 & 6 & 1 & 0 & 1 \\ 0 & 3 & 9 & 3 & 0 \\ 0 & 2 & 0 & 6 & 9 \end{bmatrix}}_{x}
\tag{3.10}
$$

The rows of the y-matrix represent the series of power spectra obtained by the PSF scan while the columns of the x-matrix contain the actual target and clutter information (in a particular frequency band) as it would appear on the ground. The analogy is similar to that of the image convolution given in Section 3.5.2. Also, the three rows and five columns of these matrices correspond to the number of cross-range cells and Doppler bins respectively. If one considers how the information is actually processed, a column of data in the x-matrix would be filtered into a single Doppler bin. However, the information in each row of that column would be scaled by the antenna gain pattern at that cell's location on

the ground. The first row of the A-matrix, must therefore be the PSF, with the main lobe properly positioned above the correct cell. The resulting superposition of power returns would then appear in the top-left element of the y-matrix, and be the total power that appears in the first Doppler bin. Similarly, as the first row of the A-matrix consecutively multiplies each column of the x-matrix, the power received in each Doppler bin appears in the proper position in the y-matrix. The information contained in the first row of the y-matrix then represents exactly what would appear after passing the time domain signal through the Doppler filter bank.

If the time delays are then changed to place the peak of the PSF on the second cell of the range bin, and the process is repeated, the new shifted PSF appears in the second row of the A-matrix, and the resulting power spectrum appears in the second row of the y-matrix. It can be seen that operationally, the scan would be performed by time shifting the data streams and recording the resulting power spectrum in the rows of the y-matrix. The A-matrix can be generated using the known geometry of the array, and provided it is non-singular, can be inverted to solve the set of equations for the x-matrix. The targets are then uniquely identified in cross-range and Doppler. The same holds true for clutter, and depending on the resolution of the Doppler bins, no targets above a very low minimum detectable velocity (corresponding to the width of a single Doppler bin) should fall in the same matrix element as clutter.

From the azimuth and elevation angles of the corresponding ground cell, it is always possible to determine which cells of the matrix should represent clutter. Because the radar is side-looking (in this example), the clutter return is found roughly along the diagonal of the x-matrix (highest Doppler shift corresponding to left-most cell of the footprint) and anything else represents a target return. Ultimately, we are able to achieve an almost complete rejection of clutter return in the received signals, thereby reducing the interference sources to system and receiver noise and giving a solely noise limited probability of detection. It is now no longer necessary to model the statistics of the clutter return, since the isolation of the clutter is not dependent on its statistical nature, but on the fact that the clutter does

not change over the dwell time. This generalized example gives only a partial demonstration of deconvolution in space-based radar. However, only an application of this signal processing technique with actual received radar signals will give us a true appreciation of the superior clutter suppression capability provided by deconvolution.

3.5.4 Deconvolution in Space-Based GMTI Radar

Expanding the simplified deconvolution example given in the last subsection to a realistic description of this signal processing method in space-based GMTI radar is fairly straightforward. From a typical ground scene in a single range bin, the interferometric image is constructed by scanning the PSF over each cross-range cell. Adding receiver noise to the result gives the power spectrum measured in the signal processor. The ground scene is subsequently reproduced by subtracting the noise power from the spectrum and deconvolving the result with the PSF matrix. Since some form of ambiguity is always present in the received signals, the processing must account for these ambiguities and remove them to obtain an accurate representation of the ground scene. The following paragraphs explain each of these steps in greater detail.

Receive Process

To illustrate the deconvolution method for space-based GMTI radar, the diagram given in Figure 3.11 serves as the framework for this discussion. Starting on the right side of the first row, the strip represents the cross-range cells in a single range bin within the footprint. To its left is a dashed box containing a gray-scale strip that displays the one-dimensional gain pattern (PSF) used to scan the range bin. The darkest region refers to the mainlobe of the PSF, meaning that the top cross-range cell is currently being scanned. Because the gain acts as a matrix multiplier, the result from this multiplication of the gain pattern row and the column of cross-range cell is demonstrated by the single entry in the dashed box at the far left of the top row. Without the frequency information in the received signals, this process would resemble the imaging example in Section 3.5.2.
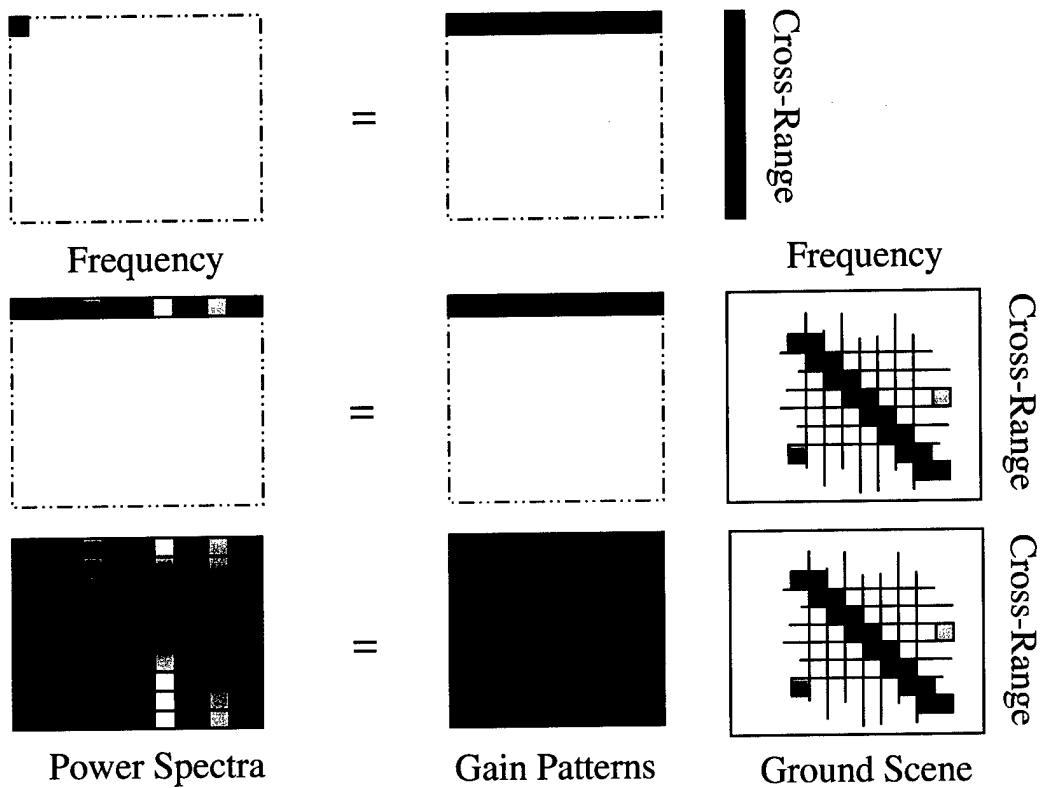
Figure 3.11   Matrix Representation of the PSF Scan Within a Single Range Bin [Sedwick et al, 2000]

Continuing with the second row in Figure 3.11, a bank of Doppler filters is provided for each cross-range cell to measure the Doppler spectrum associated with the clutter and any targets it may contain. This information adds a second frequency dimension to the cross-range cells, shown on the far right of the figure. The strip represents the return from ground clutter because it is present in every cross-range cell and has a predictable Doppler profile based on its location relative to the radar (Sections 2.6.1 and 4.2.4). The returns from moving targets are located in the ground scene matrix according to their individual locations and Doppler shifts. Keep in mind that this matrix is an exact replication of the true ground scene and is the information we ultimately wish to reproduce. As before, the antenna gain pattern, acts as a multiplier on the range bin data and amplifies all frequencies at each cross-range point by the same amount. The top cross-range cell experiences the highest amplification since it is being scanned by the mainlobe. The result at the far

right is a Doppler spectrum for the top cross-range cell where the target signals are embed-ded within the clutter.

The third row in Figure 3.11 represents the complete PSF scan of the range bin. As the mainlobe of the antenna pattern is scanned across the range bin, the distribution of the gain pattern shifts to place the mainlobe over each cross-range cell. The power spectrum that results from the PSF scan is illustrated at the far left. We can tell from this diagram that target echoes are present in the received signals. However, the only way that we can char-acterize the locations and Doppler shifts of these targets is to compute the inverse of the gain pattern matrix and used it to deconvolve the power spectrum to yield the true ground scene. At the end of this process, the target signals will be completely separated from the clutter return as long as their respective Doppler shifts exceed the spectral width of the clutter. As we have said all along, the sole source of interference in the detection process after deconvolution is noise, so the target detection capability of the radar system is deter-mined by the post-processing signal-to-noise ratio.

Reproducing the Ground Scene

The illustration of the receive process in Figure 3.11 is not completely accurate. The sig-nals received by the radar also contain noise which can be represented as an additive term to the power spectrum resulting from the PSF scan. This corrected version is demon-strated in Figure 3.12. Even this version is not completely accurate because the noise and

$$\begin{pmatrix} \text{Measured} \\ \text{Power} \\ \text{Spectra} \end{pmatrix} = \begin{pmatrix} \text{Channel} \\ \text{Noise} \end{pmatrix} + \begin{pmatrix} \text{PSF} \\ \text{Variations} \end{pmatrix}\begin{pmatrix} \text{True} \\ \text{Ground} \\ \text{Scene} \end{pmatrix}$$

Figure 3.12 Deconvolution Process for a Single Range Bin

signal amplitudes are added and then squared, which would give a different result than simply adding the noise power. However, since the noise in each channel has the same

statistics but is uncorrelated with either the signal or the noise from other channels, it is sufficient to subtract off the mean noise power allowed through each of the channels. Therefore, the mathematical representation of the deconvolution process, based on Figure 3.12, is given in equation 3.11

$$y = n + A \cdot x \tag{3.11}$$

The goal of the deconvolution algorithm then is to reproduce the true ground scene by using equation 3.12.

$$x = A^{-1} \cdot (y - n) \tag{3.12}$$

This calculation would give the spectral content of the clutter return as well as the locations and Doppler shifts of any targets in the range bin. The entire process is repeated for each range bin to produce a three-dimensional representation of the spatial (range and cross-range) and frequency properties of all objects in the footprint.

Removing Ambiguities

If the PRF is too high, the returns from more than one range in the footprint are received simultaneously by the radar, making the range measurement ambiguous. Lowering the PRF causes Doppler ambiguities as the Doppler spectra of the received signals, repeated at
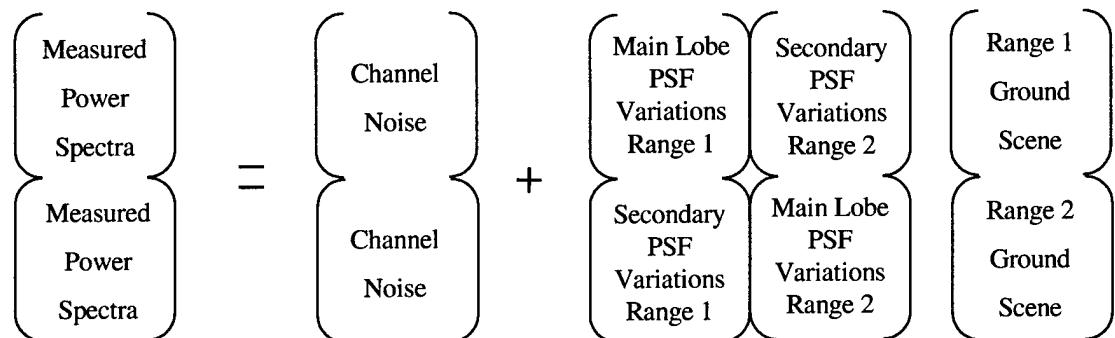
Figure 3.13 Deconvolution with Range Ambiguities

intervals equal to the PRF, begin to overlap. Please refer to Section 2.4.3 for a more thorough presentation of range and Doppler ambiguities.

When the range is ambiguous, power return is received from multiple areas in the footprint through the grating lobes as the PSF is scanned across a range bin. Simply scanning one range bin does not generate enough independent measurements to separate the information between the ambiguities. In this case, all of the ambiguous range bins must be processed simultaneously. Figure 3.13 demonstrates this process for two range ambiguities. In theory, we could process all of the range bins at once regardless of the number of range ambiguities in the footprint. However, the computational burden of inverting such a large gain pattern matrix scales as the number of bins squared, and would be prohibitive in most situations. Instead, there is a computational advantage to making the range unambiguous and removing the resulting Doppler ambiguities.
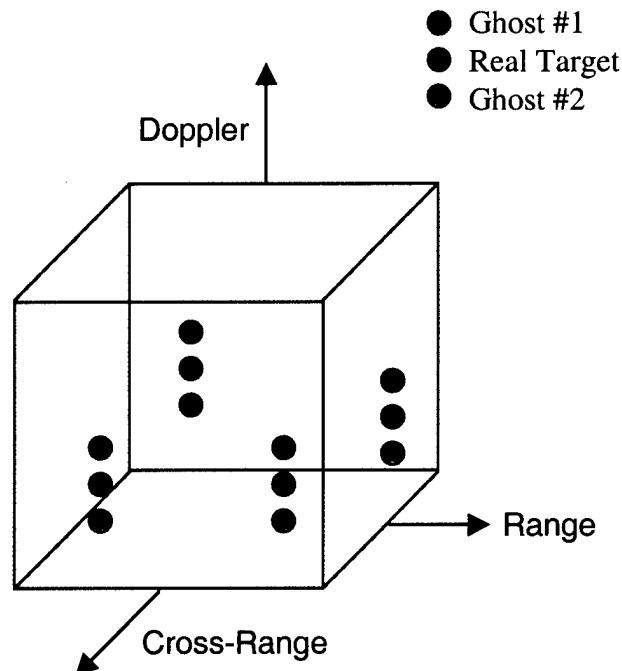
Figure 3.14   Effect of PRF Switching on the Frequency Location of Targets and Ghosts [Sedwick et al, 2000]

When the the measured Doppler frequency is ambiguous, ghost images of the targets appear in the incorrect Doppler bins. This is a result of the PRF being too low, and causing replicated target frequencies to alias into the primary frequency band. The frequency where the aliased target (ghost) appears depends on the value of the PRF. As a result, the PRF can be varied between successive coherent pulse intervals to identify which targets are actually ghost images. This technique is known as PRF switching (Section 2.4.3). The effect on target signals and their ghost images from PRF switching is illustrated in Figure 3.14. As a number of these data cubes are noncoherently integrated to reduce the variations in noise, the true targets continue to grow in strength. The ghost images, which do not occur in the same cell from one interval to the next, do not combine, and therefore remain at the same level during the integration in much the same way the noise does. In this way the Doppler ambiguities can be suppressed, so ghost images do not exceed the target detection threshold and indicate a false alarm.

Chapter 4

REPRESENTATIVE SPACE-BASED RADAR SYSTEM MODEL

The performance of a multiple aperture radar system is somewhat difficult to assess in a clear and concise manner. Furthermore, defining a single metric to use in comparing system architectures that captures all of the necessary radar performance parameters can be a monumental task. However, a quantitative systems analysis methodology known as GINA [Shaw, 1998] has been applied to this problem to identify certain performance metrics applicable to space-based radar systems (Section 4.1). These metrics center around the probability that a valid target is detected in the presence of noise and clutter. The radar performance model presented in this chapter analyzes the radar performance from two unique perspectives. Section 4.2 focuses on the performance variations within a single radar footprint. Depending on the location of the ground area under surveillance, the ability to detect targets ultimately depends on the projection of the satellite cluster in the direction of interest. The study is expanded in Section 4.3 to evaluate the global system performance of the complete constellation of satellites based on the statistical availability of all ground locations within the coverage area of the clusters. The model breaks the analysis into a series of modules that take a set of design parameters, such as the number of satellites in each cluster, the aperture diameter, the orbital altitude, and the antenna transmission power, and steps through the calculations necessary to evaluate the performance metrics. This approach is very useful because each module can be easily corrected, upgraded, or integrated into a larger system-wide model that incorporates other key design issues including the bus, payload, operations, etc. The model was constructed from the

current design for TechSat 21. However, the hope is that the reader will realize that any radar system can be modeled in this manner as long as each module accurately captures the physics that govern their overall performance capabilities.

4.1 Radar System Design Trades: Application of the GINA Methodology

Modern advancements in satellite technology continue to drive the development of state-of-the-art systems that provide a wide range of services such as navigation, communication, information transfer, and global surveillance. Many applications that were once thought impossible from space-based platforms are now readily available worldwide. But how do we progress from the individual needs of multiple customers to a system design that can best satisfy these demands? Better yet, how do we translate a set of system requirements into a detailed blueprint of an actual system that provides the highest benefit for the lowest cost to the end user? This task may seem rather daunting at first without a rigorous framework to guide the system engineering process. Fortunately, a generalized information network analysis methodology (GINA) has been developed that allows the system engineer to characterize the quality of service provided by a system with a set of standardized and measurable quantities [Shaw, 1998]. These parameters can be used to assess the performance of different system architectures to identify the most capable yet cost-effective design.

Previous work has shown that all envisioned satellite systems can be represented as information transfer networks that gather information of interest, perform some amount of interpretation, and disseminate the data to other system components. The quantity, quality, and availability of information provided to the end user is a meaningful gauge of the quality of service provided by the system over all likely operating conditions. Four parameters can be defined to evaluate the system capabilities [Shaw, 1998]:

- **Isolation** characterizes the system's ability to isolate and classify the information signals from different sources within the field of regard

- **Rate** measures the time required to transfer useful information from its source to anywhere it is needed

- **Integrity** evaluates the probability of making an error in the interpretation of information caused by outside interference

- **Availability** represents the instantaneous probability that given isolation, rate, and integrity demands are being satisfied

For space-based radar, isolation is specified by the ground resolution, MDV, and velocity precision of the system. Rate refers to the total time required to search a theater of interest (area search rate) as well as the time between searches (revisit rate). The probability that a target echo is detected in the presence of noise and clutter defines the integrity of the system. Finally, availability is again a measure of the probability that specified values of the other capability metrics are achieved. These values can be derived from the system requirements and constraints provided by the customer. The degree to which a system fulfills these needs is a critical consideration in the analysis process. By adapting these metrics to the system of interest, valuable design trades can be conducted to help the system engineer recognize viable architectures that provide the required level of performance.

Starting with the capability metrics for space-based radar, the framework of GINA can be applied to develop a model that allows us to trade various elements of the system design. The goal is to discover the key design trends that have a considerable impact on the performance capability of the system. Unique system architectures for TechSat 21 are described by four parameters: number of satellites in a cluster, orbital altitude, aperture diameter, and antenna transmission power. Other parameters, such as the number of clusters in the global constellation, also specify distinct system designs, but the quantities listed above represent the overall performance of the radar. In addition, a number of constants are included in the model based on the requirements and constraints of the operational system. Using the concepts developed in Chapter 2, the TechSat 21 radar model is divided into a series of modules that capture the various operational and performance considerations of this system. The system architecture used throughout this chapter to describe the individual modules is given in Table 4.1. The complete model can be used to

TABLE 4.1 Example TechSat 21 Architecture

Parameter	Value
Number of Satellites	8
Orbital Altitude	800 km
Aperture Diameter	2.4 m
Antenna Transmission Power	200 W
Ground Location (Elevation)[a]	45°
Ground Location (Azimuth)[a]	90°

a. Only applies to the radar footprint model.

conduct design trades particular to the radar system and can also be incorporated into a larger system-wide model that includes all the important aspects of the entire TechSat 21 system design.

4.2 Radar Footprint Model

Now that we have a systematic framework provided by GINA for our performance analysis of TechSat 21, we need to figure out the best approach to modeling the radar system. There are two unique perspectives we can use to guide us in this process. First of all, we can evaluate the variations in performance across the footprint projected by the satellite cluster. Our other option is to characterize the performance capability within the cluster's field of regard (coverage area). Models of the footprint and the coverage area have been developed for this study. This section deals with the footprint model while the coverage area model is saved for the next section. Beginning with the general parameters of the system, the footprint model calculates the receive antenna pattern based on the projection of the individual satellite locations on the ground and combine it with the properties of the footprint to evaluate the probability of target detection in the presence of noise and clutter. The resulting availability plot illustrates the performance capability that we can expect from a single footprint. The actual MATLAB code for this model is contained in Appendix A.

4.2.1 General Radar Parameters

The first step to follow in modeling the TechSat 21 radar footprint involves the calculation of certain general characteristics based on the operational constraints of the system. These range from the properties of the pulse waveform to various physical specifications pertaining to the cluster. The following paragraphs explain the most meaningful parameters that are evaluated within this module.

Maximum Detection Range

The maximum distance at which a space-based radar can detect targets depends on three properties of the system. The first two are geometrical while the third is a requirement on signal-to-noise ratio. The orbital altitude sets the absolute maximum range for the radar, according to equation 4.1, based on the distance to the horizon [Cantafio, 1989].

$$R_{max} = R_e \, \mathrm{acos}\left(\frac{R_e}{R_e + h}\right) \tag{4.1}$$

The other geometric quantity that can limit the radar detection range is the maximum off-boresight look angle for the electronic antenna. As the antenna beam is steered away from nadir, the projected length of the antenna is shortened by the cosine of the look angle. Although negligible at small angles, this effect becomes increasingly severe at larger angles. The reduced aperture area in the direction of illumination, which causes an increase in beamwidth and a decrease in gain, effectively restricts the maximum off-bore-sight angle to $\pm 60°$ [Stimson, 1998].

Beyond these geometrical constraints, the received signals must still meet a minimum SNR limit to permit target detection. In most situations, the customer sets a minimum probability of detection in the system requirements. This quantity, combined with the number of integrated pulses and the false alarm probability, defines the minimum SNR needed to detect target signals in the presence of noise (see equation 4.12 in Section 4.2.6). The most restrictive value from the location of the horizon, the maximum

look angle of the antenna, and the minimum SNR is used to establish the maximum detection range based on the chosen TechSat 21 architecture.

Cluster Baseline

The maximum separation distance between the individual apertures in a satellite cluster is known as the cluster baseline. This parameter can be thought of as the diameter of the synthesized aperture that results from the combination of the received signals from an array of sparse apertures located on separate spacecraft. As will be explained in Section 4.3.4, the baseline determines both the cross-range resolution and minimum detectable velocity of the cluster. Therefore, the required isolation capabilities of the radar system establish the minimum baseline for a TechSat 21 cluster.

While the range resolution is set by the received pulse width after pulse compression (Section 2.5.3), the cross-range resolution of the cluster results from the projection of the baseline in the direction the radar is looking. Since this projection decreases as the elevation angle moves from nadir to the horizon, the cluster baseline is sized to achieve the required cross-range resolution at the maximum detection range. Alternatively, the MDV comes from the frequency spread of the mainlobe clutter, which again is a function of the illuminated ground location and the baseline. It is assumed that targets cannot be detected if their echoes fall in the spectrum of the mainlobe clutter, so the required MDV also fixes the minimum baseline to ensure detection of slow-moving targets. The actual cluster baseline is chosen from the largest result from these two considerations.

Additional Pulse Properties

The properties of the transmitted pulse are also calculated in this module. Based on the maximum detection range of the cluster, the pulse repetition frequency is selected such that no range ambiguities are present in the footprint (Section 2.4.3). The PRF and the antenna duty cycle establish the width of the transmitted pulse while the required range resolution at nadir sets the compressed pulse width. Although the received signals contain Doppler ambiguities caused by such a low PRF, the frequency range of the mainlobe clut-

ter plus the maximum anticipated target Doppler shift is calculated assuming that these ambiguities are resolved using the deconvolution signal processing method described in Section 3.5. The area search rate for this model is found using equation 4.2 based on a continuous search of the field of regard by the cluster.

$$ASR_{search} = 2v_p R_{max} \sin(EL_{max}) \tag{4.2}$$

Finally, the spatial and velocity resolution are evaluated for the specified location of the footprint. A more complete discussion of these resolution parameters is given in Section 4.3.4. All of these quantities are used by other modules in the model to properly assess the capability to detect targets in the radar footprint. With these basic parameters, we now need to figure out how to optimize the satellite locations in the cluster to maintain the best configuration for maximum performance.

4.2.2 Satellite Configuration

Based on the cluster baseline set by either the required MDV or cross-range resolution, the chosen configuration of the satellites in the cluster must maintain an adequate spatial diversity of the apertures to ensure that a sufficient target detection capability is provided in all directions. In Section 3.2.2, we presented a free orbit solution for a separated space-craft radar interferometer that fulfills this condition. However, the actual placement of the individual satellites in these orbits has yet to be addressed. The only requirement here is to prevent the cluster geometry from degenerating to an unacceptable distribution as the satellites move in their orbits.

The satellite locations used in this module are derived from the spacings with non-redundant baselines for three to eleven apertures calculated by Leech, 1956, and applied by Shaw, 1998, to linear, side-looking TechSat 21 arrays. To accommodate clusters with up to sixteen satellites, the eleven aperture array is expanded in a manner where the spacing between the individual satellites is still non-redundant. However, it must be pointed out that some of the baselines in the cluster are now repeated because the non-redundancy
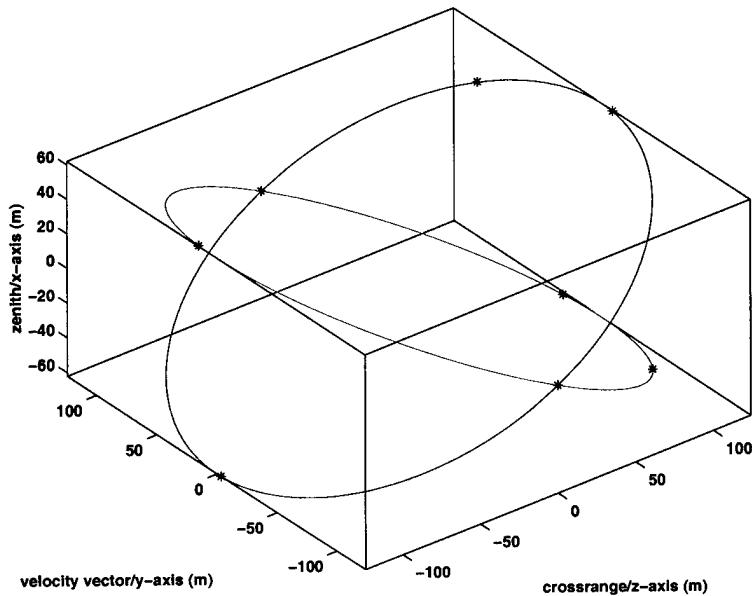
Figure 4.1 Satellite Orbits in Each Cluster

property cannot be achieved with more than eleven apertures [Leech, 1956]. Applying these aperture spacings along the velocity vector of the cluster, the satellite positions are extended to the two-orbit solution in Hill's frame from Section 3.2.2. Figure 4.1 illustrates an example geometry for an eight-satellite cluster. These configurations are fixed for only an instant before the orbital motion of the satellites produces a new geometry. Fortunately, the distribution of the satellites never degenerates to a single line over the entire orbital period, so a nominal spatial separation for processing the received radar signals is always maintained [Sedwick et al, 1999]. Using these satellite configurations, we can now compute the receive gain for the antenna based on the projection of the satellite positions at the ground location of interest.

4.2.3 Transmit and Receive Gain

The overall gain pattern of the signal reflections that arrive at a radar antenna is affected by the transmission wavelength, but it mainly depends on the effective area of the aperture on transmit and receive (Section 2.3.2). For a single aperture system, these gains are the same. On the other hand, the transmit gain for a multiple aperture system is again the

same for a single aperture, but the receive gain depends on the characteristics of the synthesized aperture. From the angular location of the footprint on the ground, the receive gain is determined in this module by projecting the satellite positions in Hill's frame to this particular point using the coordinate transformation matrices in equations 4.3 and 4.4.

$$T_x = \begin{bmatrix} 1 & 0 & 0 \\ 0 & \cos AZ & \sin AZ \\ 0 & -\sin AZ & \cos AZ \end{bmatrix} \tag{4.3}$$

$$T_z = \begin{bmatrix} \cos\left(\dfrac{\pi}{2} - EL\right) & \sin\left(\dfrac{\pi}{2} - EL\right) & 0 \\ -\sin\left(\dfrac{\pi}{2} - EL\right) & \cos\left(\dfrac{\pi}{2} - EL\right) & 0 \\ 0 & 0 & 1 \end{bmatrix} \tag{4.4}$$

Figure 4.2 demonstrates this ground projection for our example eight-satellite cluster at forward and lateral ($AZ = 0°$ and $90°$) locations. We see here that one of the orbits in the side-looking case is almost degenerate. Without the opposing orbit for a portion of the satellites, the radar performance of the system would be unacceptable at these locations.
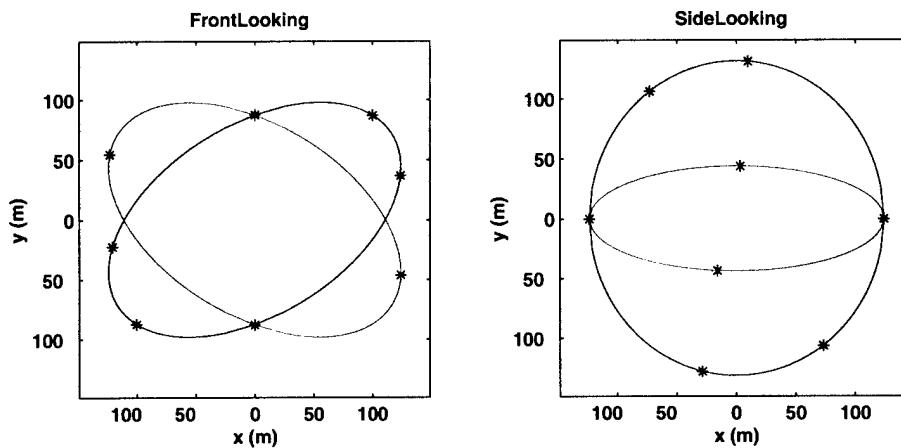
Figure 4.2 Ground Projection for a Front and Side-Looking Cluster
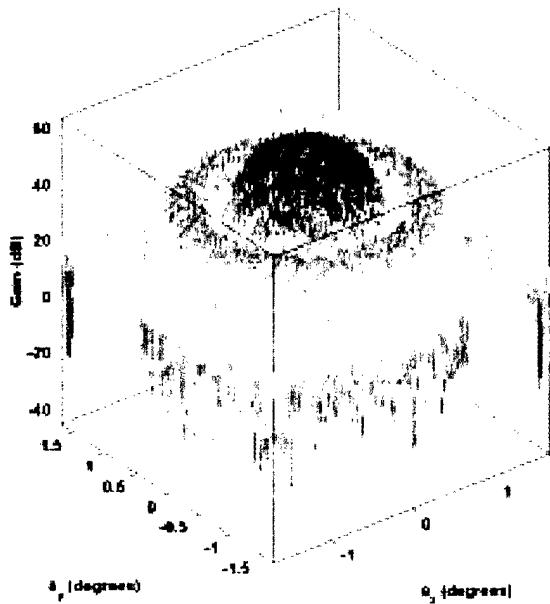
Figure 4.3 Example Point Spread Function of a Sparse Aperture Interferometer

The cluster ground projection is used to calculate the array factor gain, which represents the energy increase in the processed signals from separated spacecraft interferometry. The product of the antenna and array factor gains gives the complete receive gain, also known as the point spread function, for this system (Section 3.3.2). Figure 4.3 illustrates the PSF for our example TechSat 21 architecture with the gain given in decibels. Two important properties of the PSF are evident in this figure: the general shape of the main and side-lobes is caused by the antenna gain of each satellite ($\propto \lambda/D$) while the spikes represent the grating lobes that result from the combination of signals received by a finite number of apertures ($\propto \lambda/B$). The transmit and receive gain influence the strength of the reflections from targets and clutter. Before we can continue with this analysis, we first need to define the properties of the ground clutter in the footprint to estimate accurately the target detection capability of the system.

4.2.4 Footprint Properties

At this point, we have nearly all of the quantities needed in the radar range equation to calculate the signal-to-noise ratio for our example TechSat 21 architecture. However, we have not considered the general geometry of the cluster and the location of interest. We must also characterize the competing clutter return in the received signals. The purpose of this module is to assess these parameters so we can complete our analysis of the radar performance within the footprint.

Radar Geometry

The geometry of this problem can be described by the radar range to target, the grazing angle of the footprint, and the footprint area. The target range is simply the distance from the cluster to the location on the ground where the footprint is projected (equation 4.5).

$$R = R_e \frac{\sin\phi_c}{\sin EL} \tag{4.5}$$

The grazing angle corrects the elevation angle of the illuminated ground location to account for the curvature of the Earth (equation 4.6).

$$\psi = a\cos\left(\sin EL \frac{(R_e + h)}{R_e}\right) \tag{4.6}$$

Finally, the footprint area is proportional to the antenna beamwidth elongated by the Earth's curvature (equation 4.7)

$$A_f = \frac{\Delta\theta^2 R^2}{\sin\psi} \tag{4.7}$$

With these quantities, we are now able to compute the SNR of the received radar signals. Still, we are not quite finished because we have not yet evaluated the characteristics of the clutter.
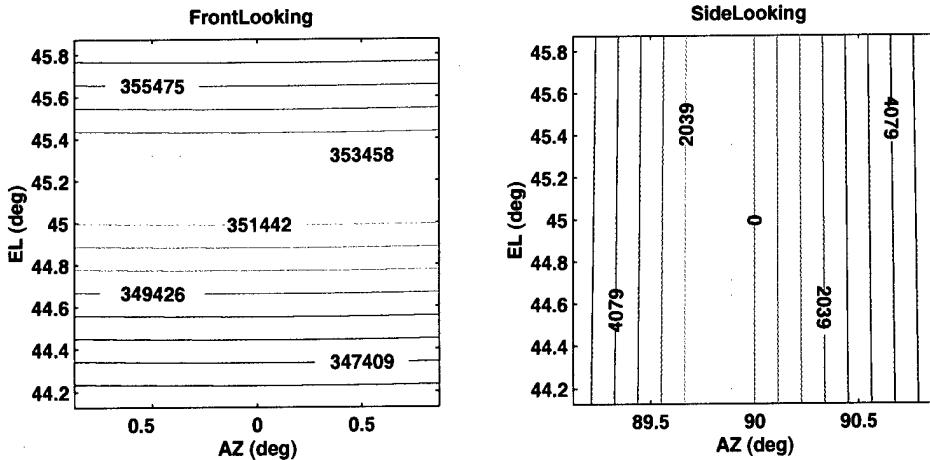
Figure 4.4 Footprint Doppler Shift (Hz) for a Front and Side-Looking Cluster

Clutter Doppler Profile

In Section 2.6.1 we learned that although objects on the ground are stationary, the clutter returns they produce in the received radar signals are shifted and spread in frequency due to the platform motion of the cluster. Equation 4.8 represents this Doppler shift in terms of the angles measured from the cluster to the ground location (neglecting Earth rotation and curvature) [Cantafio, 1989].

$$f_D = \frac{2v_p}{\lambda} \sin EL \cos AZ \tag{4.8}$$

The clutter signals are blue-shifted in the direction of the cluster motion and red-shifted in the opposite direction. In addition, the Doppler shift decreases as the elevation angle moves from the horizon to nadir. Figure 4.4 contains a contour plot of the Doppler shift for our example eight-satellite cluster in the front and side-looking directions.

Since the cells in the footprint have a finite area, the Doppler shift of the clutter they each contain is spread over a range of frequencies, causing the clutter return from a single cell to fall in multiple Doppler filters. This Doppler spread, given in equation 4.9, is set by the beamwidth of the synthesized aperture and is simply the magnitude of the differential of equation 4.8.

$$\Delta f_D = \frac{4v_p}{B}\sqrt{(\sin AZ \sin EL)^2 + (\cos AZ \cos EL)^2} \qquad (4.9)$$

The other property of the clutter that must also be determined is the radar cross section of the ground reflectors in the footprint.

Clutter Cross Section

The clutter located in each footprint cell has a certain RCS based on the reflective and directive qualities of the illuminated terrain. Equation 4.10 defines the clutter cross section as the product of the clutter backscattering coefficient (Section 2.6.1) and the physical area of a single cell.

$$\bar{\sigma} = \sigma_0 A_{cell} = \gamma \Delta \theta_{cell}^2 R^2 \qquad (4.10)$$

Since the $\sin\psi$ terms in σ_0 and A_{cell} cancel out, the clutter cross section simply increases with R^2 as the grazing angle is decreased from nadir to the horizon. This behavior is clearly demonstrated in Figure 4.5. In most cases, especially for space-based GMTI radar, the clutter cross section is orders of magnitude larger than the RCS of any realistic target. Therefore, techniques for clutter suppression must be implemented in the processing of the received signals to enable detection of target echoes. The parameters describing the properties of the radar footprint for the given architecture are the last pieces of data we need to complete the received signal analysis.

4.2.5 Processing of Received Signals

We now have all the necessary information to evaluate the strength of the target returns in the presence of interference from noise and clutter. The analysis of these signals must be conducted within the framework of the signal processing performed to suppress the competing clutter. From the arguments developed in Section 3.5, the signal processing technique that provides the best performance for a separated spacecraft GMTI radar system is deconvolution. This results from the fact that the clutter return in this method is not esti-
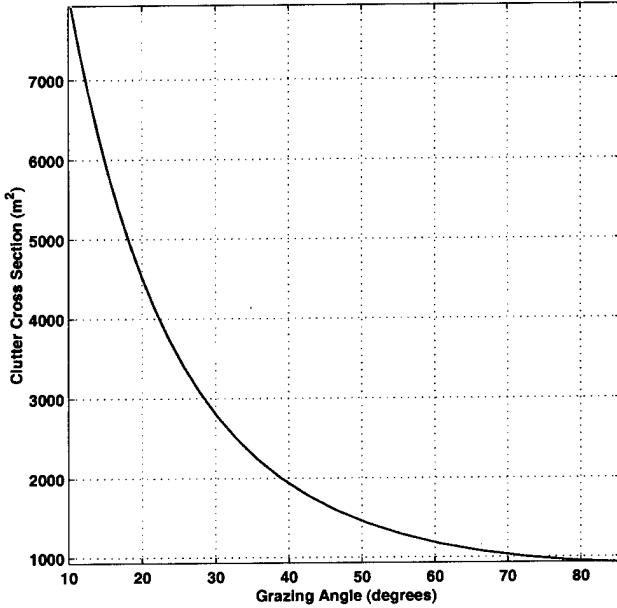
Figure 4.5 Clutter Cross Section as a Function of Grazing Angle

mated from a statistical model but is classified based on its exact Doppler profile, thus allowing the complete elimination of clutter in the received radar signals to yield a strictly noise-limited probability of detection. The purpose of this module is not to demonstrate the successful implementation of this method in actual sparse aperture radar applications. Rather, it is assumed that the deconvolution method works according to the mathematics at its foundation. In this context, we can calculate the SNR for each cell in the footprint.

The end product of the deconvolution processing is a three-dimensional matrix that contains the spatial location in range and cross-range of each target in the footprint as well as their individual Doppler shifts. Since we are binning the received signals in range, it is easiest to evaluate the cross-range and Doppler parameters for each range bin, which is analogous to the PSF scan of the footprint from Section 3.3.2. The module begins with the first range bin at the toe of the footprint and constructs the cross-range/Doppler matrix from the illuminated ground location. Each data point in the matrix contains a target RCS estimate because we are interested in the average SNR for each cell and not in the actual

target locations. The clutter cross section is then added to the matrix elements where the clutter is located based on its Doppler profile. For all cells outside this clutter band, the SNR is calculated from equation 4.11 and represents the value we can expect for each cross-range cell in the range bin.

$$SNR = \frac{P_{avg}\lambda^2 G_{ap}G_{af}\sigma_T CR}{(4\pi)^3 R^4 L_s kT_s BW_n} \tag{4.11}$$

In this equation, notice the improvements in the SNR discussed earlier resulting from pulse compression (Section 2.5.3) and sparse aperture interferometry (Section 3.3.2). The entire procedure is then repeated for each range bin in the footprint under the assumption that the received signals are range unambiguous. Once complete, the SNR variations across the footprint can be described (Figure 4.6). Again, refer to Section 3.5 for a more in-depth discussion of deconvolution. The SNR must reach a minimum level, usually 12
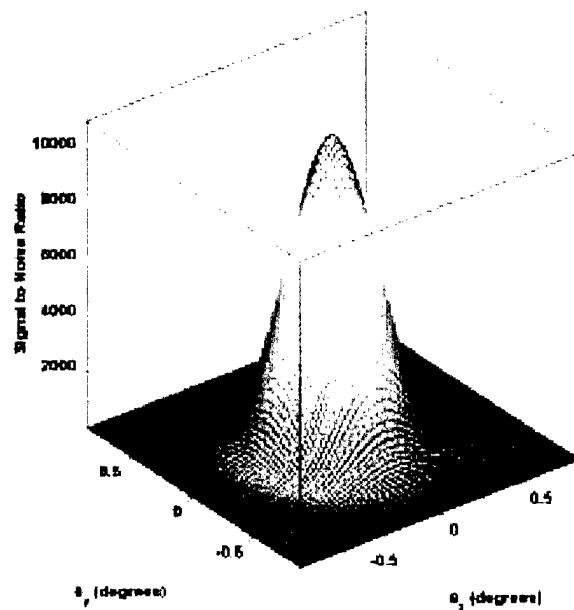
Figure 4.6 Footprint Variations in the Signal-to-Noise Ratio

to 15 dB for space based radar systems, to ensure detection of valid targets in the presence of noise [Cantafio, 1989]. This quantity essentially relates the performance of the system, but it needs to be expressed in a more intuitive manner.

4.2.6 Radar Integrity Metric

The final module in this footprint analysis evaluates the radar performance of the cluster. Although there are many different measures of performance available, the probability of detection is the best integrity metric for radar systems within the GINA framework used to guide the construction of the model (Section 4.1). The probability of detection is actually a statistical parameter based on the joint statistics of the noise and the target signal. Most likely, the target signal in space-based radar fluctuates from pulse to pulse, which can be characterized by the Case II Swerling model [Swerling, 1960]. From this model, we can approximate the probability of detection after pulse integration with equation 4.12 based on an acceptable false alarm probability [Neuvy, 1970].

$$\log\left(\frac{1}{P_d}\right) = \left(\frac{\log(n_{fa})}{n_i^{2/3} n_c SNR}\right)^{1/\beta} \tag{4.12}$$

where $\beta = 1/6 + \exp(-n_i/3)$ and n_{fa} is the false alarm number given in equation 4.13

$$n_{fa} = \frac{\ln 0.5}{\ln(1 - P_{fa})} \tag{4.13}$$

The result from equation 4.12 by itself is still not a clear metric to use for comparing various system architectures. Most of the time, the end user cares about the availability of certain detection probabilities. For instance, the user may require that the radar system provide a 85% probability of detection 80% of the time or some other combination. Therefore, the availability of certain levels of detection probability is the more important measure of performance. The target detection availability for our example radar system architecture is illustrated in Figure 4.7. The initial dip in the availability curve is caused by the finite number of cells near the edge of the footprint where targets cannot be
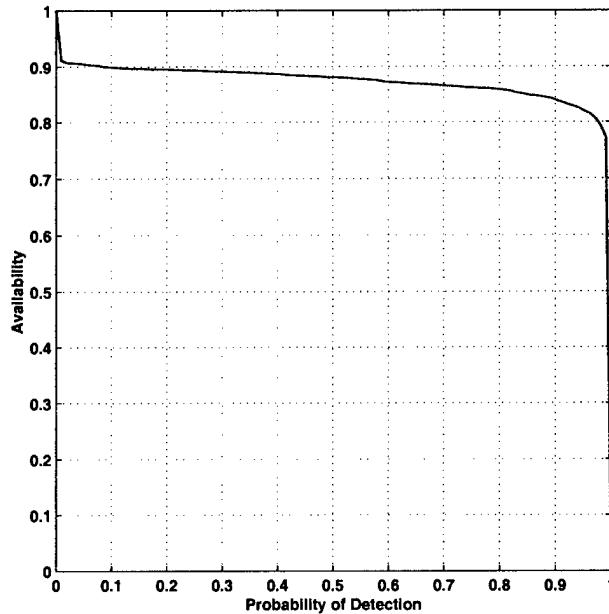
Figure 4.7 Radar Performance Availability Within a Footprint

detected ($P_d = 0$). From this plot, we see that radar performance at the chosen ground location maintains a high probability of detection in the majority of the footprint cells. This model of the radar footprint can now be used to evaluate the performance of any TechSat 21 architecture at all locations within the cluster's field of regard.

4.3 Coverage Area Model

Although the target detection capability of a footprint is an important performance gauge of a TechSat 21 cluster, expanding this analysis to the total field of regard of the cluster is inherently more useful because it captures the overall performance of the entire global constellation of clusters. Based on the statistical likelihood of all ground locations in the cluster coverage area, the geometry of the footprint and the cluster is first calculated followed by the properties of the transmitted waveform. The model then proceeds to characterize the variations in performance and isolation throughout the coverage area. With these variations and the aforementioned statistics, the overall performance capabilities of

the given TechSat 21 architecture are determined to help identify viable design alternatives for the radar system. Again, the MATLAB code for this model can be found in Appendix B.

4.3.1 Radar-Earth Geometry

The first module in this expanded model describes the relative geometry of the cluster and the ground. Since we are gauging the system performance on the constellation level, each cluster of satellites can be thought of as a single entity. The location of the horizon specifies the outer extent of the field of regard. Figure 4.8 illustrates the important geometrical parameters for this model. After selecting a linearly spaced set of the Earth angles (ϕ_c)
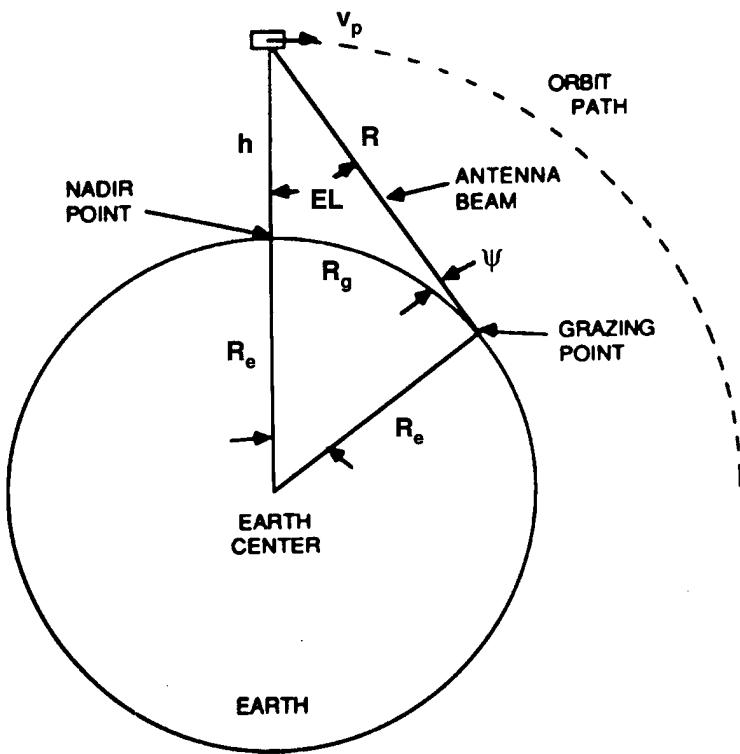
Figure 4.8   Radar-Earth Geometry [Cantafio, 1989]

from the horizon to nadir, we can calculate the radar range and elevation and grazing angles using the following equations.

$$R = \sqrt{(R_e + h)^2 - 2R_e(R_e + h)\cos\phi_c + R_e^2} \tag{4.14}$$

$$EL = \operatorname{asin}\left(\frac{R_e \sin\phi_c}{R}\right) \tag{4.15}$$

$$\psi = \frac{\pi}{2} - EL - \phi_c \tag{4.16}$$

The final geometrical parameter of interest is the azimuth angle, which are also linearly spaced over the complete 360° range of the field of regard.

Outside the geometry of the coverage area, this module also computes the cluster baseline and the area search rate for the TechSat 21 architecture. Similar to the footprint model (Section 4.2.1), the cluster baseline is set by the required cross-range resolution for the system. Eventually, the projection of this baseline is used to evaluate the minimum detectable velocity throughout the field of regard (Section 4.3.4). The ASR, on the other hand, depends on the chosen operating mode for the system. In the search mode, the cluster continuously scans all ground locations in view as it orbits the Earth. Otherwise, the cluster in the stare mode focuses on a particular region or theater in its field of regard until it is no longer in view. In this case, the ASR is simply the area of the theater divided by the average visit time. The search mode obviously requires a higher total ASR, meaning there is less reflected energy received from each location. For most reasonable TechSat 21 architectures, the ASR for the search mode is too high to provide a sufficient probability of detection, so the stare mode is the only viable option. With these quantities, the next step in this model is to determine the properties of the transmitted signal.

4.3.2 Pulsed Waveform Parameters

This module is similar to the one described in Section 4.2.1 for the footprint model. For each grazing angle, the maximum range unambiguous PRF is calculated followed by other properties such as the number of pulses, the pulse width, and the pulse compression parameters. As the length of the footprint shortens from the horizon to nadir, the PRF is increased while still preventing range ambiguities in the footprint. This means that the transmitted waveform is tuned to the various ground locations in the coverage area. These fluctuations in the pulse waveform parameters can be used to characterize the variations in performance over the cluster's field of regard.

4.3.3 Performance Variations

Up to this point, the modules in this coverage area model have followed a progression similar to the footprint analysis. In this subsection, the differences between these two models will become more apparent. We again evaluate the performance of the radar system in the context of the various techniques executed in the signal processor that enhance the power of the target echoes in the presence of noise and clutter. In the beginning processing stages, the received pulses are compressed, causing a boost in the signal power equal to the pulse compression ratio (Section 2.5.3). The interferometric combination of the signals received by a series of apertures gives an increase in the signal power proportional to the square of the number of apertures (Section 3.3.2). After this step, coherent and noncoherent integration of the combined pulses also strengthens the signal power (Section 2.5.4). All of these improvements are included in equation 4.17 to calculate the signal-to-noise ratio that results after processing.

$$SNR = \frac{P_t \sigma_T A_e^2 \tau}{4\pi\lambda^2 k T_s L_s R^4} CR_{min} \frac{N^2}{4} n_i^{2/3} n_c \qquad (4.17)$$

Taking a closer look at this equation, we realize that variations in the SNR within the field of regard are only caused by changes in the grazing angle. This allows us to reduce the analysis of the probability of detection to a single dimension in this model. The SNR vari-
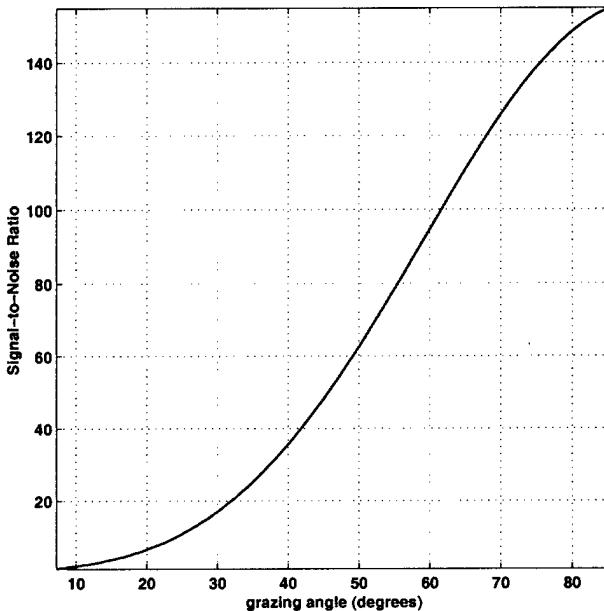
Figure 4.9 Coverage Area Variations in the Signal-to-Noise Ratio

ations as a function of the grazing angle for the example TechSat 21 architecture can be seen in Figure 4.9.

It is important to note that the parameters representing the processing gains in equation 4.17 are more or less determined in this module from a worst case scenario. For instance, we use the minimum compression ratio because we are unsure of the realistic amount of pulse compression that will be provided by the operational system. The maximum number of noncoherent integrations is similarly capped based on the limited computational resources for each satellite. Finally, an estimate of the mean array factor gain is used to reduce the complexity of the analysis. The SNR values from the horizon to nadir establish the target detection probabilities from equation 4.12 in Section 4.2.6. Before we evaluate the availability of the probability of detection within the cluster coverage area, we first need to investigate the level of isolation attainable by the cluster to give a further description of the radar system performance.

4.3.4 Isolation Capability

In the footprint model, the performance of the system was solely represented by the probability of detection. We can now expand this analysis to include the isolation capability of the system. The level of isolation in space-based GMTI radars is represented by the achievable spatial and frequency resolution in received signal processing as well as the minimum detectable velocity. Along with the probability of detection, these isolation parameters provide another useful piece of information to help characterize the performance of candidate TechSat 21 architectures.

Spatial and Frequency Resolution

From Section 3.1 we know that the spatial resolution of the synthesized aperture in a sparse array interferometer is proportional to the maximum separation distance between the apertures. The range resolution is also affected by the width of the compressed pulse. In most cases, it is easier to achieve fine range resolution with pulse compression rather than interferometry. Therefore, the range resolution for TechSat 21 results from the pulse compression while the cross-range resolution is set by the cluster baseline.

$$\Delta R = \frac{c\tau_c}{2}\sec\psi$$

$$\Delta XR = \frac{2\lambda}{B}\frac{R}{\cos EL}$$

(4.18)

Equation 4.18 shows us that the range resolution is poorest at nadir where the $\sec\psi$ term approaches infinity. The opposite is true for the cross-range resolution because the projection of the cluster baseline has the smallest extent at the horizon.

The achievable frequency resolution of the system is limited by the amount of time when coherence is maintained between successive pulses received by the radar (Section 2.4.2). In space-based radar, the orbital motion of the platform restricts the coherent dwell time, thus specifying the frequency resolution. This resolution sets the width of the filters in the

Doppler bank, which defines the precision of the target velocity measurement according to equation 4.19.

$$\Delta v = \frac{\lambda}{2}\Delta f \qquad (4.19)$$

Unfortunately, the parameters that determine the resolution capability of the cluster are not constrained by the system design and are not useful in evaluating the performance. The other parameter that relates the isolation capability is the MDV.

Minimum Detectable Velocity

The MDV is derived from the spectral width of the mainlobe clutter return based on the projected cluster baseline (Section 2.6.1). In the footprint model, we did not fully examine how the projected baseline changes with ground location. As before in Section 4.2.2, the cluster baseline is used to size the two possible satellite orbits in Hill's frame. For each
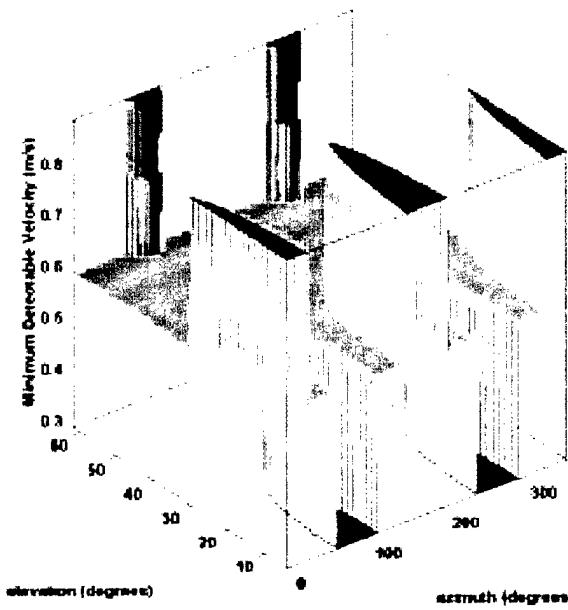
Figure 4.10 Coverage Area Variations in the Minimum Detectable Velocity

location in the coverage area, the projection of the orbits sets the average baseline to give the clutter Doppler spread. With this value, the MDV is calculated from equation 4.20 in the same manner as the velocity precision above.

$$MDV = \frac{\lambda}{2}\left(\frac{4v_p}{B}\sqrt{(\sin AZ \sin EL)^2 + (\cos AZ \cos EL)^2}\right) \qquad (4.20)$$

Since the Doppler bank filters have a finite width and we are assuming that any filter containing clutter is unusable, the MDV can only take on discrete values. This feature is apparent in Figure 4.10, which gives the MDV over the entire field of regard. The availability of both the MDV and the probability of detection can now be determined to demonstrate the overall radar performance for the TechSat 21 system.

4.3.5 Overall System Performance

Once again, the availability is used to characterize the performance for TechSat 21. It is here that we will gain an appreciation of the major differences between the footprint model and this coverage area model. Because the MDV does not have an appreciable variation within the footprint, it cannot be used as a measure of performance in the footprint model, so we are limited to using the probability of detection. By expanding our analysis to the complete coverage area, the MDV gives us another metric to help us compare system architectures. However, the most significant difference between these two models lies in their treatment of ground location. The location of interest must be specified for the footprint model while the coverage area model relies on the statistical likelihood of these locations. The performance for a single location is somewhat meaningless because it is not tied to a specific system constellation. Stated another way, the performance at specified azimuth and elevation/grazing angles does not tell us anything about the performance we can expect as the cluster orbits the Earth. In the coverage area model, the system constellation directly affects the location statistics over the field of regard. This means that although we focus our analysis on a single cluster in this model, we actually characterize the performance availability of the entire constellation as a result of the
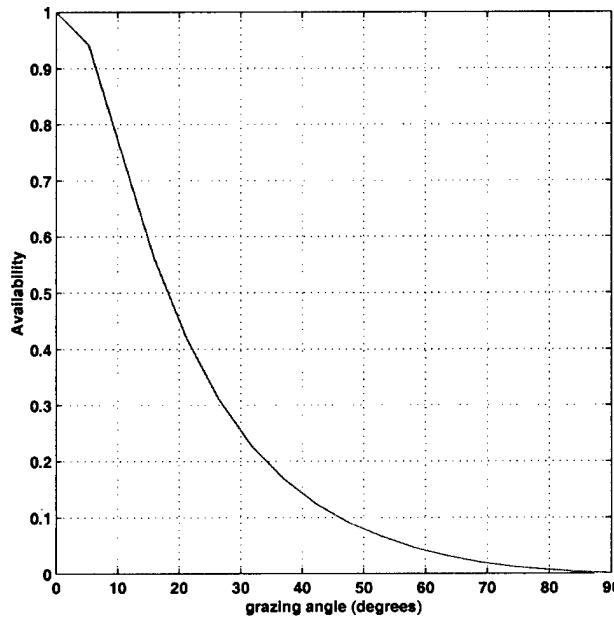
Figure 4.11 Grazing Angle Availability in the Field of Regard

statistical distribution of the ground locations. Before we look at the individual availabilities of the isolation and integrity metrics, we first need to understand how the statistical distribution of the coverage area is determined.

Statistics Interpolation

Based on the design parameters of the TechSat 21 constellation, including the total number of clusters and their orbit properties, the grazing angle availability can be evaluated from the horizon to nadir. Figure 4.11 gives this availability for our example system architecture. From this plot, we can find the probability that a particular grazing angle is illuminated by the radar, otherwise known as the probability density function. While the probability of detection is a function of the grazing angle, the MDV depends on the elevation angle. This requires that we also compute the elevation angle PDF for the MDV availability calculation. The same process can be followed for the azimuth angles, but the PDF in this case is uniformly distributed, meaning that there is an equal probability of
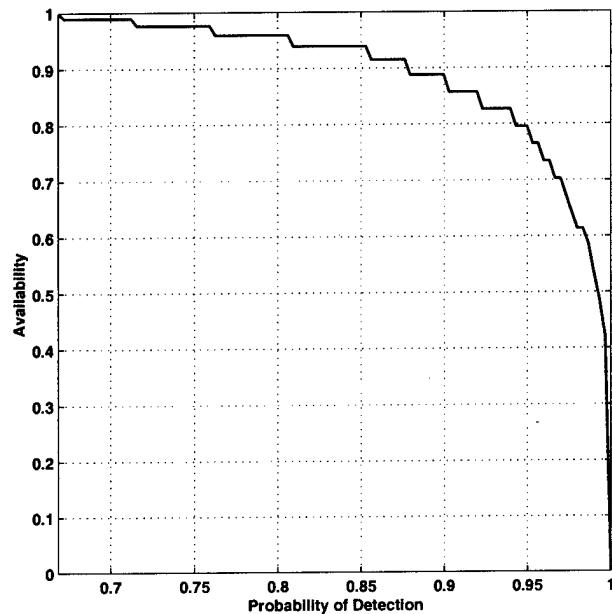
Figure 4.12   Radar Performance Availability Within the System Coverage Area

being at any azimuth angle in the field of regard. Using these PDFs, we can now evaluate the availabilities of the probability of detection and the MDV.

Performance Availability

The first step in finding the isolation and integrity availabilities is to match the number of data points in the probability of detection and the MDV arrays with the discretization of the coverage area statistics. For a particular probability of detection or MDV, the locations that equal or exceed this specified value are determined. The performance availability is then calculated by summing the probabilities that correspond to these locations. From our example TechSat 21 architecture, Figures 4.12 and 4.13 give the availability plots for the probability of detection and the MDV. We can now use both of these metrics to identify viable system architectures for TechSat 21 by figuring out which combinations of the design vector parameters meet the performance requirements set by the end user.   Most of the time, the user will care more about the probability of detection than the MDV, but
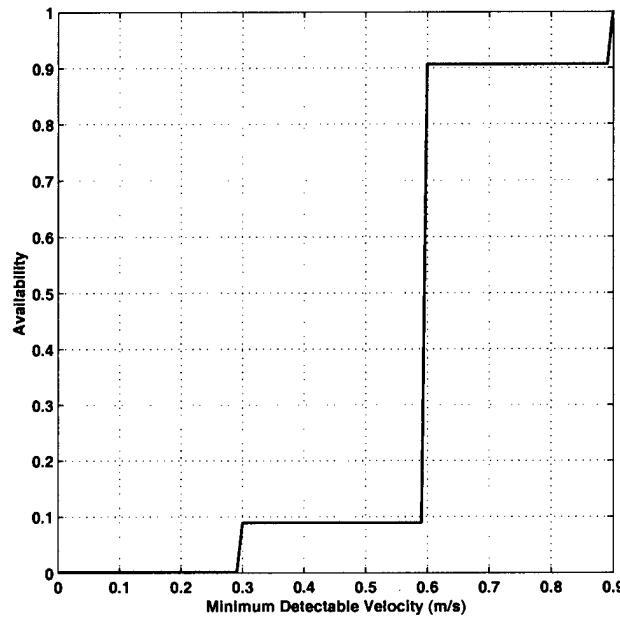
Figure 4.13 Isolation Capability (MDV) Within the System Coverage Area

both metrics can still be used to characterize the TechSat 21 system performance and can also identify key design trends for the system or which architectures will never provide adequate levels of performance.

Chapter 5

KEY RADAR PERFORMANCE
RESULTS FOR TECHSAT 21

All of the previous chapters in this thesis have discussed the background research and analysis that together form the foundation of the model used to evaluate the radar performance of various architectures for TechSat 21. As the development of this space-based GMTI radar system continues, critical decisions concerning the system design will soon be made. Accurate assessment of the impact on performance resulting from the selection of certain major design parameters is crucial in this decision-making process to define a preferred system concept. Rather than characterizing the performance capabilities of specific system architectures, it is much more useful to the system engineer to discover the subset of the total possible architectures that satisfy the performance requirements set by the end user. This chapter presents a design study that determines which combinations of the design parameters (number of satellites per cluster, aperture diameter, and antenna transmission power) fulfill specified minimums placed on the probability of detection and the availability. After motivating the framework of this design study for the TechSat 21 radar system in Section 5.1, Section 5.2 introduces a new radar performance metric for multiple aperture systems, termed the $P_t N^2$ product, used to identify viable design candidates for an example TechSat 21 system constellation. The problem of choosing the better option is now reduced to a simple cost and reliability analysis to ensure that the final design for the operational system will provide the best possible performance for the lowest cost to the end user.

5.1 Design Study for TechSat 21

The design of any space system requires careful examination of myriad interrelated issues including operational complexity, system reliability, computational workload, level of autonomy, physical dimensions, total mass, and overall cost. If we narrow our focus to space-based radar systems, additional concerns are raised by certain requirements imposed on global coverage, detection range, angular resolution, and frequency sensitivity. The primary goal of the systems engineering process is to understand how the different parameters of the system design affect operational performance by evaluating the functionality of the system as a whole. An appropriate design study in this process must be able to quantify the relative impacts of the most significant architecture variables on performance and cost [Shaw, 1998]. In this section, the framework for a design study of TechSat 21 is developed to assist in the identification of viable design candidates for this space-based GMTI radar system based on radar performance metrics. Expanding the evaluation to include cost considerations is beyond the scope of this study because many other elements of the complete system contribute to the total cost but have no impact on the performance assessment of the radar system. However, a proposed format for a comprehensive design analysis of TechSat 21 will eventually be presented in Chapter 6.

5.1.1 Study Development

A complete analysis and evaluation of every component relevant to the operation of the TechSat 21 radar system is far too complicated to yield practical results. Instead, this design study concentrates on the performance impact of the most significant radar system design parameters. These variables are: the number of satellites in the cluster, the aperture diameter, and the antenna transmission power. In selecting a framework for this design study, there are two distinct paths we can take. Starting with a specific system architecture, we can construct a detailed model to estimate the overall performance capabilities of the radar system. This is precisely the underlying concept of the coverage area model presented in Section 4.3. Our other choice is to set bounds on performance based on the

needs of the end user and separate out the architectures that satisfy these requirements. While the former is helpful in evaluating the affect on performance of each design parameter, the latter is often much more effective in the systems engineering process because it can reduce the design space available to the system by identifying viable candidate architectures and eliminating inadequate options. Therefore, we adapt the coverage area model from Section 4.3 to this alternative framework in this design study (see Appendix C for the MATLAB code). This adjusted model uses the same modules from the coverage area model to determine radar-Earth geometry (Section 4.3.1), the pulsed waveform parameters (Section 4.3.2), and the statistics interpolation (Section 4.3.5). The new modules are discussed in the remainder of this subsection.

Variational Parameters

Since the performance of the TechSat 21 radar system is defined by the signal-to-noise ratio of the received signals after processing (Section 3.5.4), we need to develop our design study by considering the dependence of this quantity on the radar design parameters. Equation 5.1 gives a different representation of a standard form of the SNR equation for sparse aperture radars (Section 4.2.5) that is better suited to this study.

$$SNR = P_t N^2 A_e^2 \cdot \frac{\tau n_i^{2/3} n_c}{R^4} \cdot \frac{\sigma_T CR_{min}}{16\pi\lambda^2 kT_s L_s} \tag{5.1}$$

This equation is divided into three components based on the origins of each parameter. The first part describes the contribution of the design parameters to the SNR. Other properties of the radar system that are functions of the footprint location on the ground are contained in the second part. The last part is simply a collection of all of the constants in the SNR equation.

The reason for classifying the SNR equation in this manner is evident from the framework for this design study. As stated previously, our goal is to figure out which combinations of the design parameters meet specific requirements on performance. This means that eventually we want to solve for the first element in equation 5.1. Since the constants are prede-

termined outside this analysis (assumed target characteristics, transmission wavelength,
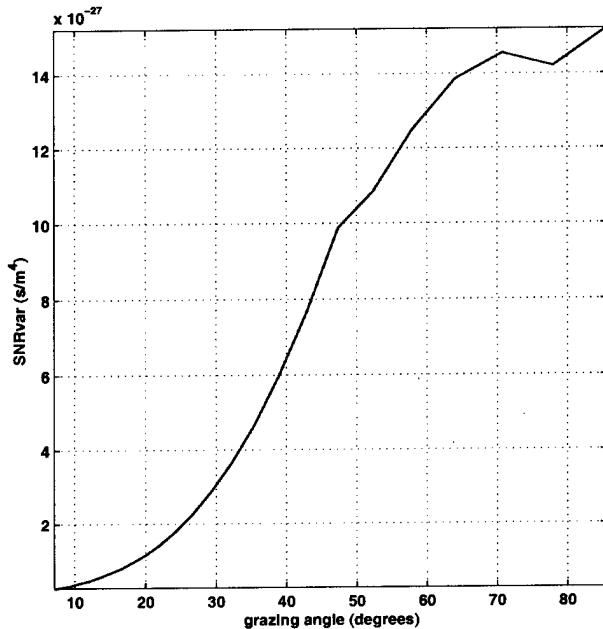
Figure 5.1 Coverage Area Variations of SNR_{var} (D = 2.5 m)

system noise temperature and losses, etc.), the basic function of the design study is to find the correct values for the second element and the required SNR based on the required performance minimums.

The second element of equation 5.1, hereafter referred to as SNR_{var}, includes the transmitted pulse width, the number of coherent and noncoherent pulse integrations, and the range to target. All of these quantities are functions of the grazing angle corresponding to the footprint location in the field of regard, meaning that the availability of their combined value can be determined. Therefore, the first step in this process is to compute SNR_{var} as a function of grazing angle (Figure 5.1). From the constellation design for the system (number of clusters, number of orbit planes, and orbital altitude), the probability distribution of the grazing angles from the horizon to nadir is estimated. From these coverage area statis-

tics, the availability of SNR_{var} is calculated based on the procedure described in Section 4.3.5 (Figure 5.2). The required availability is ultimately applied to this availability curve to find the corresponding value of SNR_{var}
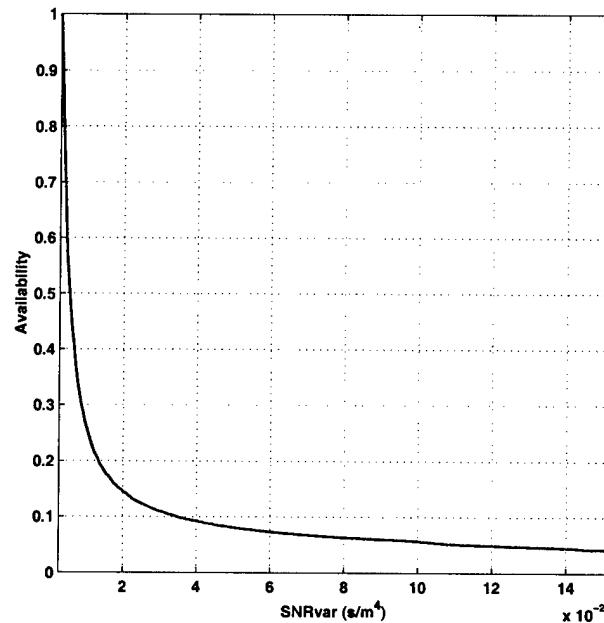
Figure 5.2 SNR_{var} Availability Within the System Coverage Area (D = 2.5 m)

Radar System Design

In the preceding chapters, we learned that the most useful performance metrics for space-based GMTI radar systems are probability of detection and availability. Demands on performance set by the end user are used to establish minimum values for these metrics. The minimum probability of detection defines the minimum SNR according to equation 5.2 (Section 4.2.6)

$$SNR_{min} = \frac{\log(n_{fa})}{\log\left(\frac{1}{P_{dmin}}\right)^{\beta}} \qquad (5.2)$$

where β is calculated based on the maximum number of noncoherent integrations (Section 4.2.5). At this point, we have all of the parameters we need to distinguish the system architectures that fulfill the specified minimums for probability of detection and availability.

5.1.2 Design Analysis Procedure

Once we have the minimum SNR and the value for SNR_{var} corresponding to the required availability, we can identify viable combinations of the design parameters. Looking again at equation 5.1, this process would be as simple as dividing the minimum SNR by SNR_{var} and the constants in the SNR equation to yield a minimum required product proportional to the transmission power, the aperture diameter, and the number of satellites. This quantity is similar to the power-aperture product for single aperture radar systems but modified by the resulting gain from the number of satellites in a sparse aperture system. However, the variables in SNR_{var} also depend on the aperture diameter, meaning that this design parameter must be specified to evaluate SNR_{var}. This is actually helpful because the performance analysis is reduced to a trade between the antenna transmission power and the number of satellites in the cluster for each value of the aperture diameter, a result clearly seen in equation 5.3

$$P_t N^2 = \frac{SNR_{min}/SNR_{var}/SNR_{const}}{D^4} \tag{5.3}$$

where the constants that specify the aperture effective area are contained in SNR_{const}. This quantity is termed the $P_t N^2$ product, and it must exceed a threshold value for a given aperture diameter to provide sufficient target detection performance.

The sequence of steps developed in the last subsection can be enumerated as follows:

- Estimate the coverage area statistics of the constellation based on the total number of clusters, their distribution around the Earth, and their orbital altitude

- For a reasonable range of aperture diameters, determine the distribution of the system parameters that vary with ground location, evaluate their combined availabilities according to the coverage area statistics, and choose the combination that corresponds to the minimum required availability

- Compute the minimum signal-to-noise ratio to meet the probability of detection requirement

- Calculate the $P_t N^2$ product for each aperture diameter with equation 5.3

With this explicit procedure for our design study now defined, we can move on to presenting some results for an example TechSat 21 constellation.

5.2 Study Results

Based on the framework used to develop this study, the results presented in this section begin with an example constellation and realistic values for the performance minimums to end up with a plot of the $P_t N^2$ product versus aperture diameter. The parameters of this example TechSat 21 constellation are given in Table 5.1. This constellation was chosen

TABLE 5.1 Constellation Architecture for the Design Study

Parameter	Value
Number of Clusters	35
Number of Orbital Planes	7
Orbital Altitude	800 km

because the revisit time for any point on the Earth is no longer than fifteen minutes. In the future, a complete set of all constellations that meet the required revisit rate could be generated, perhaps as a function of orbital altitude, to create a family of $P_t N^2$ curves that would be used to conduct a full system-wide analysis and optimization of the TechSat 21 design.

A number of constants are included in the system model but are not considered tradeable design parameters. These quantities and their values are listed in Table 5.2. Some of

TABLE 5.2   Constant System Parameters for the Design Study

Parameter	Value
Carrier Frequency	10 GHz
Transmission Duty Cycle	5%
Target RCS	10 m^2
Coherent Dwell Time	50 ms
Receiver Noise Temperature	290 K
False Alarm Time	1000 s
System Losses	3 dB

these values are standard approximations common to most space-based GMTI radar systems while others are conservative estimates of certain system constraints. Note that the only constant from equation 5.1 that is not found in Table 5.2 is the minimum pulse compression ratio because this value is a function of the aperture diameter in this model. As the capabilities and technology of space-based radar continue to advance, these constants can be adjusted to account for these improvements.

Following the example constellation and the system constants, the probability of detection and availability requirements need to be specified to calculate the $P_t N^2$ product curve. One approach is to set the required availability and allow the probability of detection to vary. Also, we can fix the minimum probability of detection for a range of required availabilities. The resulting $P_t N^2$ curves for both these options with aperture diameters extending from one to four meters are illustrated in Figures 5.3 and 5.4. In general, a lower value for the $P_t N^2$ product corresponds to a less expensive system with diminished capability. For each probability of detection-availability pair, any combination of transmission power and number of satellites greater than the $P_t N^2$ product for a given aperture diameter represents a viable system architecture. If we have a 2.5 meter aperture, for example, the $P_t N^2$ product for an 85% probability of detection and a 90% availability is 1.07×10^4. With six satellites per cluster, the antenna transmission power must be around 300 watts to achieve the performance requirements. If more satellites per cluster are needed (increased reliability, computational capacity, etc.), then the minimum transmission power can be decreased.
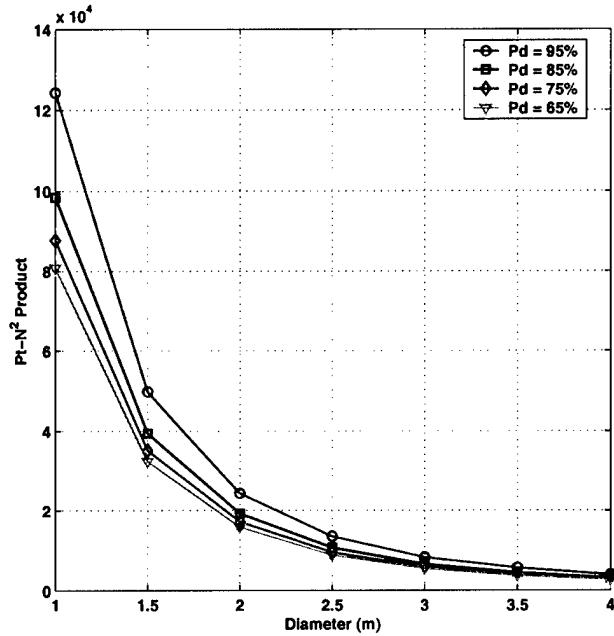
Figure 5.3 Acceptable System Design Architectures (av = 90%)

The optimal transmission power and number of satellites for a given $P_t N^2$ product involves a trade between cost, reliability, hardware, maintenance, data processing, technology status, and other similar issues.

A number of interesting relationships can be drawn from these Figures 5.3 and 5.4. First, the $P_t N^2$ product curves are inversely proportional to the aperture diameter. This suggests a diminishing return as the aperture diameter is increased, meaning that it is more advantageous to increase the aperture diameter for radars with small antennas compared to architectures that already have large diameter antennas. In addition, this diminishing rate of return is also demonstrated in Figure 5.3 as the probability of detection requirement is decreased. Starting with the highest probability of detection, the largest declines in the $P_t N^2$ product curves occur when this requirement is initially reduced then taper off as the minimum probability of detection continues to be lowered. Therefore, the largest cost benefit occurs when the probability of detection requirement is decreased from 95% to 85% compared to 75% to 65%. A comparable diminishing return as the required avail-
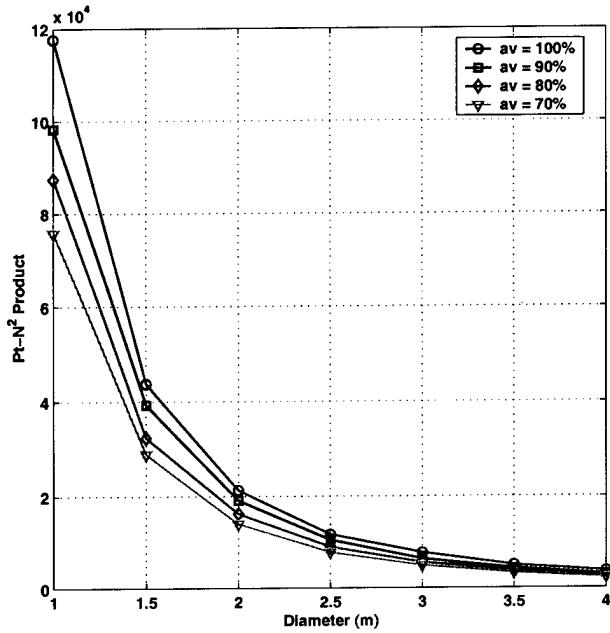
Figure 5.4 Acceptable System Design Architectures ($P_d = 85\%$)

ability is reduced is not evident in Figure 5.4. Overall, these results represent only a small fraction of the possible applications of this design study. As alluded to before, the viable parameters for the constellation and cluster design can be incorporated into a comprehensive model that includes launch, operations, payload, and bus considerations to characterize the overall performance, costs, and reliabilities of candidate TechSat 21 architectures. This system-wide analysis would be extremely beneficial in the development process of this sparse aperture space-based GMTI radar system.

Chapter 6

CONCLUSIONS

6.1 Thesis Summary

The main objective of this thesis was to evaluate the radar performance capabilities of various TechSat 21 system architectures. Using the fundamentals of space-based radar and separated spacecraft interferometry as a foundation, a model was developed to assess performance based on the probability of detection and availability metrics. The model was used to conduct a design study where minimum performance requirements were specified to identify viable system candidates and eliminate alternatives. Eventually, these results will be used to establish key design trends and find optimal configurations for the operational TechSat 21 system. The remainder of this section summarizes the important results contained in this thesis.

Detecting targets and determining their locations is the basic premise behind radar. The frequency content of the target echoes provides additional information used to measure the range rates of each target. When designing a radar system, careful consideration must be give to the chosen frequency and waveform of the transmitted signal, the properties of the antenna beam, and the parameters of the pulsed signal. From these concerns, the measurement of target ranges and range rates is evaluated, including the impact of range and Doppler ambiguities. The presence of interference in the received signals limits the target detection capabilities of the radar. Noise reduces the maximum detection range of the radar, but its adverse effects are mitigated with certain techniques that improve the signal-

to-noise ratio such as pulse compression and pulse integration. Clutter, on the other hand, is produced by the unwanted reflections from objects on the ground. Although clutter return is orders of magnitude stronger than target echoes, sometimes these target signals are isolated based on the different Doppler profiles of stationary clutter and moving targets. Most of the time, however, some form of signal processing is necessary to separate target returns from clutter.

Most modern space-based radar systems incorporate large antennas to detect targets at the required range and angular resolution. The excessive deployment and maintenance costs with these single aperture systems warrant a better alternative. The interferometric combination of the signals received by an array of sparse apertures synthesizes an aperture based on the maximum separation distance of the satellites. This gives a significant improvement in angular resolution while maintaining the same area search rate. The cluster of satellites must maintain an adequate spatial distribution of the apertures in all directions of interest. Certain free orbit trajectories satisfy this condition to help minimize the propulsive demands of the system. In radar interferometry, the footprint projected by the cluster is divided into a cell grid based on the spatial resolution of the synthesized aperture. Each cell is scanned by the point spread function to maximize the probability of detecting targets. Unfortunately, none of this is possible unless some form of signal processing is performed to suppress the contribution of clutter in the received radar signals. While certain signal processing methods such as DPCA and STAP have demonstrated high levels of clutter suppression in existing airborne and space-based radar systems, the perfect cancellation of clutter provided by deconvolution has the potential to significantly enhance the performance of space-based GMTI radar.

With this comprehensive background on space-based radar and separated spacecraft interferometry, we developed a model to evaluate the performance of the TechSat 21 radar system within the framework provided by the GINA methodology. Applying GINA to space-based radar, the probability of detection was the integrity metric and the minimum detectable velocity was the isolation metric, each with their associated availabilities. Unique

radar system architectures were defined by the number of satellites in the cluster, the orbital altitude, the aperture diameter, and the antenna transmission power. Our first approach was to construct the model based on the performance variations within a footprint. Starting with general parameters of the radar system, the satellite configuration was determined to characterize the receive gain (PSF) at a specified ground location. From the properties of the clutter in the footprint and the mean noise level in the system, the probability of detection was calculated for each cell to determine the performance availability of the system. Although this model produced meaningful results, they could not identify viable TechSat 21 system architectures because the performance at the constellation level was not considered. Therefore, the model was expanded to evaluate the radar performance over the entire field of regard of the system. The parameters defining the constellation from the total number of clusters and their chosen orbits were used to compute the statistical distribution of grazing angles in the coverage area. Using these statistics and other generic system parameters, the variations in the probability of detection and MDV over the coverage area set the availabilities of these performance metrics for the TechSat 21 constellation. We now had a tool to accurately analyze the performance of candidate TechSat 21 architectures.

An easy design study well suited to this model would have simply evaluated the performance metrics for a limited selection of reasonable TechSat 21 architectures and compared the results to identify the best option. While this is a valid approach, we could generate much more useful results with the opposite idea. Instead of characterizing the performance of TechSat 21 system configurations, the better alternative is to set a minimum level of performance and figure out which configurations satisfy these requirements. By taking a closer look at the SNR equation, we realized that some parameters specified the system design, others varied with aperture diameter and ground location of the footprint in the cluster coverage area, and the remainders were predetermined constants. Again using the coverage area statistics defined by the constellation design, a value for the variational parameters was selected based on a required performance availability. Similarly, the minimum probability of detection specified the required SNR in the received

radar signals after processing. Combining these quantities yielded the minimum value for the product of the antenna transmission power and the number of satellites squared for a given aperture diameter. This $P_t N^2$ product identifies which TechSat 21 architectures meet the performance requirements of the system. Further cost, reliability, and performance analysis is needed to decide the optimal combination of transmission power and the number of satellites.

6.2 Future Work

This thesis addresses only a small fraction of the numerous design considerations for a sparse aperture space-based GMTI radar system such as TechSat 21. There remain additional unanswered questions that warrant further investigation. Those listed here are a summary of the various issues discussed throughout the thesis.

- Consolidate into a larger system-wide model - The performance results presented in this thesis are limited to the design of the radar system. The $P_t N^2$ product is a valuable quantity to distinguish viable system architectures. However, true design optimization requires a more comprehensive system model that includes bus, payload, operations, and launch considerations to characterize the overall capability and performance of the complete system. This expanded model will eventually permit a complete exploration of the TechSat 21 trade space.

- Validate the proposed signal processing strategies - A number of novel signal processing methods were discussed in previous chapters, but very few have been demonstrated experimentally. Computer testbeds will simulate the real-time combination of radar receiver inputs in severe clutter backgrounds. One such testbed under development at the MIT Space Systems Laboratory is known as GFLOPS. This will investigate a wide variety of issues including the footprint scan, clutter rejection with the deconvolution algorithm, pulse compression, pulse integration, resolving ambiguities, and operational autonomy. This validation is needed before we can proceed with the actual implementation of these concepts in an operational distributed satellite system.

- Update the model to continually improve the results - The coverage area and design study models contain certain simplifications that should be relaxed if possible. For instance, the array factor gain is approximated by its mean value because it is assumed that variations in the point spread function do

not significantly impact the ability to detect targets. However, spatial variations over the cluster coverage area and temporal variations from satellite orbital motion may limit the synthesis of a reliable sparse aperture. Also, target detection may be possible in the outer extents of the clutter band, meaning that fairly accurate clutter models are needed to evaluate its power contribution in the received radar signals.

This thesis represents a preliminary radar performance analysis of two-dimensional Tech-Sat 21 clusters. Initial results indicate a substantial improvement in performance provided by clusters of cooperative microsatellites in the space-based GMTI radar mission, but many avenues still need to be explored to fully understand and realize the potential benefits of this concept.

6.3 Closing Remarks

Although some useful results are presented in this thesis, the main value is contained in the background discussion on space-based GMTI radar using separated spacecraft interferometry as well as the overall development process for the TechSat 21 radar performance model. This model demonstrates the superior performance capabilities of this system provided by the distribution of satellite resources within a cluster of microsatellites. The ability to represent the radar system performance with a single parameter (the $P_t N^2$ product) is a powerful tool in identifying viable system design configurations.

REFERENCES

[AFRL, 1998] Air Force Research Laboratory - Space Vehicles Directorate, *TechSat 21 - Space Missions Using Satellite Clusters*, <URL:http://www.vs.afrl.af.mil/fact-sheets/TechSat21.html>, June 1998.

[Barton, 1988] Barton, D. K., *Modern Radar System Analysis*, Artech House, Inc., 1988.

[Cantafio, 1989] Cantafio, L. J., ed., *Space-Based Radar Handbook*, Artech House, Inc., 1989.

[Das et al, 1998] Das, A., Cobb, R., and Stallard, M., *TechSat 21 - A Revolutionary Concept in Distributed Space Based Sensing*, AIAA Defense and Civil Space Programs Conference and Exhibit, AIAA 98-5255, October 1998.

[Enright, 1999] Enright, J. P., *Investigation of Spacecraft Cluster Autonomy Through an Acoustic Imaging Interferometric Testbed*, Masters Thesis, Department of Aeronautics and Astronautics, Massachusetts Institute of Technology, September 1999.

[Hacker et al, 1999] Hacker, T. L. and Sedwick, R. J., *Space-Based GMTI Radar Using Separated Spacecraft Interferometry*, AIAA Space Technology Conference and Exposition, AIAA 99-4634, September 1999.

[Hill, 1878] Hill, G. W., *Researches in the Lunar Theory*, American Journal of Mathematics, Vol. 1, No. 1, 1878.

[Jilla, 1998] Jilla, C. D., *Separated Spacecraft Interferometry - System Architecture Design and Optimization*, Masters Thesis, Department of Aeronautics and Astronautics, Massachusetts Institute of Technology, December 1998.

[Klemm, 1998-1] Klemm, R., *Introduction to Space-Time Adaptive Processing*, IEE Colloquium on Space-Time Adaptive Processing, Ref. No. 1998/241, April 1998.

[Klemm, 1998-2] Klemm, R., *Space-Time Adaptive Processing: Principles and Applications*, Peter Peregrinus Limited, 1998.

[Kogon et al, 1999] Kogon, S. M., Rabideau, D. J., and Barnes, R. M., *Clutter Mitigation Techniques for Space-Based Radar*, IEEE International Conference on Acoustics, Speech, and Signal Processing, Vol. 4, March 1999.

[Kong, 1998] Kong, E. M. C., *Optimal Trajectories and Orbit Design for Separated Spacecraft Interferometry*, Masters Thesis, Department of Aeronautics and Astronautics, Massachusetts Institute of Technology, November 1998.

[Leech, 1956] Leech, J., *On the Representation of 1,2,....n by Differences*, Journal of the London Mathematical Society, Vol. 31, 1956.

[Mahafza, 1998] Mahafza, B. R., *Introduction to Radar Analysis*, CRC Press LLC, 1998.

[Martin et al, 1999] Martin, M. and Stallard, M. J., *Distributed Satellite Missions and Technologies - The TechSat 21 Program*, AIAA Space Technology Conference and Exposition, AIAA 99-4479, September 1999.

[Miller, 1999] Miller, R. W., *Space-Time Adaptive Processing for TechSat 21 MTI Radar*, May 1999.

[Murray et al, 1997] Murray, D. J., Coe, D. J., and White, R. G., *Experimental MTI with Spaceborne Geometries*, IEE Colloquium on Radar Interferometry, Ref. No. 1997/153, April 1997.

[Nathanson, 1969] Nathanson, F. E., *Radar Design Principles*, McGraw-Hill, 1969.

[Neuvy, 1970] Neuvy, J., *An Aspect of Determining the Range of Radar Detection*, IEEE Transactions on Aerospace and Electronic Systems, Vol. 6, No. 4, July 1970.

[Nohara, 1995] Nohara, T. J., *Comparison of DPCA and STAP for Space-Based Radar*, IEEE International Radar Conference, May 1995.

[Rabideau et al, 1999] Rabideau, D. J. and Kogon, S. M., *A Signal Processing Architecture for Space-Based GMTI Radar*, Proceedings IEEE Radar Conference, April 1999.

[Sedwick et al, 1998] Sedwick, R. J., Kong, E. M. C., and Miller, D. W., *Exploiting Orbital Dynamics and Micropropulsion for Aperture Synthesis Using Distributed Satellite Systems: Applications to TechSat 21*, AIAA Defense and Civil Space Programs Conference and Exhibit, AIAA 98-5289, October 1998.

[Sedwick et al, 1999] Sedwick, R. J., Hacker, T. L., and Miller, D. W., *Optimum Aperture Placement for a Space-Based Radar System Using Separated Spacecraft Interferometry*, AIAA Guidance, Navigation, and Control Conference and Exhibit, AIAA 99-4271, August 1999.

[Sedwick et al, 2000] Sedwick, R. J., Hacker, T. L., and Marais, K., *Performance Analysis for an Interferometric Space-Based GMTI Radar System*, IEEE International Radar Conference - RADAR 2000, May 2000.

[Shaw, 1998] Shaw, G. B., *The Generalized Information Network Analysis Methodology for Distributed Satellite Systems*, Ph.D. Thesis, Department of Aeronautics and Astronautics, Massachusetts Institute of Technology, 1998.

[Skolnik, 1980] Skolnik, M. I., *Introduction to Radar Systems*, McGraw-Hill Book Com-

pany, 1980.

[Skolnik, 1990] Skolnik, M. I., *Radar Handbook*, McGraw-Hill Book Company, 2nd edition, 1990.

[Stimson, 1998] Stimson, G. W., *Introduction to Airborne Radar*, SciTech Publishing, Inc., 2nd edition, 1998.

[Swerling, 1960] Swerling, P., *Probability of Detection for Fluctuating Targets*, IRE Transactions IT-6, No. 2, April 1960.

[Thompson et al, 1994] Thompson, A. R., Moran, J. M., and Swenson, G. W. Jr., *Interferometry and Synthesis in Radio Astronomy*, Krieger Publishing Co., 1994.

[Ward, 1994] Ward, J., *Space-Time Adaptive Processing for Airborne Radar*, MIT Lincoln Laboratory Training Report 1015, ESC-TR-91-109, December 1994.

[Wickert, 1997] Wickert, D. P., *Space Based Radar - System Architecture Design and Optimization for a Space Based Replacement to AWACS*, Masters Thesis, Department of Aeronautics and Astronautics, Massachusetts Institute of Technology, May 1997.

[Winings, 1997] Winings, M. J. and Jamieson, J. A., *Infrared Imaging Spatial Spectral Interferometer for Spaceborne Rapid-Response, Global-Surveillance*, Proceedings of SPIE, Vol. 3063, 1997.

Appendix A

FOOTPRINT MATLAB CODE

A.1 Master File

```
%TechSat 21 Footprint Model - Master File


clear all
tic


%design vector variables
N = 8;        %number of satellites
h = 8e5;      %orbital altitude (m)
D = 2.4;      %aperture diameter (m)
Pt = 200;     %transmission power (W)


%constants vector inputs
f = 10e9;           %frequency (Hz)
DC = 0.05;          %antenna tranmission duty cycle
sigmaT = 10;        %target radar cross section (m^2)
reqrngres = 250;    %required range ground resolution (m)
reqXrngres = 1000;  %required cross range ground resolution (m)
Pdmin = 0.85;       %minimum probability of detection
FAR = 1e-3;         %false alarm rate
reqMDV = 1.5;       %required minimum detectable velocity (m/s)
vTmax = 20;         %maximum target velocity (m/s)
nadirhole = 5*pi/180;   %grazing angle nadir hole (deg)


disp('Enter the terrain type according to the following table:')
disp('   1 - Sea')
```

```
disp('   2 - Deserts and roads')
disp('   3 - Cultivated land')
disp('   4 - Open woods')
disp('   5 - Wooded hills')
disp('   6 - Cities')
type = input('Terrain Type: ');      %terrain type (used to find
                                     %the clutter reflectivity)
while (type < 1) | (type > 6)
    disp('The terrain type is invalid.')
    type = input('Please reenter the terrain type (1-6).');
end


%other module variables
c = 2.998e8;         %speed of light (m/s)
lamda = c/f;         %wavelength (m)
Pavg = Pt*DC;        %antenna average power (W)
k = 1.381e-23;       %Boltzmann constant (J/K)
Tdwell = 0.050;      %dwell time (s)
Ts = 290;            %antenna temperature (K)
LsdB = 3;            %system losses (dB)
Re = 6.378e6;        %Earth radius (m)
theta = 2.44*lamda/D;    %antenna beamwidth (rad)
vp = 1.9964e7/sqrt(h + Re);    %velocity of the satellite cluster (m/s)
ESAmax = 60*pi/180;   %maximum off-boresight angle for the ESA (rad)


%input ground location
dec = 45*pi/180;
az = 90*pi/180;
while dec < acos(Re/(Re + h))
    disp('The satellite footprint does not fall on the Earth surface')
    dec = input('Please reenter the declination angle.')*pi/180;
end




%calculate the isolation and rate parameters as well as other radar quan-
tities of interest
PARAMETER = radarparameter(D,vp,lamda,FAR,Pdmin,Pt,sigmaT,...
    N,k,Ts,LsdB,Tdwell,Re,h,ESAmax,reqrngres,reqXrngres,DC,...
    c,reqMDV,vTmax,nadirhole,dec)
```

```
%calculate the 3D Hill's frame coordinates for each satellite
[S,j] = spacing(N,PARAMETER.baseline);
COORD = Hillcoords(N,PARAMETER.baseline,S,j)


%find the ground projection
NSATGROUND = satground(COORD,PARAMETER.baseline,j,dec,az)


%calculate the PSF
NSATPSF = psf1D(NSATGROUND,N,D,PARAMETER.matrix_res,lamda)


%determine the radar footprint parameters
NSATFOOTPRINT = footprint(dec,az,D,PARAMETER.matrix_res,...
    lamda,Re,h,vp,type)


%calculate the signal-to-noise ratio for the footprint
PROCESSING = deconvolve(PARAMETER,NSATPSF,NSATFOOTPRINT,...
    N,Pavg,D,lamda,sigmaT,k,Ts,LsdB)


%determine the performance metrics
CAPABILITY = radarcapability(PROCESSING,NSATFOOTPRINT,...
    PARAMETER,D,lamda,Tdwell)


toc
```

A.2 Radar Parameters Module

```
%TechSat 21 Footprint Model - Radar Parameters Module


function [PARAMETER] = radarparameter(D,vp,lamda,FAR,Pdmin,Pt,sigmaT,...
    N,k,Ts,LsdB,Tdwell,Re,h,ESAmax,reqrngres,reqXrngres,DC,c,...
    reqMDV,vTmax,nadirhole,dec)
%calculates some of the key radar parameters that affect isolation and
%rate and other properties of the transmitted pulse train based on the
%constraints in the design and constants vectors
```

```
%calculate the PRF from geometric constraints
elhzn = asin(Re/(Re+h)) - 1.22*lamda/D;   %horizon elevation angle (rad)
psihzn = acos((Re+h)*sin(elhzn)/Re);
Rmaxhzn = Re*sin(pi/2-elhzn-psihzn)/sin(elhzn); %horizon max range (m)
psiESA = acos((Re+h)*sin(ESAmax)/Re); %max ESA grazing angle (rad)
RmaxESA = Re*sin(pi/2-ESAmax-psiESA)/sin(ESAmax);       %ESA max range (m)
if RmaxESA < Rmaxhzn     %find the smallest geometric max range
    Rmaxgeo = RmaxESA;
    Rgeoflag = 'ESA';
    elmax = ESAmax;
    psimin = psiESA;
else
    Rmaxgeo = Rmaxhzn;
    Rgeoflag = 'horizon';
    elmax = elhzn;
    psimin = psihzn;
end
psitmin = acos((Re+h)/Re*...
    sin(elmax+1.22*lamda/D));  %toe grazing angle (rad)
psihmin = acos((Re+h)/Re...
    *sin(elmax-1.22*lamda/D));    %heel grazing angle (rad)
Lmax = Re*(psihmin - psitmin - 2.44*lamda/D);   %footprint length (m)
PRFgeo = c/2/cos(psimin)/Lmax;   %max range unambiguous PRF


%determine the signal frequency properties
BWr = 1/Tdwell;   %receiver bandwidth/Doppler bin width (Hz)
velres = BWr*lamda/2;   %velocity resolution (m/s)
fdTmax = 2*vTmax/lamda;    %max target Doppler shift (Hz)
Nfdbins = floor(Tdwell*4*vp/lamda*sin(pi/2-dec)*sin(1.22*lamda/D)) +...
    ceil(2*fdTmax/BWr);
if round(Nfdbins/2) == Nfdbins/2
    Nfdbins = Nfdbins + 1;     %required number of Doppler bins
end


%find the smallest maximum range (SNR vs geometric constraints)
Pfa = FAR/BWr;    %false alarm probability
nfa = log(0.5)/log(1 - Pfa);  %number of false alarms
taup = DC/PRFgeo;     %pulse width (s)
np = floor(Tdwell*PRFgeo);      %number of pulses in a CPI
```

```
Rstart = 1;
Rflag = 1;
while Rflag == 1   %find optimal PRF-max range combination for min SNR
    beta = 1/6;
    SNRmin = log10(nfa)/np/log10(1/Pdmin)^beta; %min SNR from required Pd
    Ls = 10^(LsdB/10);
    RmaxSNR = (Pt*sigmaT*(0.9*pi)^2*(D/2)^4*N^2*taup/...
        (4*pi*lamda^2*k*Ts*Ls*SNRmin))^0.25;    %max range from min SNR
    if RmaxSNR < Rmaxgeo     %determine smallest max range
        Rmax = RmaxSNR;
        Rmaxflag = 'SNR';
        phic = acos((Re^2+(Re+h)^2-Rmax^2)/(2*Re*(Re+h)));
        elmax = asin(Re*sin(phic)/Rmax);
        psimin = acos((Re+h)*sin(elmax)/Re);
        psitmin = acos((Re+h)/Re*sin(elmax+1.22*lamda/D));
        psihmin = acos((Re+h)/Re*sin(elmax-1.22*lamda/D));
        Lmax = Re*(psihmin - psitmin - 2.44*lamda/D);
        PRF = c/2/cos(psimin)/Lmax;
        taup = DC/PRF;
        np = floor(Tdwell*PRF);
        if Rmax > Rstart
            Rflag = 1;
            Rstart = Rmax;
        else
            Rflag = 2;
            Rmax = Rstart;
        end
    else
        Rflag = 2;
        Rmax = Rmaxgeo;
        Rmaxflag = Rgeoflag;
        PRF = PRFgeo;
    end
end
if Rmax < h     %error message when max range is less than altitude
    disp('The chosen values for the design vector are too small to')
    disp('provide adequate SNR for target detection.')
    disp('Please reselect design vector inputs.')
    pause
end
```

```
%determine the remaining pulse properties
taucp = 2*reqrngres/c*cos(pi/2-nadirhole);    %compressed pulse width (s)
BWs = 1/taucp;    %signal bandwidth (Hz)
taup = DC/PRF;    %pulse width (s)
CR = taup/taucp;   %pulse compression ratio


%calculate the cluster baseline
B_Rmax = ceil(2*lamda*Rmax/reqXrngres/...
    cos(elmax));   %max radius cluster baseline (m)
cellwidth = floor(2*reqMDV/lamda/BWr)*BWr;   %Doppler bin bandwidth (Hz)
B_MDV = ceil(lamda/asin(cellwidth*lamda/...
    4/vp/sin(elmax)));  %required MDV cluster baseline (m)
if B_Rmax > B_MDV    %choose larger baseline
    B = B_Rmax;
    Bflag = 'Rmax';
elseif B_MDV > B_Rmax
    B = B_MDV;
    Bflag = 'MDV';
end
n = round(B/D);   %matrix dimension constant (footprint resolution)


%calculate the minimum area search rate (assuming search mode operation)
ASR = 2*Rmax*sin(elmax)*vp;   %area search rate (m^2/s)


%calculate the minimum detectable velocity
Dopspread = 4*vp/lamda*sin(lamda/B)...
    *sin(elmax);        %clutter Doppler spread (Hz)
Dopbinscell = ceil(Dopspread/BWr);   %number of Doppler bins with clutter
MDV = lamda/2*Dopbinscell*BWr;    %minimum detectable velocity (m/s)


%determine the range and cross-range resolution at the ground location
psi = acos((Re+h)*sin(pi/2-dec)/Re);   %ground location grazing angle
(rad)
rngres = c/2*taucp*sec(psi);     %range resolution (m)
if psi == dec
    Rs = h;
else
    Rs = Re*sin(dec-psi)/sin(pi/2-dec);    %radar range (m)
```

```
end
Xrngres = 2*lamda*Rs/B/cos(pi/2-dec);   %cross-range resolution (m)


%output data structures
PARAMETER.pulse_rep_freq = PRF;
PARAMETER.num_Doppler_bins = Nfdbins;
PARAMETER.num_pulses = np;
PARAMETER.pulse_width = taup;
PARAMETER.comp_pulse_width = taucp;
PARAMETER.comp_ratio = CR;
PARAMETER.signal_bandwidth = BWs;
PARAMETER.receive_bandwidth = BWr;
PARAMETER.range_res = rngres;
PARAMETER.Xrange_res = Xrngres;
PARAMETER.vel_res = velres;
PARAMETER.prob_false_alarm = Pfa;
PARAMETER.max_elev_angle = elmax;
PARAMETER.min_grazing_angle = psimin;
PARAMETER.footprint_length = Lmax;
PARAMETER.max_range = Rmax;
PARAMETER.limit_max_range = Rmaxflag;
PARAMETER.baseline = B;
PARAMETER.limit_baseline = Bflag;
PARAMETER.matrix_res = n;
PARAMETER.area_search_rate = ASR;
PARAMETER.min_detect_vel = MDV;
```

A.3 Satellite Configuration Module

A.3.1 Spacing Function

```
%TechSat 21 Footprint Model - Spacing Function


function [S,j] = spacing(N,B)
%determines the normalized satellite spacing along the velocity
%vector (y-axis) and the orbit based on the number of satellites
```

```
while (N < 3) | (N > 16)
    disp('The number of satellites does not fall within the')
    disp('acceptable range.')
    N = input('Please reenter the number of satellites (3-16).');
end
if N == 3
    s = [1 2];
    j = [1];
elseif N == 4
    s = [1 3 2];
    j = [1 4];
elseif N == 5
    s = [3 1 5 2];
    j = [1 4];
elseif N == 6
    s = [1 3 6 2 5];
    j = [1 4 5];
elseif N == 7
    s = [8 1 3 6 5 2];
    j = [1 4 5];
elseif N == 8
    s = [8 10 1 3 2 7 8];
    j = [1 4 5 8];
elseif N == 9
    s = [1 2 3 7 7 4 4 1];
    j = [1 4 5 8 9];
elseif N == 10
    s = [7 15 5 1 3 8 2 16 7];
    j = [1 4 5 8 9];
elseif N == 11
    s = [18 1 3 9 11 6 8 2 5 28];
    j = [1 4 5 8 9];
elseif N == 12
    s = [18 1 3 9 11 6 8 2 5 28 7];
    j = [1 4 5 8 9 12];
elseif N == 13
    s = [18 1 3 9 11 6 8 2 5 28 7 15];
    j = [1 4 5 8 9 12 13];
elseif N == 14
    s = [18 1 3 9 11 6 8 2 5 28 7 15 4];
```

```
      j = [1 4 5 8 9 12 13];
elseif N == 15
      s = [18 1 3 9 23 6 8 2 5 28 7 15 4 11];
      j = [1 4 5 8 9 12 13];
elseif N == 16
      s = [18 1 3 9 23 6 8 10 5 28 7 15 4 11 2];
      j = [1 4 5 8 9 12 13 15];
end
S = s * B/sum(s);     %actual satellite spacing (m)
```

A.3.2 Hill's Coordinates Function

```
%TechSat 21 Footprint Model - Hill's Coordinates Function


function COORD = Hillcoords(N,B,S,j)
%converts a given satellite spacing along the y-axis into the
%3D Hill's frame coordinates and places each satellite into
%its proper orbit


a = round(B/4);    %height of the orbit ellipse
b = round(B/2);    %width of the orbit ellipse
i = atan(a/b);     %inclination of the elliptical orbits (rad)


county = 1;
y(county) = 0;
for county = 1:(N-1)
    y(county + 1) = y(county) + S(county);    %1D satellite coordinates
end
y = y - 0.5*B;
x = real(sqrt(a^2 * (1 - y.^2/b^2)));
for countx = 2:2:N
    x(countx) = -x(countx);        %2D satellite coordinates
end
z = real(sqrt(b^2 - y.^2));
z(j) = -z(j);      %two ellipse z coordinates


%satellite elliptical orbits
y1 = linspace(-b,b,B);
```

```
x1 = sqrt(a^2 * (1 - y1.^2/b^2));
x2 = -x1;
z1 = sqrt(b^2 - y1.^2);
z2 = -z1;

%plot the satellites in Hill's frame
figure
clf
plot3(z,y,x,'k*',z1,y1,x1,'b-',z2,y1,x2,'b-',...
    z1,y1,x2,'r-',z2,y1,x1,'r-')
axis square
axis equal
set(gca,'fontweight','bold')
box on
xlabel('crossrange/z-axis (m)')
ylabel('velocity vector/y-axis (m)')
zlabel('zenith/x-axis (m)')
title('3D Satellite Locations')

alpha = atan2(-y/(2*a),x/a);
beta = alpha;   %satellite phase angles (equal because the orbit
                %projects a circle on the ground at nadir)

%output data structures
COORD.ellipse_height = a;
COORD.ellipse_width = b;
COORD.inclination = i;
COORD.xy_phase = alpha;
COORD.z_phase = beta;
```

A.4 Ground Projection Module

```
%TechSat 21 Footprint Model - Ground Projection Module

function NSATGROUND = satground(COORD,B,j,dec,az)
%N satellite configuration coordinates at a specific location
```

```
%inputs from other radar modules
a = COORD.ellipse_height;
b = COORD.ellipse_width;
alpha = COORD.xy_phase;
beta = COORD.z_phase;

%determine the ground projection
x = a*cos(alpha);
y = -2*a*sin(alpha);
z = b*cos(beta);       %simplified Hill's frame equations
z(j) = -z(j);       %projects satellites onto 2 elliptical orbits
coord = [x;y;z];   %satellite Hill's frame coordinates
Tz = [cos(dec) sin(dec) 0;-sin(dec) cos(dec) 0;0 0 1]; %coordinate trans-
Tx = [1 0 0;0 cos(az) sin(az);0 -sin(az) cos(az)];    %formation matrices
prime = Tz*Tx*coord;
xg = prime(3,:);
yg = prime(1,:);       %satellite 2D ground coordinates

%plot the ground locations
ground = xg + i*yg;
figure
clf
plot(ground,'k*')
axis square
axis([-0.6*B 0.6*B -0.6*B 0.6*B])
axis equal
set(gca,'fontweight','bold')
box on
xlabel('x (m)')
ylabel('y (m)')
title('Satellite Ground Projections')

%output data structures
NSATGROUND.x_ground = xg;
NSATGROUND.y_ground = yg;
```

A.5 Point Spread Function Module

```
%TechSat 21 Footprint Model - Point Spread Function Module


function [NSATPSF] = psf1D(NSATGROUND,N,D,n,lamda)
%calculates the point spread function (PSF) for a satellite
%configuration based on the ground projection


%inputs from other radar modules
xaper = NSATGROUND.x_ground;
yaper = NSATGROUND.y_ground;


%define the image angular coordinates
thetax = linspace(-2.44*lamda/D,2.44*lamda/D,2*n+1);
thetax = unique(thetax) + eps;
thetax = repmat(thetax,length(thetax),1);
thetay = thetax.';
theta = sqrt(thetax.^2 + thetay.^2);


%calculate the single antenna gain
Gapert = real(((pi*D*(1 + cos(theta))/lamda).^2).*...
    (besselj(1,pi*D*sin(theta)/lamda)./(pi*D*sin(theta)/lamda)).^2);
for j = 1:n+1
    for k = 1:n+1
        Gant(j,k) = Gapert((j+floor(n/2)),(k+floor(n/2)));
    end
end


%calculate the array factor gain
AF = zeros(2*n+1);
for count = 1:length(xaper)
    AF = AF + exp(-2*pi*i*(thetay*yaper(count) +...
        thetax*xaper(count))/lamda);
end
Gaf = abs(AF).^2;        %array factor gain
Gr = Gaf.*Gapert;        %receive gain
PSF = 10*log10(Gr);      %point spread function
normGaf = Gaf/N^2;       %normalized array facto gain
[r,s] = max(max(normGaf));
Gafstrip = normGaf(s,:);    %only need center strip (range unambiguous)
```

```
%graph the PSF
figure
clf
mesh(thetax/pi*180,thetay/pi*180,PSF)
set(gca,'fontweight','bold')
view(3)
xlabel('\theta_x (degrees)')
ylabel('\theta_y (degrees)')
zlabel('Gain (dB)')
axis square
colorbar
title('Point Spread Function')
xlim = round(max(max(thetax/pi*180))*10)/10;
axis([-xlim xlim -xlim xlim min(min(PSF)) max(max(PSF))])
box on

%output data structures
NSATPSF.gain_antenna = Gant;
NSATPSF.gain_array_factor = Gafstrip;
```

A.6 Footprint Properties Module

A.6.1 Clutter Reflectivity Function

```
%TechSat 21 Footprint Model - Clutter Reflectivity Function

function [sigmanot] = clutter(type,psi)
%determines the clutter reflectivity per unit area based on
%the terrain type and grazing angle

%the values for gamma (with the exception of sea clutter)
%were obtained from Radar Design Principles
%by Nathanson, Table 7-13, pg 273
if type == 1
    gamma = -30;        %sea clutter return (dB)
elseif type == 2
```

```
    gamma = -25;        %desert and roads clutter return (dB)
elseif type == 3
    gamma = -22;        %cultivated land clutter return (dB)
elseif type == 4
    gamma = -16;        %open woods clutter return (dB)
elseif type == 5
    gamma = -14;        %wooded hills clutter return (dB)
elseif type == 6
    gamma = -11;        %cities clutter return (dB)
end
sigmanot = 10^(gamma/10)*sin(psi);   %clutter reflectivity per unit area
```

A.6.2 Footprint Properties Function

```
%TechSat 21 Footprint Module - Footprint Properties Function


function [NSATFOOTPRINT] = footprint(dec,az,D,n,lamda,Re,h,vp,type)
%determines the properties of the footprint projected on the ground
%by the given satellite configuration


%create a grid for the footprint centered on ground location
delta_az = linspace(az - 1.22*lamda/D,az + 1.22*lamda/D,n+1);
delta_az = unique(delta_az) + eps;
delta_az = fliplr(delta_az);
delta_dec = linspace(dec - 1.22*lamda/D,dec + 1.22*lamda/D,n+1);
delta_dec = unique(delta_dec) + eps;
thetaant = 2.44*lamda/D;    %antenna beamwidth (rad)
thetacell = 2*thetaant/n/2.44;      %cell beamwidth (rad)


%calculate the grazing angle (psi) and the radar range (Rs)
delta_el = pi/2 - delta_dec;      %elevation angle (rad)
psi = acos((Re + h)*sin(delta_el)/Re);      %grazing angle (rad)
phic = pi/2 - delta_el - psi;       %Earth angle (rad)
for k = 1:n+1  %correction for nadir
    if psi(k) == delta_dec(k)
        Rs(k) = h;
    else
        Rs(k) = Re*sin(phic(k))./sin(delta_el(k));    %radar range (m)
```

```
    end
end


%calculate the cell area and clutter cross section
fparea = thetaant^2*Rs(round(n/2))^2/...
    sin(psi(round(n/2)));    %footprint area (m^2)
cellarea = thetacell^2*Rs.^2./sin(psi);        %cell area (m^2)
sigmanot = clutter(type,psi);    %clutter reflectivity per unit area
sigma_c = sigmanot.*cellarea;    %clutter cross section (m^2)


%calculate the Doppler shift and Doppler spread for each cell
delta_Az = repmat(delta_az,length(delta_az),1);
delta_Dec = repmat(delta_dec,length(delta_dec),1);
delta_Dec = delta_Dec';
delta_El = repmat(delta_el,length(delta_el),1);
delta_El = delta_El';
fd = 2*vp*sin(delta_El).*cos(delta_Az)/lamda;    %Doppler shift (Hz)
deltafd_az = 2*vp*sin(delta_Az).*sin(delta_El)*...
    (cos(pi/2 - thetacell/2) - cos(pi/2 + thetacell/2))/lamda;
deltafd_el = 2*vp*cos(delta_Az).*(sin(delta_El - thetacell/2)...
    - sin(delta_El + thetacell/2))/lamda;
deltafd = sqrt(deltafd_az.^2 + deltafd_el.^2);


%plot the cell parameters for the radar footprint
figure
clf
contour(delta_Az/pi*180,delta_El/pi*180,fd,27);
grid off
set(gca,'fontweight','bold')
xlabel('Azimuth (degrees)')
ylabel('Elevation (degrees)')
axis square
axis([min(delta_az)*180/pi max(delta_az)*180/pi min(delta_el)*180/pi
max(delta_el)*180/pi])
colorbar
title('Properties of the Radar Footprint: Doppler Shift (Hz)')
box on


figure
```

```
clf
plot(psi/pi*180,sigma_c,'m-','linewidth',1.5)
grid on
set(gca,'fontweight','bold')
xlabel('Grazing Angle (degrees)')
ylabel('Clutter Cross Section (m^2)')
axis square
axis([min(psi)*180/pi max(psi)*180/pi min(sigma_c) max(sigma_c)])
title('Properties of the Radar Footprint: Clutter Cross Section')
box on

%output data structures
NSATFOOTPRINT.radar_range = Rs;
NSATFOOTPRINT.footprint_area = fparea;
NSATFOOTPRINT.Doppler_shift = fd;
NSATFOOTPRINT.Doppler_spread = deltafd;
NSATFOOTPRINT.clutter_cross_section = sigma_c;
```

A.7 Signal Processing Module

```
%TechSat 21 Footprint Module - Signal Processing Module

function PROCESSING = deconvolve(PARAMETER,NSATPSF,NSATFOOTPRINT,...
    Nsat,Pavg,D,lamda,sigmaT,k,Ts,LsdB)
%calculates the results from the processing of the received radar signals
%for a given satellite configuration (assume no range ambiguities)

%inputs from other radar modules
Gant = NSATPSF.gain_antenna;        %antenna gain
Gaf = NSATPSF.gain_array_factor;        %array factor gain
Rs = NSATFOOTPRINT.radar_range;     %radar range (km)
fd = NSATFOOTPRINT.Doppler_shift;    %cell Doppler shift (Hz)
deltafd = NSATFOOTPRINT.Doppler_spread;    %cell Doppler spread (Hz)
sigmac = NSATFOOTPRINT.clutter_cross_section;    %clutter RCS (m^2)
Nfdbins = PARAMETER.num_Doppler_bins;   %number of Doppler bins
BWr = PARAMETER.receive_bandwidth;   %Doppler bin bandwidth (Hz)
CR = PARAMETER.comp_ratio;        %pulse compression ratio
n = PARAMETER.matrix_res+1;       %matrix index
```

```
theta = linspace(-1.22*lamda/D,1.22*lamda/D,n); %antenna beamwidth (rad)


%clutter and target contributions in each cell
%(assume Doppler ambiguities are resolved)
N = k*Ts*BWr*ones(n,Nfdbins);          %system noise power (W)
W = waitbar(0,'Computing Footprint SNR...');
for p = 1:n     %footprint scan of all range bins
    midfd = round(min(fd(p,:)) + (max(fd(p,:))-min(fd(p,:)))/2);
    fdbinsH = zeros(1,floor(Nfdbins/2));
    fdbinsL = zeros(1,floor(Nfdbins/2));
    fdbinsH(1) = midfd + BWr;
    fdbinsL(1) = midfd - BWr;
    for m = 2:length(fdbinsH)
        fdbinsH(m) = fdbinsH(m-1) + BWr;
        fdbinsL(m) = fdbinsL(m-1) - BWr;
    end
    fdbins = [fliplr(fdbinsL) midfd fdbinsH];    %assign Doppler
                                                 %bin frequencies


    M = sigmaT*ones(n,length(fdbins));   %target RCS contribution
    for a = 1:n
        minfd = fd(p,a) - deltafd(p,a)/2;
        if minfd < min(fdbins)
            minfd = min(fdbins);
        end
        maxfd = fd(p,a) + deltafd(p,a)/2;
        if maxfd > max(fdbins)
            maxfd = max(fdbins);
        end
        CperHz = sigmac(p)/deltafd(p,a);
        b = find((fdbins >= maxfd) & (fdbins-BWr < maxfd));
        c = find((fdbins >= minfd) & (fdbins-BWr < minfd));
        for d = (b+1):(c-1)
            M(a,d) = M(a,d) + CperHz*BWr;
        end
        M(a,b) = M(a,b) + CperHz*(maxfd-(fdbins(b)-BWr));
        M(a,c) = M(a,c) + CperHz*(fdbins(c)-minfd); %clutter RCS
                                                    %contribution
    end
```

```matlab
    Ls = 10^(LsdB/10);
    X = Pavg*CR*lamda^2*Nsat^2*Gant(p,:).^2./...
        ((4*pi)^3*Rs(p)^4*Ls);        %constant radar equation parameters
    X = repmat(X,size(M,2),1);
    X = X';
    R = X.*M;    %true ground scene

    [r,s] = max(max(Gaf));
    for u = 1:n
        for v = 1:n
            Gscan(v) = Gaf(v+(u-1));
        end
        Gend(u,:) = Gscan;
    end
    PSFmtx = flipud(Gend);        %point spread function matrix

    S = PSFmtx*R;        %received power from targets and clutter (W)
    SCNR = R./N;    %signal-plus-clutter-to-noise ratio
    for q = 1:n    %find cells without clutter
        SNR(p,q) = min(SCNR(q,:));        %signal-to-noise ratio
    end
    waitbar(p/n,W)
end
close(W)

%plot the SNR variations for the entire footprint
figure
clf
mesh(theta/pi*180,theta/pi*180,SNR)
grid on
set(gca,'fontweight','bold')
xlabel('\theta_x (degrees)')
ylabel('\theta_y (degrees)')
zlabel('Signal to Noise Ratio')
axis square
axis([min(theta)*180/pi max(theta)*180/pi min(theta)*180/pi
max(theta)*180/pi min(min(SNR)) max(max(SNR))])
colorbar
title('Footprint Variations in the Signal to Noise Ratio')
box on
```

```
%output data structures
PROCESSING.ground_scene = R;
PROCESSING.receive_scene = S;
PROCESSING.gain_matrix = PSFmtx;
PROCESSING.signal_clutter_noise = SCNR;
PROCESSING.signal_noise = SNR;
```

A.8 Radar Capability Module

```
%TechSat 21 Footprint Model - Radar Capability Module


function CAPABILITY = radarcapability(PROCESSING,NSATFOOTPRINT,...
    PARAMETER,D,lamda,Tdwell)
%calculates the probability of detection, availability, and
%performance of a given satellite configuration


%input parameters from other radar modules
SNR = PROCESSING.signal_noise;    %footprint signal-to-noise ratio
fparea = NSATFOOTPRINT.footprint_area;       %footprint area (m^2)
PRF = PARAMETER.pulse_rep_freq;  %pulse repetition frequency (Hz)
nc = PARAMETER.num_pulses;        %number of pulses in CPI
Pfa = PARAMETER.prob_false_alarm;   %false alarm probability
ASR = PARAMETER.area_search_rate;    %area search rate (m^2/s)
n = length(SNR);        %matrix index
theta = linspace(-1.22*lamda/D,1.22*lamda/D,n); %antenna beamwidth (rad)


%calculate the probability of detection
nfa = log(0.5)/log(1 - Pfa);  %number of false alarms
Tfp = fparea/ASR;    %total available dwell time for a footprint (s)
if Tfp >= Tdwell  %determine if noncoherent integration is possible
   ni = floor(Tfp/Tdwell);        %number of noncoherent integrations
   if ni == 0
      ni = 1;
   end
   beta = 1/6 + exp(-ni/3);
   X = (log10(nfa)./(ni^(2/3)*nc*SNR)).^(1/beta);
```

```
    Pd = 10.^-X;
elseif Tfp < Tdwell
    np = floor(Tfp*PRF);
    beta = 1/6;
    X = (log10(nfa)./(np*SNR)).^(1/beta);
    Pd = 10.^-X;
end


%correct Pd for circular footprint
Theta = repmat(theta,length(theta),1);
cell = sqrt(Theta.^2 + (Theta').^2);
for j = 1:n
    for k = 1:n
        if cell(j,k) > 1.22*lamda/D
            Pd(j,k) = -1e-12;
        end
    end
end


%determine the availability of various levels of detection probability
a = find(Pd == -1e-12);
b = n^2 - length(a);
for j = 1:n+1
    x = find(Pd >= (j-1)/n);
    availPd(j) = length(x)/b;
    p(j) = (j-1)/n;
end


%plot the Pd availability curve
figure
clf
plot(p,availPd,'r-','linewidth',1.5)
grid on
set(gca,'fontweight','bold')
xlabel('Probability of Detection')
ylabel('Availability')
axis square
title('Radar Performance Availability')
```

```
%output data structures
CAPABILITY.time_footprint = Tfp;
CAPABILITY.prob_detect = Pd;
CAPABILITY.availability = availPd;
```

Appendix B

COVERAGE AREA MATLAB CODE

B.1 Master File

```
%TechSat 21 Coverage Area Model - Master File


clear all
tic


%design vector variables
N = 8;         %number of satellites
h = 8e5;       %orbital altitude (m)
D = 4;         %aperture diameter (m)
Pt = 200;      %transmission power (W)


%constants vector inputs
f = 10e9;          %frequency (Hz)
DC = 0.05;         %antenna tranmission duty cycle
sigmaT = 10;       %target radar cross section (m^2)
reqrngres = 250;   %required range ground resolution (m)
reqXrngres = 500;  %required cross range ground resolution (m)
FAR = 1e-3;        %false alarm rate
maxni = 10;        %maximum number of nocoherent integrations
nadirhole = 0.5*pi/180;    %Earth angle nadir hole (rad)
mode = 1;          %operating mode for the system (1=scan, 2=search)
theater = 1e6^2;   %area (m^2) of a region of interest
avail_res = 25;    %resolution of the availability calculations


%other module variables
```

```
c = 2.998e8;        %speed of light (m/s)

lamda = c/f;        %wavelength (m)

Pavg = Pt*DC;       %antenna average power (W)

k = 1.381e-23;      %Boltzmann constant (J/K)

Tdwell = 0.050;     %dwell time (s)

Ts = 290;           %antenna temperature (K)

Ls = 2;             %system losses

Re = 6.378e6;       %Earth radius (m)

theta = 2.44*lamda/D;   %antenna null-to-null beamwidth (rad)

vp = 1.9964e7/sqrt(h + Re);   %velocity of the satellite cluster (m/s)


%input variables from other modules
load cons_stats(35at8)
psistats = CONSTELLATION.avgelv';    %grazing angle statistics
avgview = mean(mean(CONSTELLATION.avgvis));   %average visit time (s)
clear CONSTELLATION




%discretize the coverage area
GEOMETRY = coveragearea(Re,h,vp,lamda,D,reqXrngres,nadirhole,mode,...
    theater,avgview)


%reduce the statistics to PDFs
STATS = coveragestats(GEOMETRY,Re,h,psistats)


%determine the important system parameters
PARAMETER = radarparameter(GEOMETRY,D,c,lamda,DC,Tdwell,FAR,...
    reqrngres,Re,theta)


%calculate the SNR and Pd variations over the coverage area
CAPABILITY = variation(GEOMETRY,PARAMETER,Pt,sigmaT,D,N,DC,c,lamda,...
    k,Ts,Ls,reqrngres,Tdwell,maxni)


%calculate the variations in isolation capability
ISOLATION = resolution(GEOMETRY,PARAMETER,c,vp,lamda,D)


%determine the performance statistics
PERFORMANCE = radarperformance(GEOMETRY,STATS,CAPABILITY,ISOLATION,...
    avail_res,Re,h)
```

toc

B.2 Radar-Earth Geometry Module

```
%TechSat 21 Coverage Model - Radar-Earth Geometry Module


function [GEOMETRY] = coveragearea(Re,h,vp,lamda,D,reqXrngres,...
    nadirhole,mode,theater,avgview)
%discretizes the coverage area of the TechSat 21 configuration


%radar-Earth geometry
elhzn = asin(Re/(Re+h)) - 1.22*lamda/D; %horizon elevation angle (rad)
psihzn = acos((Re+h)/Re*sin(elhzn));    %horizon grazing angle (rad)
phichzn = pi/2 - elhzn - psihzn;        %Earth angle at the horizon
phic = linspace(nadirhole,phichzn,25);    %Earth angle discretization
phic = fliplr(phic);    %Earth angles from horizon to nadir
Rs = ((Re+h)^2 - 2*Re*(Re+h)*cos(phic) + Re^2).^0.5;   %radar range (m)
el = asin(Re*sin(phic)./Rs);   %coverage area elevation angles (rad)
psi = pi/2 - el - phic;    %coverage area grazing angles (rad)
psit = acos((Re+h)/Re*sin(el+1.22*lamda/D)); %toe grazing angle (rad)
psih = acos((Re+h)/Re*sin(el-1.22*lamda/D)); %heel grazing angle (rad)
az = linspace(0,(359)*pi/180,90); %coverage area azimuth angles (rad)


%cluster parameters
B = ceil(2*lamda*max(Rs)/reqXrngres/cos(max(el))); %cluster baseline (m)
if mode == 1    %scan mode
    ASR = theater/avgview;   %area search rate (m^2/s)
elseif mode == 2   %search mode
    ASR = 2*max(Rs)*sin(max(el))*vp;    %area search rate (m^2/s)
end


%output data structures
GEOMETRY.earth_angle = phic;
GEOMETRY.radar_range = Rs;
GEOMETRY.elevation = el;
GEOMETRY.grazing_angle = psi;
```

```
GEOMETRY.grazing_angle_toe = psit;
GEOMETRY.grazing_angle_heel = psih;
GEOMETRY.azimuth = az;
GEOMETRY.baseline = B;
GEOMETRY.area_search_rate = ASR;
```

B.3 Statistics Module

```
%TechSat 21 Coverage Area Model - Statistics Module


function [STATS] = coveragestats(GEOMETRY,Re,h,stats_psi)
%calculates the grazing and elevation angle PDFs


%inputs from other radar modules
az = GEOMETRY.azimuth;       %azimuth angle (rad)


%turn stats files into PDFs
CDF_psi = 1 - stats_psi;    %grazing angle CDF
PDF1 = diff(CDF_psi);
psi1 = linspace(0,pi/2,length(PDF1));
PSI = linspace(0,pi/2,length(stats_psi));
PDF_psi = interp1(psi1,PDF1,PSI);
PDF_psi = PDF_psi/sum(PDF_psi);   %grazing angle PDF


EL = asin(Re*cos(PSI)/(Re+h));
PDF_el = interp1(PSI,PDF_psi,EL);
PDF_el = PDF_el/sum(PDF_el);
PDF_el_3D = PDF_el/length(az);    %elevation angle PDF


%plot the grazing angle availability
figure
clf
plot(PSI*180/pi,stats_psi,'g-','linewidth',1.5)
grid on
set(gca,'fontweight','bold')
xlabel('grazing angle (degrees)')
ylabel('Availability')
```

```
axis square
axis([min(PSI)*180/pi max(PSI)*180/pi 0 1])
box on

%output data structures
STATS.grazing_angle_PDF = PDF_psi;
STATS.elevation_angle_PDF_3D = PDF_el_3D;
```

B.4 Radar Parameters Module

```
%TechSat 21 Coverage Are Model - Radar Parameters Module

function [PARAMETER] = radarparameter(GEOMETRY,D,c,lamda,DC,Tdwell,...
    FAR,reqrngres,Re,theta)
%calculates some of the key radar parameters based on constraints
%in the design and constants vectors

%inputs from other radar modules
psi = GEOMETRY.grazing_angle;        %grazing angle (rad)
psit = GEOMETRY.grazing_angle_toe;   %toe grazing angle (rad)
psih = GEOMETRY.grazing_angle_heel;   %heel grazing angle (rad)
Rs = GEOMETRY.radar_range;           %radar range to target (m)
el = GEOMETRY.elevation;             %elevation angle (rad)

%determine the pulse properties
L = Re*(psih - psit - theta);     %footprint length (m)
PRF = c/2./cos(psi)./L;     %pulse repetition frequency (Hz)
np = floor(Tdwell*PRF);     %number of pulses
taup = DC./PRF;        %pulse width (s)
taucp = 2*reqrngres/c*cos(max(psi));     %compressed pulse width (s)
CR = taup/taucp;  %pulse compression ratio
BWs = 1/taucp;    %signal bandwidth (Hz)
BWr = 1/Tdwell;   %receive bandwidth (Hz)
Pfa = FAR/BWr;    %false alarm probability

%output data structures
PARAMETER.pulse_rep_freq = PRF;
```

```
PARAMETER.num_pulses = np;
PARAMETER.pulse_width = taup;
PARAMETER.comp_pulse_width = taucp;
PARAMETER.comp_ratio = CR;
PARAMETER.signal_bandwidth = BWs;
PARAMETER.receive_bandwidth = BWr;
PARAMETER.prob_false_alarm = Pfa;
```

B.5 Performance Variations Module

```
%TechSat 21 Coverage Area Model - Performance Variations Module


function [CAPABILITY] = variation(GEOMETRY,PARAMETER,Pt,sigmaT,D,N,...
    DC,c,lamda,k,Ts,Ls,reqrngres,Tdwell,maxni)
%calculates the SNR and Pd variations over the radar coverage area


%inputs from radar other modules
psi = GEOMETRY.grazing_angle;       %grazing angle (rad)
Rs = GEOMETRY.radar_range;          %radar range to target (m)
el = GEOMETRY.elevation;          %elevation angle (rad)
az = GEOMETRY.azimuth;           %azimuth angle (rad)
ASR = GEOMETRY.area_search_rate;      %area search rate (m^2/s)
taup = PARAMETER.pulse_width;        %transmitted pulse width (s)
CR = PARAMETER.comp_ratio;          %pulse compression ratio
Pfa = PARAMETER.prob_false_alarm;      %probability of false alarm
nc = PARAMETER.num_pulses;         %number of CPI pulses


%SNR and corresponding Pd variations over coverage area
SNR = Pt*sigmaT*0.85^2*pi*(D/2)^4*taup*N^2*min(CR).*nc./...
    (16*lamda^2*k*Ts*Ls*Rs.^4);      %signal-to-noise ratio


Tfp = pi*(1.22*Rs*lamda/D).^2./...
    sin(psi)/ASR;      %time available to scan a specific location (s)
ni = floor(Tfp/Tdwell);     %number of incoherent integrations
A = find(ni > maxni);
ni(A) = maxni;      %max number of noncoherent integrations
B = find(ni == 0);
```

```
ni(B) = 1;   %enough time for coherent integration only
nfa = log(0.5)/log(1 - Pfa);   %number of false alarms
beta = 1/6 + exp(-ni/3);
X = (log10(nfa)./(ni.^(2/3).*SNR)).^(1./beta);
Pd = 10.^-X;    %probability of detection


%plot the coverage area variations in SNR
figure
clf
plot(psi*180/pi,SNR,'g-','linewidth',1.5)
grid on
set(gca,'fontweight','bold')
xlabel('grazing angle (degrees)')
ylabel('Signal-to-Noise Ratio')
axis square
axis([min(psi)*180/pi max(psi)*180/pi min(SNR) max(SNR)])
title('Coverage Area Variations in the Signal-to-Noise Ratio')
box on


%output data structures
CAPABILITY.time_footprint = Tfp;
CAPABILITY.num_incoherent_int = ni;
CAPABILITY.signal_noise = SNR;
CAPABILITY.prob_detect = Pd;
CAPABILITY.SNRvar = SNRvar;
```

B.6 System Isolation Module

```
%TechSat 21 Coverage Area Model - System Isolation Module


function [ISOLATION] = resolution(GEOMETRY,PARAMETER,c,vp,lamda,D)
%calculates the variations in MDV over the coverage area


%inputs from other radar modules
el = GEOMETRY.elevation;        %elevation angle (rad)
az = GEOMETRY.azimuth;          %azimuth angle (rad)
psi = GEOMETRY.grazing_angle;    %grazing angle (rad)
```

```matlab
Rs = GEOMETRY.radar_range;         %radar range to target (m)
B = GEOMETRY.baseline;            %cluster baseline (m)
BWr = PARAMETER.receive_bandwidth;  %receive bandwidth (Hz)
taucp = PARAMETER.comp_pulse_width;    %compressed pulse width (s)


%determine the projection of the satellite orbits and the corresponding
baseline
a = round(B/4);    %height of the orbit ellipse
b = round(B/2);    %width of the orbit ellipse
y1 = linspace(-b,b,100);
x1 = sqrt(a^2 * (1 - y1.^2/b^2));
x2 = -x1;
z1 = sqrt(b^2 - y1.^2);
z2 = -z1;
coord1 = [x1;y1;z1];
coord2 = [x2;y1;z2];
coord3 = [x2;y1;z1];
coord4 = [x1;y1;z2];    %satellite orbits in Hill's frame
W = waitbar(0,'Computing Projected Baselines...');
for r = 1:length(el)    %find the ground projection of the orbits
   Tz = [cos(pi/2-el(r)) sin(pi/2-el(r)) 0;-sin(pi/2-el(r)) cos(pi/2-
el(r)) 0;0 0 1];
    for s = 1:length(az)
        Tx = [1 0 0;0 cos(az(s)) sin(az(s));0 -sin(az(s)) cos(az(s))];
                                %coordinate transformation matrices
        prime1 = Tz*Tx*coord1;
        prime2 = Tz*Tx*coord2;
        prime3 = Tz*Tx*coord3;
        prime4 = Tz*Tx*coord4;
        xg1 = prime1(3,:);
        yg1 = prime1(1,:);
        dist1 = sqrt(xg1.^2 + yg1.^2);
        xg2 = prime2(3,:);
        yg2 = prime2(1,:);
        dist2 = fliplr(sqrt(xg2.^2 + yg2.^2));
        xg3 = prime3(3,:);
        yg3 = prime3(1,:);
        dist3 = sqrt(xg3.^2 + yg3.^2);
        xg4 = prime4(3,:);
        yg4 = prime4(1,:);    %orbit projection ground coordinates
```

```
        dist4 = fliplr(sqrt(xg4.^2 + yg4.^2));
        Bproj = [(dist1+dist2)' (dist3+dist4)'];   %projected baselines (m)
        avgBproj(r,s) = max(mean(Bproj)); %average projected baseline (m)
    end
    waitbar(r/length(el),W)
end
close(W)


%plot the ground projection of the satellite orbits
ground1 = xg1 + i*yg1;
ground2 = xg2 + i*yg2;
ground3 = xg3 + i*yg3;
ground4 = xg4 + i*yg4;
figure
clf
plot(ground1,'b-')
hold on
plot(ground2,'b-')
hold on
plot(ground3,'r-')
hold on
plot(ground4,'r-')
axis square
axis([-0.6*B 0.6*B -0.6*B 0.6*B])
axis equal
set(gca,'fontweight','bold')
box on
xlabel('x (m)')
ylabel('y (m)')
title('Satellite Ground Projections')


%calculate the MDV variations over coverage area
for u = 1:length(el)
    for v = 1:length(az)
        deltaDop(u,v) = 4*vp/avgBproj(u,v)*...%clutter Doppler spread (Hz)
            sqrt((sin(az(v))*sin(el(u)))^2 + (cos(az(v))*cos(el(u)))^2);
    end
end
Dopbinscell = ceil(deltaDop/BWr); %Doppler bins containing clutter
```

```
MDV = lamda/2*Dopbinscell*BWr;    %minimum detectable velocity (m/s)


%plot the coverage area variations in MDV
figure
clf
mesh(az*180/pi,el*180/pi,MDV)
grid on
set(gca,'fontweight','bold')
xlabel('azimuth (degrees)')
ylabel('elevation (degrees)')
zlabel('Minimum Detectable Velocity (m/s)')
axis square
axis([min(az)*180/pi max(az)*180/pi min(el)*180/pi max(el)*180/pi...
      min(min(MDV)) max(max(MDV))])
colorbar
title('Coverage Area Variations in the Minimum Detectable Velocity')
box on


%determine the spatial and velocity resolution of the cluster over the
coverage area
rngres = c*taucp/2*sec(psi);      %range resolution (m)
Xrngres = 2*lamda/B*Rs./cos(el);    %cross range resolution (m)
velres = BWr*lamda/2;    %velocity resolution (m/s)


%output data structures
ISOLATION.avg_proj_baseline = avgBproj;
ISOLATION.min_detect_vel = MDV;
ISOLATION.range_res = rngres;
ISOLATION.cross_range_res = Xrngres;
ISOLATION.vel_res = velres;
```

B.7 Radar Performance Module

```
%TechSat 21 Coverage Area Model - Radar Performance Module


function [PERFORMANCE] = radarperformance(GEOMETRY,STATS,CAPABILITY,...
    ISOLATION,res,Re,h)
```

```
%calculates the radar performance statistics for a given TechSat 21 con-
stellation

%inputs from other radar modules
psiPDF = STATS.grazing_angle_PDF;    %grazing angle PDF
elPDF_3D = STATS.elevation_angle_PDF_3D;   %3D elevation angle PDF
el = GEOMETRY.elevation;    %elevation angle (rad)
az = GEOMETRY.azimuth;      %azimuth angle (rad)
psi = GEOMETRY.grazing_angle;       %grazing angle (rad)
Pd = CAPABILITY.prob_detect;  %probability of detection
MDV = ISOLATION.min_detect_vel;   %minimum detectable velocity (m/s)

%increase the resolution of all geometric parameters
A = linspace(min(psi),max(psi),length(psi));
B = linspace(0,pi/2,length(psiPDF));
C = linspace(min(psi),max(psi),res);
D = linspace(0,pi/2,res);
psiPd = interp1(A,psi,C);
psiPDFnew = interp1(B,psiPDF,D);
psiPDFnew = psiPDFnew/sum(psiPDFnew);

elhzn = asin(Re/(Re+h));
E = linspace(min(el),max(el),length(el));
F = linspace(0,elhzn,length(elPDF_3D));
G = linspace(min(el),max(el),res);
H = linspace(0,elhzn,res);
elMDV = interp1(E,el,G);
elPDF_3Dnew = interp1(F,elPDF_3D,H);
elPDF_3Dnew = elPDF_3Dnew/sum(elPDF_3Dnew)/length(az);

%determine the performance capability of the system
Pdnew = interp1(psi,Pd,psiPd);
Pdrange = linspace(min(Pdnew),1,length(Pdnew));

MDVnew = interp1(el,MDV,elMDV,'nearest');
MDVrange = linspace(0,max(max(MDVnew)),size(MDVnew,1));
MDVrange = fliplr(MDVrange);

W = waitbar(0,'Computing Availabilities...');
```

```
for m = 1:res
    a = find(Pdnew >= Pdrange(m));
    if sum(a) == 0
        PdPDF = 0;
    else
        for b = 1:length(a)
            PdPDF(b) = psiPDFnew(a(b));
        end
    end
    av_Pd(m) = sum(PdPDF);


    [x,y] = find(MDVnew <= MDVrange(m));
    if sum(x) == 0
        MDVPDF = 0;
    else
        for z = 1:length(x)
            MDVPDF(z) = elPDF_3Dnew(x(z));
        end
    end
    av_MDV(m) = sum(MDVPDF);
    clear PdPDF MDVPDF
    waitbar(m/res,W)
end
close(W)

%plot the integrity (Pd) and isolation (MDV) availabilities
figure
clf
plot(Pdrange,av_Pd,'b-','linewidth',1.5)
grid on
set(gca,'fontweight','bold')
xlabel('Probability of Detection')
ylabel('Availability')
axis square
axis([min(Pdrange) max(Pdrange) 0 1])
title('Radar Performance Availability')

figure
clf
```

```
plot(MDVrange,av_MDV,'b-','linewidth',1.5)
grid on
set(gca,'fontweight','bold')
xlabel('Minimum Detectable Velocity (m/s)')
ylabel('Availability')
axis square
axis([floor(min(MDVrange)*10)/10 ceil(max(MDVrange)*10)/10 0 1])
title('Radar Isolation Availability')

%output data structures
PERFORMANCE.range_prob_detect = Pdrange;
PERFORMANCE.range_min_detect_vel = MDVrange;
PERFORMANCE.avail_prob_detect = av_Pd;
PERFORMANCE.avail_min_detect_vel = av_MDV;
```

Appendix C

DESIGN STUDY MATLAB CODE

C.1 Master File

```
%TechSat 21 Design Study - Master File


clear all
tic


%design vector variables
h = 8e5;      %orbital altitude (m)
D = 0.5:0.5:4;     %aperture diameter (m)


%constants vector inputs
f = 10e9;          %frequency (Hz)
DC = 0.05;         %antenna tranmission duty cycle
sigmaT = 10;       %target radar cross section (m^2)
reqrngres = 250;   %required range ground resolution (m)
reqXrngres = 500;  %required cross range ground resolution (m)
Pdmin = 0.85;      %minimum probability of detection
avmin = 0.9;       %minimum availability of Pdmin
FAR = 1e-3;        %false alarm rate
maxni = 10;        %maximum number of nocoherent integrations
nadirhole = 0.5*pi/180;     %Earth angle nadir hole (rad)
mode = 1;          %operating mode for the system (1=scan, 2=search)
theater = 1e6^2;   %area (m^2) of a region of interest
avail_res = 300;   %resolution of the availability calculations


%other module variables
```

```
c = 2.998e8;        %speed of light (m/s)

lamda = c/f;        %wavelength (m)

Pavg = Pt*DC;       %antenna average power (W)

k = 1.381e-23;      %Boltzmann constant (J/K)

Tdwell = 0.050;     %dwell time (s)

Ts = 290;           %antenna temperature (K)

Ls = 2;             %system losses

Re = 6.378e6;       %Earth radius (m)

theta = 2.44*lamda./D;   %antenna null-to-null beamwidth (rad)

vp = 1.9964e7/sqrt(h+Re);   %velocity of the satellite cluster (m/s)


%input variables from other modules
load cons_stats(35at8)
psistats = CONSTELLATION.avgelv';      %grazing angle statistics
avgview = mean(mean(CONSTELLATION.avgvis));   %average visit time (s)
clear CONSTELLATION



%reduce the statistics to PDFs
STATS = coveragestats(Re,h,psistats);


for n = 1:length(D)   %repeat for each aperture diameter
    %discretize the coverage area
    GEOMETRY(n) = coveragearea(Re,h,vp,lamda,D(n),reqXrngres,...
        nadirhole,mode,theater,avgview,theta(n));

    %determine the important system parameters
    PARAMETER(n) = radarparameter(GEOMETRY(n),D(n),c,lamda,DC,...
        Tdwell,FAR,reqrngres,Re,theta(n),maxni);

    %evaluate the variational parameters in the SNR equation
    VARIABLE(n) = statscurve(STATS,GEOMETRY(n),PARAMETER(n),...
        avail_res,avmin);
end


%calculate the PtN2 product for each aperture diameter
DESIGN = radardesign(PARAMETER,VARIABLE,D,sigmaT,DC,lamda,k,Ts,...
    Ls,Pdmin,maxni);
```

```
toc
```

C.2 Statistics Module

```
%TechSat 21 Design Study - Statistics Module


function [STATS] = coveragestats(Re,h,stats_psi)
%calculates the grazing angle PDF


%turn stats files into PDFs
CDF_psi = 1 - stats_psi;    %grazin angle CDF
PDF1 = diff(CDF_psi);
psi1 = linspace(0,pi/2,length(PDF1));
PSI = linspace(0,pi/2,length(stats_psi));
PDF_psi = interp1(psi1,PDF1,PSI);
PDF_psi = PDF_psi/sum(PDF_psi);     %grazing angle PDF


%output data structures
STATS.grazing_angle_PDF = PDF_psi;
```

C.3 Radar-Earth Geometry Module

```
%TechSat 21 Design Study - Radar-Earth Geometry Module


function [GEOMETRY] = coveragearea(Re,h,vp,lamda,D,reqXrngres,...
    nadirhole,mode,theater,avgview,theta)
%discretizes the coverage area of the TechSat 21 configuration


%radar-Earth geometry
elhzn = asin(Re/(Re+h)) - theta/2;   %horizon elevation angle (rad)
psihzn = acos((Re+h)/Re*sin(elhzn));    %horizon grazing angle (rad)
phichzn = pi/2 - elhzn - psihzn;        %horizon Earth angle (rad)
phic = linspace(nadirhole,phichzn,25);    %Earth angle discretization
phic = fliplr(phic);    %Earth angles from horizon to nadir
Rs = ((Re+h)^2 - 2*Re*(Re+h)*cos(phic) + Re^2).^0.5;    %radar range
(m)
```

```
el = asin(Re*sin(phic)./Rs);   %coverage area elevation angles (rad)
psi = pi/2 - el - phic;          %coverage area grazing angles (rad)
psit = acos((Re+h)/Re*sin(el+theta/2));   %toe grazing angle (rad)
psih = acos((Re+h)/Re*sin(el-theta/2));   %heel grazing angle (rad)
az = linspace(0,(359)*pi/180,90);   %coverage area azimuth angles (rad)


%cluster parameters
B = ceil(2*lamda*max(Rs)/reqXrngres/cos(max(el)));  %cluster baseline (m)
if mode == 1    %scan mode
    ASR = theater/avgview;   %area search rate (m^2/s)
elseif mode == 2   %search mode
    ASR = 2*max(Rs)*sin(max(el))*vp;     %area search rate (m^2/s)
end


%output data structures
GEOMETRY.earth_angle = phic;
GEOMETRY.radar_range = Rs;
GEOMETRY.elevation = el;
GEOMETRY.grazing_angle = psi;
GEOMETRY.grazing_angle_toe = psit;
GEOMETRY.grazing_angle_heel = psih;
GEOMETRY.azimuth = az;
GEOMETRY.baseline = B;
GEOMETRY.area_search_rate = ASR;
```

C.4 Radar Parameters Module

```
%TechSat 21 Design Study - Radar Parameters Module


function [PARAMETER] = radarparameter(GEOMETRY,D,c,lamda,DC,...
    Tdwell,FAR,reqrngres,Re,theta,maxni)
%calculates some of the key radar parameters based on constraints
%in the design and constants vectors


%inputs from other radar modules
psi = GEOMETRY.grazing_angle;        %grazing angle (rad)
psit = GEOMETRY.grazing_angle_toe;   %toe grazing angle (rad)
```

```
psih = GEOMETRY.grazing_angle_heel;     %heel grazing angle (rad)
Rs = GEOMETRY.radar_range;              %radar range to target (m)
el = GEOMETRY.elevation;                %elevation angle (rad)
ASR = GEOMETRY.area_search_rate;        %area search rate (m^2/s)


%determine the pulse properties
L = Re*(psih - psit - theta);    %footprint length (m)
PRF = c/2./cos(psi)./L;     %pulse repetition frequency (Hz)
nc = floor(Tdwell*PRF);     %number of coherent pulses
taup = DC./PRF;        %pulse width (s)
taucp = 2*reqrngres/c*cos(max(psi));    %compressed pulse width (s)
CR = taup/taucp;  %pulse compression ratio
Tfp = pi*(Rs*theta/2).^2./...
   sin(psi)/ASR;  %time available to scan a specific location (s)
ni = floor(Tfp/Tdwell);     %number of noncoherent integrations
A = find(ni > maxni);
ni(A) = maxni;     %max number of noncoherent integrations
B = find(ni == 0);
ni(B) = 1;          %enough time for coherent integration only
BWs = 1/taucp;     %signal bandwidth (Hz)
BWr = 1/Tdwell;    %receive bandwidth (Hz)
Pfa = FAR/BWr;     %false alarm probability


%output data structures
PARAMETER.pulse_rep_freq = PRF;
PARAMETER.num_coherent_pulses = nc;
PARAMETER.pulse_width = taup;
PARAMETER.comp_pulse_width = taucp;
PARAMETER.comp_ratio = CR;
PARAMETER.num_incoherent_pulses = ni;
PARAMETER.signal_bandwidth = BWs;
PARAMETER.receive_bandwidth = BWr;
PARAMETER.prob_false_alarm = Pfa;
```


C.5 Variational Parameters Module

```
%TechSat 21 Design Study - Variational Parameters Module
```

```
function [VARIABLE] = statscurve(STATS,GEOMETRY,PARAMETER,res,avmin)
%evaluates the variational parameters from the SNR equation


%inputs from radar other modules
psi = GEOMETRY.grazing_angle;        %grazing angle (rad)
Rs = GEOMETRY.radar_range;           %radar range to target (m)
ASR = GEOMETRY.area_search_rate;     %area search rate (m^2/s)
taup = PARAMETER.pulse_width;        %transmitted pulse width (s)
nc = PARAMETER.num_coherent_pulses;       %number of coherent pulses
ni = PARAMETER.num_incoherent_pulses;   %number on incoherent pulses
psiPDF = STATS.grazing_angle_PDF;        %grazing angle PDF


%calculate the SNR variational parameters at each grazing angle
var = taup.*nc.*ni.^(2/3)./Rs.^4;


%increase the resolution of all parameters
A = linspace(min(psi),max(psi),length(psi));
B = linspace(0,pi/2,length(psiPDF));
C = linspace(min(psi),max(psi),res);
D = linspace(0,pi/2,res);
PSI = interp1(A,psi,C);
psiPDFnew = interp1(B,psiPDF,D);
psiPDFnew = psiPDFnew/sum(psiPDFnew);


%determine the availability of the SNR variational parameters
varnew = interp1(psi,var,PSI);
varrange = linspace(min(varnew),max(varnew),length(varnew));
W = waitbar(0,'Computing Availabilities...');
for m = 1:res
   a = find(varnew >= varrange(m));
   if sum(a) == 0
      varPDF = 0;
   else
      for j = 1:length(a)
         varPDF(j) = psiPDFnew(a(j));
      end
   end
   av_var(m) = sum(varPDF);
   waitbar(m/res,W)
```

```
end
close(W)

%plot the SNR variational parameters availability curve
figure
clf
plot(varrange,av_var,'b-','linewidth',1.5)
plot(psi*180/pi,var,'g-','linewidth',1.5)
grid on
set(gca,'fontweight','bold')
xlabel('SNRvar (s/m^4)')
ylabel('Availability')
axis square
axis([min(varrange) max(varrange) 0 1])
axis([min(psi)*180/pi max(psi)*180/pi min(var) max(var)])
title('SNR Statistical Quantities')

%find the value of the SNR variable that corresponds to the required
availability
if avmin == 1
    x = 1;
else
    x = find(av_var >= avmin);
end
SNRvar = (varrange(max(x)) + varrange(max(x)+1))/2*(av_var(max(x)) +
av_var(max(x)+1))/avmin/2;

%output data structures
VARIABLE.avail_SNR_var = av_var;
VARIABLE.range_SNR_var = varrange;
VARIABLE.SNR_var = SNRvar;
```

C.6 Radar Design Module

```
%TechSat 21 Design Study - Radar Design Module


function [DESIGN] = radardesign(PARAMETER,VARIABLE,D,sigmaT,DC,...
```

```
    lamda,k,Ts,Ls,Pdmin,maxni)
%compute the PtN2 product curve


%constant inputs from other modules
Pfa = PARAMETER(1).prob_false_alarm;    %false alarm probability
nfa = log(0.5)/log(1 - Pfa);   %number of false alarms
beta = 1/6 + exp(-maxni/3);
SNRreq = log10(nfa)/log10(1/Pdmin)^beta;   %minimum SNR from required Pd


%calculate the PtN2 product for each aperture diameter
for j = 1:length(D)
    CR = min(PARAMETER(j).comp_ratio);   %min pulse compression ratio
    SNRvar = VARIABLE(j).SNR_var;        %SNR variational parameters
    SNRconst = 0.85^2*pi*sigmaT*CR/...
        (16^2*lamda^2*k*Ts*Ls);      %SNR constants
    PD4N2(j) = SNRreq/SNRconst/SNRvar;   %power-aperture-num_sats product
end
PN2 = PD4N2./D.^4;    %PtN2 product


%plot the PtN2 product curve
figure
clf
plot(D,PN2,'r-','linewidth',1.5)
grid on
set(gca,'fontweight','bold')
xlabel('Diameter (m)')
ylabel('Pavg-N^2 Product')
axis square
axis([min(varrange) max(varrange) 0 1])
title('Acceptable Design Parameter Combinations')


%output data structures
DESIGN.power_diameter_numsats = PD4N2;
DESIGN.power_numsats = PN2;
```